รายงานวิจัยฉบับสมบูรณ์

โครงการ : Nonlinear Frame Model for Large Displacement Inelastic Analysis of Frame Structures

โดย รองศาสตราจารย์ ดร.สุชาติ ลิ่มกตัญญู

19 กันยายน 2557

สัญญาเลขที่ RSA 5480001

รายงานวิจัยฉบับสมบูรณ์

โครงการ : Nonlinear Frame Model for Large Displacement Inelastic Analysis of Frame Structures

รองศาสตราจารย์ ดร.สุชาติ ลิ่มกตัญญู

ภาควิชาวิศวกรรมโยธา คณะวิศวกรรมศาสตร์
มหาวิทยาลัยสงขลานครินทร์

สนับสนุนโดยสำนักงานกองทุนสนับสนุนการวิจัย
และสำนักงานคณะกรรมการการอุดมศึกษา

กิตติกรรมประกาศ

รายงานวิจัยฉบับนี้ ได้รับการสนับสนุนทุนวิจัยจาก สำนักกองทุนสนับสนุนการวิจัย (สกว.) ผู้วิจัยใคร่ขอขอบพระคุณเป็นอย่างสูงมา ณ ที่นี้ นอกจากนี้ในช่วงเวลาที่ทำงานวิจัยนี้ทางสำนักกองทุนสนับสนุนการวิจัย (สกว.) ยังสร้างโอกาสและเปิดช่องทางในการแลกเปลี่ยนความรู้ระหว่างผู้วิจัยและเมธีวิจัยอาวุโส ผู้วิจัยอื่น ๆ ที่อยู่ในสายงานวิจัยเดียวกันหรือใกล้เคียง และผู้วิจัยที่อยู่ในสายงานอื่น

ผู้วิจัยขอขอบคุณภาควิชาวิศวกรรมโยธา คณะวิศวกรรมศาสตร์ มหาวิทยาลัยสงขลานครินทร์ ที่ให้ความอนุเคราะห์ในการใช้อุปกรณ์ และเครื่องมือต่าง ๆ ในงานวิจัย รวมทั้ง ศ.ดร. ปณิธาน ลักคุณะประสิทธิ์ และ ศ.ดร.สมชาย ชูชีพสกุล ที่ให้ความกรุณาเขียนจดหมายรับรองในการสมัครทุนวิจัย

สุดท้ายนี้ขอขอบคุณเจ้าหน้าที่ของสำนักกองทุนสนับสนุนการวิจัย (สกว.) ที่อำนวยความสะดวกในด้านต่าง ๆ เพื่อให้งานวิจัยนี้สำเร็จลุล่วงไปด้วยดี

รองศาสตราจารย์ ดร. รศ.ดร.สุชาติ ลิ่มกตัญญู
ผู้วิจัย

ABSTRACT

Project Code: RSA 5480001

Project Title: Nonlinear Frame Model for Large Displacement Inelastic Analysis of Frame Structures

Investigator: Associate Professor Dr. Suchart Limkatanyu

Department of Civil Engineering, Faculty of Engineering,

Prince of Songkla University

Project Period: 2 Years

The main goal of this research is to develop and implement the simple but efficient nonlinear frame models (bar and beam) that take into account geometric and material nonlinearities. These frame elements can be used to model both elastic and inelastic behaviors of slender framed structures undergoing large displacements and large rotations. The material nonlinearity is included into the models through the fiber-section discretization. This could be done with ease since the Euler-Bernoulli-von Karman beam theory will be used in describing the frame section kinematics. Therefore, the local geometric nonlinearity ($P-\delta$ effect) is automatically accounted for. However, the use of standard displacement-based frame element with this nonlinear beam theory can lead to the so-called *membrane-locking* problem, thus resulting in an over-stiff frame model. One way to remedy this locking phenomenon is to use the reduced integration technique. In this research, both Hellinger-Reissner mixed and force-hybrid variational principles are used to develop the nonlinear frame elements within the corotating local framework. This stems from the fact that the resulting frame elements are locking free and have superb performance in describing the inelastic actions when compared with the standard displacement-based frame models. The global geometric nonlinearity ($P-\Delta$ effect) is introduced into the models via the corotational approach.

Keywords: Corotational formulation; Large displacement/rotation; Hellinger-Reissner mixed functional; Nonlinear bar element; Nonlinear beam element; Geometric nonlinearity; Material nonlinearity; Euler-Bernoulli-von Karman beam theory; Total Lagrangian formulation.

CONTENTS

CHAPTER 1 Introduction 1

1.1 Importance and Motivation of This Research 1

1.2 Objectives of This Research 3

1.3 Literature Review 5

1.3.1 Material Nonlinearity 5

1.3.1.1 Lumped Nonlinear Frame Models 6

1.3.1.1.1 Pros and Cons of Nonlinear Frame Models 6

1.3.1.2 Distributed Nonlinear Frame Models 7

1.3.2 Geometric Nonlinearity 9

1.4 Research Methodology 13

1.4.1 The Formulation and Implementation of the Finite Element Model for Large Displacement Elastic and Inelastic Analyses of Frame Structures 13

1.4.2 The Development and Implementation of Constitutive Relations for Steel and Concrete 13

1.4.2.1 Confined and Unconfined Concrete 15

1.4.2.2 Steel 16

1.4.3 Verification of the Model Accuracy 16

1.4.3 Correlation Studies between the Experimental and Numerical Results 17

1.5 Scope of This Research Area 17

CHAPTER 2 Uniaxial Constitutive Laws 18

2.1 General 18

2.2 Steel Constitutive Law 18

2.3 Concrete Constitutive Law 23

2.3.1 Concrete Stress-Strain Relation in Compression 24

2.3.2 Concrete Stress-Strain Relation in Tension 28

CHAPTER 3 Total Lagrangian Formulation of Planar Bar Element Using Vectorial Kinematical Description 32

3.1 Introduction 32

3.2 Total Lagrangian Formulation 34

3.2.1 Element Kinematics and Green-Lagrange Strain 36

3.2.2 Material Constitutive Law 39

3.2.3 Element Equilibrium: The Virtual Displacement Principle 40

3.3 Incremental Equilibrium Equations 42

3.4 Incremental-Iterative Solution Procedure 44

3.4.1 Generalized Displacement Control Method 46

3.4.2 Step-by-step Algorithm for Generalized Displacement Control Method 48

3.5 Numerical Examples 50

CHAPTER 4 Finite Frame Element for Large Displacement Elastic and Inelastic Analyses of Frame Structures.....61

4.1 Introduction.....61

4.2 Corotational Formulation of Planar Frames 66

4.2.1 Frame Kinematics and Kinetics.....66

4.2.2 Global and Basic Element Stiffness Matrices.....70

4.3 Basic (Local) Beam System: Euler-Bernoulli-von Karman Beam Theory 72

4.3.1 Compatibility: Motion, Deformation, and Strain.....72

4.3.2 Equilibrium: Direct Approach vs. Variational Approach.....75

4.3.3 Sectional Deformation-Force Relations.....78

4.4 Local Euler-Bernoulli-von Karman Finite Beam Formulation.....79

4.4.1 Hellinger-Reissner Mixed Functional.....79

4.4.2 Incremental Element Equations 81

4.4.3 Displacement and Force Interpolation Functions 84

4.5 Element State Determination 86

4.6 Model Evaluation by Benchmark Examples.....87

CHAPTER 5 Summary and Conclusions Remarks.....106

5.1 Total Lagrangian Formulation of Planar Bar Element Using Vectorial Kinematical Description 106

5.2 Finite Frame Element for Large Displacement Elastic and Inelastic Analyses of Frame Structures.....107

BIBLIOGRAPHY

OUTPUTS

APPENDIX

CHAPTER 1
INTRODUCTION

1.1 Importance and Motivation of This Research

During the last sixty years, the level of structural analysis needed to assess and analyze structural performance has been more and more sophisticated especially with drastic advances on computer technology as well as a better understanding of the physical and mathematical principles governing the behavior of complex structures. The driving forces for higher requirement on structural analysis are partly due to the occurrence of catastrophic damages, loss of human lives, etc. during exceptional and extreme events (e.g. rare earthquakes, terrorist attacks, construction errors, etc.). These force structural engineers to rely on more advanced structural modeling techniques in order to understand and trace the structural behavior under abnormal loading conditions. Generally, abnormal loads are categorized as exerted forces not accounted for in the design of structures during their service lives. In the worst case scenario, these abnormal loads can eventually result in the structural collapse. Therefore, nonlinear behaviors of structures due to material properties and geometric changes are necessarily included in more reliable structural models. This leads to a need for the simple but efficient numerical model capable of simulating the nonlinear behavior of structures undergoing large displacements and rotations associated with several collapse limit states. Such a numerical model is also essential to assess the safety of structural design for progressive collapse resistance. Progressive collapse of structures is characterized by local failure of primary structural components leading to the collapse of entire structures or disproportionately large parts of them. Following the tragic loss due to the collapse of the Ronan Point Apartment building in London in

1968 as shown Figure 1, progressive collapse of structures has become a growing concern among structural engineers to include it as an important consideration for structural design. The use of finite element models that fail to account for either material or geometric nonlinearity is inadequate to give accurate and reliable analysis results, thus preventing structural engineers from understanding the whole process of structural collapse. Consequently, the primary focus of this work is to develop and implement simple but efficient nonlinear frame elements capable of taking into account both material (inelastic) and geometric (large displacements and rotations) nonlinearities.

Figure 1: Ronan Point Apartment Building

(http://en.wikipedia.org/wiki/Ronan_Point)

Furthermore, the drastic advance in material technology has resulted in engineering structures with high-strength but lightweight in nature (e.g. aerospace structures, marine vehicles, innovative structural buildings, etc.). Such structures often fail by losses of their stability and may behave elastically well into the post-buckling regime. During the post-buckling regime, these structures generally experience large

displacements and rotations. Therefore, the use of nonlinear frame elements developed herein is also essential in predicting the pre and post buckling responses of these structures.

1.2 Objectives of This Research

The main goal of this research is to develop and implement the simple but efficient nonlinear frame models that take into account geometric and material nonlinearities. These frame elements can be used to model both elastic and inelastic behaviors of slender framed structures undergoing large displacements and large rotations. The material nonlinearity is included into the models through the fiber-section discretization. This could be done with ease since the Euler-Bernoulli-von Ka′rma′n beam theory will be used in describing the frame section kinematics. Therefore, the local geometric nonlinearity ($P-\delta$ effect) is automatically accounted for. However, the use of standard displacement-based frame element with this nonlinear beam theory can lead to the so-called *membrane-locking* problem, thus resulting in an over-stiff frame model (Reddy, 2005). One way to remedy this locking phenomenon is to use the reduced integration technique (Hughes, 1987). In this research, both Hellinger-Reissner mixed and force-hybrid variational principles (Limkatanyu and Spacone, 2006) are used to develop the nonlinear frame elements within the corotating local framework. This stems from the fact that the resulting frame elements are locking free and have superb performance in describing the inelastic actions when compared with the standard displacement-based frame models (Limkatanyu and Spacone, 2002). The global geometric nonlinearity ($P-\Delta$ effect) is introduced into the models via the corotational approach.

The objectives of this research can be summarized as follows:

1. Develop and implement the efficient nonlinear finite element models as a reliable numerical tool for large displacement elastic and inelastic analyses of frames.
2. Explore the importance of including the rotational-related quadratic terms in the local strain-displacement equations (Euler-Bernoulli-von Ka′rma′n beam theory).
3. Explore the feasibility of formulating the Hellinger-Reissner mixed frame elements within the framework of the Euler-Bernoulli-von Ka′rma′n beam theory.
4. Explore the feasibility of merging the Hellinger-Reissner mixed fiber frame elements with the corotational approach.
5. Compare the performance of the developed frame elements with the standard displacement-based frame elements formulated based on total Lagrangian, updated Lagrangian, and corotational approaches and indicate their pros and cons.
6. Validate the accuracy of the developed frame elements by comparing their numerical results to benchmark analytical results, to results obtained from other finite element software, and to experimental results published in the literature.

1.3 Literature Review

To certain extent, all engineering structures response nonlinearly to their applied loads. In particular, structural collapse may be induced by both material failures and geometric changes. Consequently, the inclusion of both material and geometric nonlinearities into the numerical models is essential in understanding the realistic collapse mechanism of engineering structures. Since the main focus in this research is on reticulated structures, only finite frame elements for large-displacement inelastic analysis of frame structures are developed. Therefore, a literature review relevant to the development of nonlinear frame models incorporating material and geometric nonlinearities is presented in this section. The review begins with frame models considering material nonlinearity and ends up with frame models considering geometric nonlinearity.

1.3.1 Material Nonlinearity

Nonlinear frame elements are used to discretize a building into a skeletal structure. The hysteretic behavior of non-linear elements is either introduced at the element ends or is spread over the entire element length. As a result, the element formulation can be classified into two groups: (a) lumped nonlinear frame models, and (b) distributed nonlinear frame models. Several nonlinear frame elements belonging to these two element formulations have been proposed by several researchers in the research community.

1.3.1.1 Lumped Nonlinear Frame Models

In lumped nonlinear frame models, inelastic zones are idealized as zero-length plastic hinges in the form of hysteretic springs. At each inelastic region, more than one hysteretic spring can be used depending on the number of nonlinear actions to be represented. Each hysteretic spring represents either flexural, shear, or bond-slip mechanism. Several lumped nonlinear frame models have been proposed by several researchers. Among others, the widely used lumped models are the two-component model by Clough et al. (1965), the one component model by Giberson (1969), and the *sandwich-like* model by Lai et al. (1984). An excellent overview of the lumped nonlinear frame models is presented in the state-of-the-art report by Comite Euro-International du Beton: Task Group III/6 (1996).

1.3.1.1.1 Pros and cons of lumped nonlinear frame models

The actual behavior of a structural member (either steel or reinforced concrete) involves the gradual penetration of inelastic deformations into the members as a function of the excitation history. The use of lumped nonlinear frame models greatly simplifies the representation of this behavior. However, the limitations of these models have been recognized in several correlation studies, especially in large resisting elements of flexural wall-frame system (Charney and Bertero, 1982; Bertero et al., 1984). The main advantages of lumped nonlinear frame models are the followings: (*a*) the compactness of their mathematical formulation, which reduces storage requirements and computational cost and improves numerical stability, and (*b*) the ease of including the effects of different inelastic actions (flexural, shear, and bond-slip) into the models. However, the lumped representation of the inelastic behavior oversimplifies certain crucial aspects of the hysteretic behavior of structural members and hence limits the applicability of the models. One such limitation derives

from an *ad-hoc* assumption needed to define the hysteretic parameters of the end-springs. Several researchers (Mahin and Bertero, 1975; Agardh, 1974; Anagnostopoulos, 1981) performed parametric and theoretical investigations of reinforced concrete beams under monotonic loadings and showed that there is a strong combination between model parameters and loading pattern. None of these two factors is expected to remain constant during the entire loading history. This problem is further magnified by the fluctuation of the axial forces in compression members. Because of this history dependence, damage predictions at the global level as well as at the local level may be completely inaccurate. Furthermore, most lumped nonlinear frame models fail to describe the deformation softening behavior of reinforced concrete members. Deformation softening is usually indicated by the reduction in loading resistance under increasing deformations.

1.3.1.2 Distributed Nonlinear Frame Models

Distributed nonlinear frame models give a more refined and accurate description of the inelastic behavior of structures. Unlike lumped nonlinear frame models, the inelastic behavior can take place in any section in the distributed nonlinear frame model. In a reinforced concrete structure, the discrete nature of cracks is represented via the smeared crack concept. The nonlinear nature of a cross-section can be formulated either by the classical plasticity theory (Prager and Hodge, 1951) in terms of the stress and strain resultants or by the fiber-section discretization. The main drawback of the first approach is the need for specific force-deformation relations for specific shapes of cross section. Due to the loss of its generality, the first approach is mostly applied to steel frame structures where standard shapes of member cross section are available. Furthermore, the difficulty of characterizing partial yielding of the cross section is another drawback of this approach. The fiber-discretized section is

a more refined and rational way to introduce the distributed nonlinear feature. The detailed discussion of the fiber-discretized section is presented in Spacone (1994). The fiber-discretized section model can be combined with the finite frame element to develop the more refined and rational distributed nonlinear numerical model for frame structures. This may lead to different nonlinear fiber frame elements derived based on different variational principles (Limkatanyu, 2002). These nonlinear fiber frame models can be classified into three groups: (*a*) displacement-based model (e.g. Hellesland and Scordelis, 1981; Rubiano-Benavides, 1998); (*b*) force-based model (e.g. Ciampi and Carlesimo, 1986; Spacone et al., 1996; Limkatanyu and Spacone, 2002); and (*c*) multi-fields (mixed) model (e.g. Limkatanyu and Spacone, 2002; Taylor et al., 2003; Lee and Filippou, 2009). The pros and cons of these three fiber frame models are comprehensively discussed in Limkatanyu (2002). Generally, the force-based and mixed frame elements are more accurate than the displacement-based element. This advantage stems from two main observations: (1) in some simplified cases the internal force distributions in frame elements are known "exactly". This is, for example, the case of the reinforced concrete element with perfect bond; (2) in general, the force fields along the element are smoother than the deformation fields, which may show large jumps in the inelastic zones, especially where plastic hinges tend to form (i.e., in the column base, girder ends, beam midspan, etc.). While the development of elements that use force shape functions is *per se* simple, the implementation of such elements in an existing nonlinear structural analysis program is the real challenge in the element formulation.

1.3.2 Geometric Nonlinearity

In recent years, the development of finite elements for the nonlinear analysis of frame structures has attracted many researchers. Depending on the choice of reference configuration and the method of kinematical description, there are three finite element models for geometrically non-linear frame problems, namely: (a) Total Lagrangian (TL) model; (b) Updated Lagrangian (UL) model; and (c) Corotational (CR) model. However, the most widely used models are derived based on the total Lagrangian and updated Lagrangian kinematical descriptions of a displaced body. Most of geometrically nonlinear finite element models implemented into commercial finite element packages available in the market (e.g. ABAQUS, ANSYS, etc.) are derived based on these two kinematical descriptions. However, during the last twenty years, the concept on the corotational kinematical description has been more understood and gained more popularity. Especially, the corotational concept is well-suited to a certain class of nonlinearly geometric frame problems in which displacements and rotations are large but strains are moderate. This is due to its natural treatment of rigid-body motions.

A brief review of these three kinematical descriptions (TL, UL, and CR) will be provided in the following. More comprehensive review can be found in Vu (2006) and Belytschko et al. (2000). To gain the big picture of the total Lagrangian, updated Lagrangian, and corotational approaches, let us consider the schematic motion of a frame element shown in Figure 1-1.

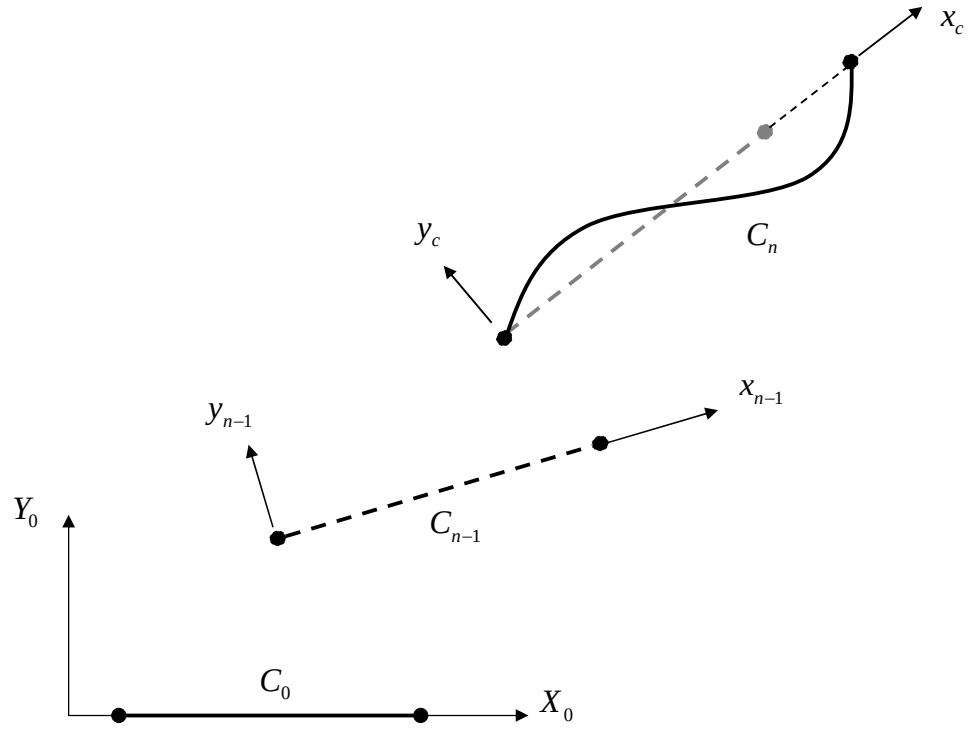

Figure 1-1: Motion of a Frame Element

In the total Lagrangian formulation, the reference system is the original undeformed element configuration C_0. All static and kinematic variables of the current element configuration C_n are referred to this reference configuration. Several total Lagrangian frame elements for large displacement problems have been proposed by several researchers in the research community (e.g. Bathe and Bolourchi, 1979; Crespo Da Silva, 1988; Iura and Atluti, 1988; Saje, 1990; Pacoste and Eriksson, 1997; Nanakorn and Vu, 2006; etc.) Within the total Lagrangian framework, a highly nonlinear beam theory (Reissner's beam theory) is usually required to simulate the frame motion even if the relative deformations of the frame experiencing finite rigid displacements are small. Using the standard Hermite frame interpolation functions leads to the problem of field inconsistency (Nanakorn and Vu, 2006). This is due to the fact that for large displacement problems, the longitudinal displacement field, the transverse displacement field, and the sectional rotation field are complicatedly dependent on

each other. In other words, these three field variables must satisfy a set of nonlinear kinematical constraints as advocated by the refined beam theory proposed by Reissner (1972). Several researches have proposed several approaches to overcome this difficulty, For example, Saje (1990) and Nanakorn and Vu (2006) proposed the semi-analytical approaches to obtain the field-consistency interpolation functions. More comprehensive explanation of the total Lagrangian formulation is given in Bathe (1996) and Belytschko et al. (2000).

In the updated Lagrangian formulation, the last computed equilibrium configuration C_{n-1} of the displaced element is used as the reference system. All static and kinematic variables of the current element configuration C_n are referred to this reference configuration. A rectangular coordinate frame (x_{n-1}, y_{n-1}) is usually attached to the last computed equilibrium configuration. In each incremental step, this attached coordinate frame is updated. Several updated Lagrangian frame element for large displacement problems have been proposed by several researchers in the research community (e.g. Bathe et al., 1975; Bathe and Bolourchi, 1979; Yang and McGuire, 1986; Gattass and Abel, 1987; Chan, 1988; Yang and Leu, 1991; Shugyo, 2003; etc.). Due to the updating nature of the reference configuration, the standard Hermite interpolation functions could be used if the displacement increment from the reference element configuration C_{n-1} to the current element configuration C_n is sufficiently small. If this is not to be the case, the use of the standard Hermite interpolation functions may lead to the field-inconsistency problem (Nanakorn and Vu, 2006).

Besides total Lagrangian and updated Lagrangian formulations used to derive geometrically nonlinear frame elements, the corotational concept is an alternative to formulate the numerical model for large displacement and large rotation analysis of frame structures and becomes extremely popular. The corotational concept, dating

back to the early 60's (Argyris et al., 1964), has employed the polar decomposition principle used in continuum mechanics in its rudimentary form. Following the polar decomposition principle (Malvern, 1969), the deformational motions of a solid body can be separated from its rigid body motions (translations and rotations). In other words, the total motion of a solid body can be decomposed into two parts, namely: rigid-body part and deformational part. In the finite frame element formulation, this decomposition can be done by attaching a local coordinate frame (x_c, y_c) corotating with the average rigid body rotation of the current element configuration C_n. Consequently, the rigid-body motions of the current element configuration can be nicely represented by the rigid-body motions of the corotating local coordinate frame and the deformations of the current element configuration can be simply measured with respect to the corotating local coordinate frame. Since the deformational part of the motion is generally small with respect to the corotating local frame, the linear beam theory (i.e. Euler-Bernoulli beam theory) can be employed to describe the relative deformations in the corotating local coordinate system. The geometric nonlinearity is introduced globally via the coordinate transformation between the displacements with respect to the corotating local coordinate system and displacements with respect to the fixed global coordinate system. Up to date, the corotational concept has been employed by several researchers to formulate geometrically nonlinear frame elements (e.g. Powell, 1968; Oran, 1973; Belytschko and Glaum, 1979; Rankin and Brogan, 1984; Crisfield, 1990; Krenk et al., 1999; Scott and Filippou, 2007; etc.).

1.4 Research Methodology

The main focus of this research is on the development and implementation of the simple but efficient nonlinear frame models accounting for geometric and material nonlinearities. The research will involve the following phases;

1.4.1 The formulation and implementation of the finite element model for large displacement elastic and inelastic analyses of frame structures.

The finite element formulation of the nonlinear frame element will start from the derivation of governing differential equations (strong form) and then the variational principle will be used to derive the finite element equation (weak form).

This finite element model will be implemented in **FEAP** (**F**inite **E**lement **A**nalysis **P**rogram). **FEAP** is the general-purpose finite element program developed by Professor R.L. Taylor at University of California, Berkeley and was extensively used by the principal investigator of this research during his doctoral work.

1.4.2 The development and implementation of constitutive relations for steel and concrete.

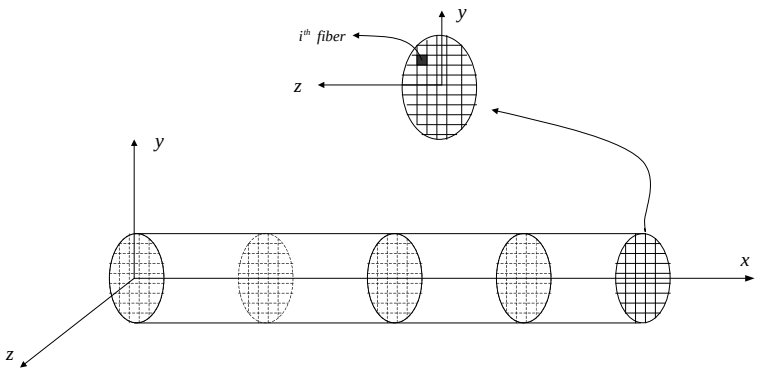

Figure 1-2: Frame Element: Discretization of Cross Section into Fibers

In this research, the fiber-section model (Figure 1-2) will be developed to model the nonlinear behavior of the frame element. The fiber-section model

automatically couples the interactions between the axial force and bending moment and allows the proposed frame element to analyze several types of frame structures (Figure 1-3).

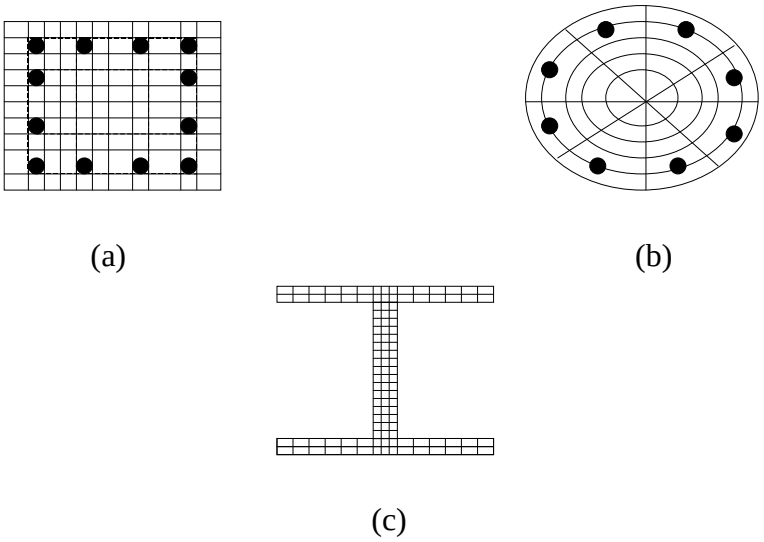

Figure 1-3: Fiber-Discretization of Frame Sections: (a) Square RC Section; (b) Circular RC Section; (c) Steel H Section.

In the fiber-section model, each fiber represents the constituent material of the section (e.g. concrete, steel). In this research, only the reinforced concrete and steel piles are of interest. Consequently, the following uniaxial laws will be developed and be implemented in the library of constitutive laws.

1.4.2.1 Confined and Unconfined Concrete

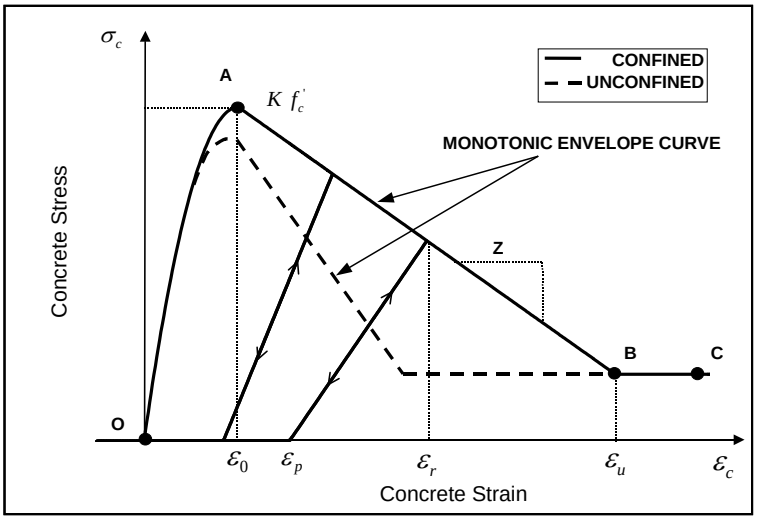

Figure 1-4: Concrete Material Model under Cyclic Loading in Compression

The concrete material model (Figure 1-4) used in this research is based on the modified Kent-and-Park model. The original model proposed by Kent and Park (1971) was modified by Scott et al. (1982) to account for the confinement effects and was later modified by Yassin (1994) to include the tensile stiffening and the tensile damage. The main features represented by this modified version of Kent-and-Park model are as follows:

- The influence of concrete confinement on the monotonic envelope curve in compression.
- The effect of tensile damage under unloading and reloading.
- The tensile stiffening
- The hysteretic response under cyclic loadings.

1.4.2.2 Steel

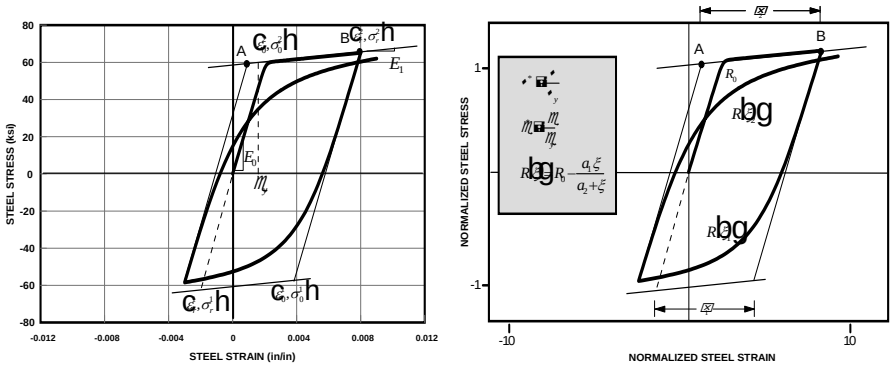

Figure 1-5: Steel Material Model under Cyclic Loading

In this research, the steel material model (Figure 1-5) under monotonic or cyclic loading is described by the nonlinear model of Menegotto and Pinto (1973), as modified by Filippou et al. (1983) to include the isotropic hardening effects.

1.4.3 Verification of the model accuracy.

The accuracy of the numerical models proposed in this research will be verified through several correlation studies between the numerical and analytical results of benchmark problems published in the literature. The following classes of problems will be considered:

(a) Cantilever beam with a concentrated load at the free end (Bisshop and Drucker, 1945).

(b) Cantilever beam with an end moment (Mattiasson, 1981).

(c) William's toggle frame (William, 1964).

(d) Lee's frame (Lee et al., 1968)

1.4.4 Correlation studies between the experimental and numerical results.

The capability of the proposed frame elements in collapse analysis will be assessed through correlation studies between the experimental and analytical results available in literature.

1.5 Scope of This Research Area

The main scope of the proposed research is to develop a set of realistic and easy to use numerical models for the nonlinear analysis of frame structures considering both geometric and material nonlinearities. The project is especially important in view of the assessment of vulnerability of framed structures against progressive collapse scenarios induced by extreme events (e.g. rare earthquakes, terrorist attacks, construction errors, etc.).

CHAPTER 2

UNIAXIAL CONSTITUTIVE LAWS

2.1 General

This chapter presents the constitutive models for reinforcing steel, concrete, and soils. The nonlinear behavior of reinforcing steel under monotonic or cyclic loading is modeled using the Menegotto and Pinto (1973) stress-strain relation. This model was later modified by Filippou et al. (1983) to include isotropic-hardening effects. As for the plain concrete, the Kent and Park (1971) stress-strain relation is used with the modification proposed by Scott et al. (1982) to include the confinement effects. This model was later modified by Yassin (1994) to include tensile strength and tensile damage. All of aforementioned constitutive laws are based on uniaxial behaviors and are expressed in the strain (deformation) space.

2.2 Steel Constitutive Law

In the present study, the reinforcing steel stress-strain behavior under monotonic or cyclic loading is described by the nonlinear model of Menegotto and Pinto (1973), as modified by Filippou et al. (1983) to include the isotropic hardening effects. The

model is computationally efficient and can closely represent experimental results from cyclic tests on reinforcing bars.

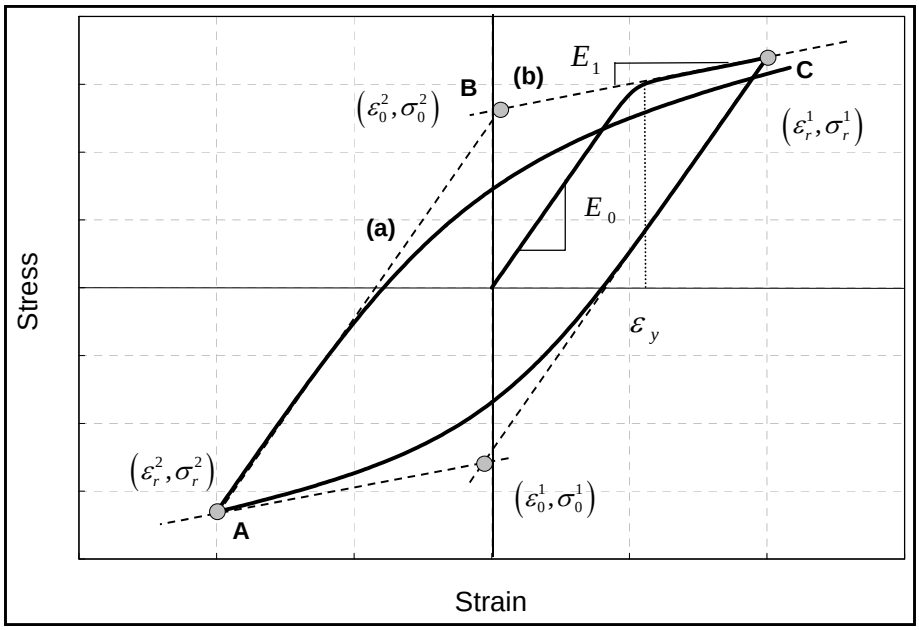

Figure 2-1 Menegotto-Pinto Model

In the Menegotto and Pinto steel model the stress-strain relation is defined by the following nonlinear equation:

$$\sigma^* = b\,\varepsilon^* + \frac{(1-b)\,\varepsilon^*}{\left(1+\left(\varepsilon^*\right)^R\right)^{1/R}} \tag{2.1}$$

where

$$\varepsilon^* = \frac{\varepsilon - \varepsilon_r}{\varepsilon_0 - \varepsilon_r} \tag{2.2}$$

and

$$\sigma^* = \frac{\sigma - \sigma_r}{\sigma_0 - \sigma_r} \tag{2.3}$$

A schematic representation of the steel model is shown in Figure 2-1. Eq. (2.1) defines a curved smooth transition from the straight-line through the origin with slope E_0 to another straight-line through the yield point $(\varepsilon_0, \sigma_0)$ with slope E_1. The tangent modulus E_t of this transition curve is obtained by differentiating Eqs. (2.1), (2.2), and (2.3), and is given by the following expression.

$$E_t = \frac{d\sigma}{d\varepsilon} = \left(\frac{\sigma_0 - \sigma_r}{\varepsilon_0 - \varepsilon_r} \right) \left(b + \left(\frac{1-b}{\left(1 + \left(\varepsilon^*\right)^R\right)^{1/R}} \right) \left(1 - \frac{\left(\varepsilon^*\right)^R}{1 + \left(\varepsilon^*\right)^R} \right) \right) \tag{2.4}$$

In the previous equations, σ_r and ε_r are the stress and strain at the point of strain reversal (point A in Figure 2-1), which also forms the origin of the asymptote with slope E_0 (line (a) Figure 2-1). σ_0 and ε_0 are the stress and strain at the point of intersection of the two asymptotes (point B in Figure 2-1). The parameter b is the strain-hardening ratio, that is $b = E_1 / E_0$. The parameter R is introduced to control the shape of the transition curve between the asymptotes and permits a good representation of the Bauschinger effect. As shown in Figure 2-1, $(\varepsilon_r, \sigma_r)$ and $(\varepsilon_0, \sigma_0)$ are updated after each strain reversal.

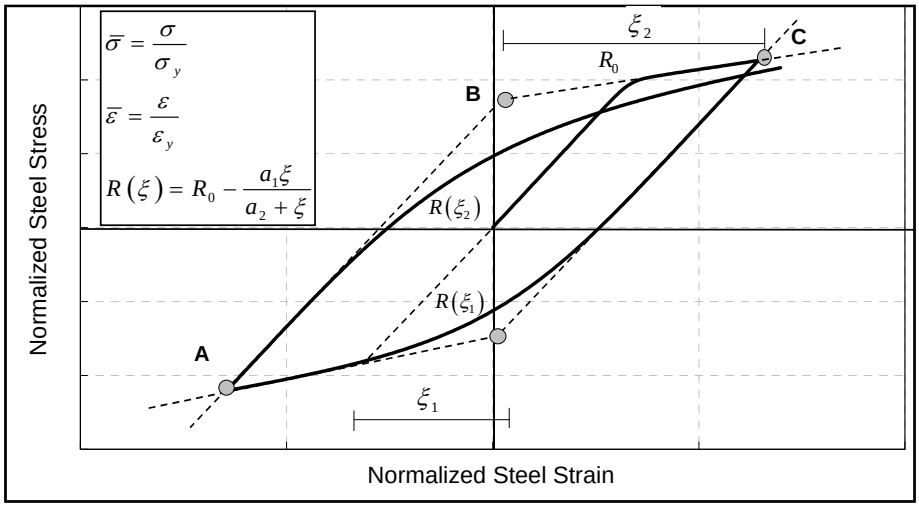

Figure 2-2 Definition of Curvature Parameter *R* in Menegotto-Pinto Steel Model

The parameter R is dependent on the absolute strain difference between the current asymptote intersection point (point B in Figure 2-2) and the previous maximum or minimum strain reversal point (point C in Figure 2-2) depending on whether the current strain is increasing or decreasing, respectively. The expression for R suggested by Menegotto and Pinto is as follows:

$$R(\xi) = R_0 - \frac{a_1 \xi}{a_2 + \xi} \tag{2.5}$$

where R_0 is the value of the parameter R during first loading and a_1 and a_2 are experimentally determined parameters to be defined together with R_0. The definition of ξ remains valid in case that reloading occurs after partial unloading

Some elucidations are needed in connection with the set of rules for unloading and reloading, which are implied by the use of Eqs. (2.1) through (2.5), allowing for a generalized load history. If the analytical model had a memory extending over all previous branches of stress-strain history, it would allow for the resumption of the previous reloading branch, as soon as the new loading curve reached it. This would

require that the model stores all necessary information to retrace all previous incomplete reloading curve. This is clearly impractical from a computational standpoint. Memory of the past stress-strain history is, therefore, limited to a predefined number of values, which in the present model are:

1. The monotonic envelope.

2. The ascending upper branch originating at the reversal point with smallest ε value.

3. The descending lower branch curve originating at the reversal point with largest ε value.

4. The current curve originating at the most recent reversal point.

Due to the above restrictions reloading after partial loading does not rejoin the original reloading curve after the point from which unloading started, but, instead, continues on the new reloading curve until reaching the monotonic envelope. However, the discrepancy between the analytical model and the actual behavior is typically very small, as discussed in details by Filippou et al. (1983).

The above implementation of the model corresponds to its simplest form, as proposed in Menegotto and Pinto (1973): Elastic and yield asymptotes are assumed to be straight lines, the position of the limiting asymptotes corresponding to the yield surface is assumed to be fixed at all times and the slope E_0 remains constant (Figure 2-1).

In spite of the simplicity in formulation, the model is capable of reproducing experimental results well. Its major drawback stems from its failure to allow for

isotropic hardening. To account for this effect Filippou et al. (1983) proposed a stress shift in the linear yield asymptote as follows:

$$\sigma_{st} = a_3 \left(\frac{\varepsilon_{\max}}{\varepsilon_y} - a_4 \right) \sigma_y \tag{2.6}$$

where $\varepsilon_{\max}$ is the absolute strain at the maximum strain reversal point if the stress shift is applied to the negative yield asymptote, or at the minimum strain reversal point if the stress shift σ_{st} is applied to the positive yield asymptote. ε_y and σ_y are the strain and stress at yield, respectively, and a_3 and a_4 are experimental determined parameters. Although the model implemented in this study has the option of including isotropic hardening, that option is not exercised in the analytical studies. Therefore, the parameter values used in this study are: $R_0 = 20$, $a_1 = 18.5$, $a_2 = 0.15$, $a_3 = 0.0$, $a_4 = 0.0$. With the exception of the last two parameters, the values used are those in the original model of Menegotto and Pinto (1973). The study by Filippou et al. (1983) also showed that the steel model with and without isotropic hardening yielded yield almost identical results.

2.3 Concrete Constitutive Law

The concrete material model used in this study is based on the modified Kent-and-Park model. The original model proposed by Kent and Park (1971) was modified by Scott et al. (1982) to account for the confinement effects and was later modified by Yassin (1994) to include the tensile stiffening and the tensile damage. The main features represented by this modified version of Kent-and-Park model are as follows:

- The influence of concrete confinement on the monotonic envelope curve in compression.
- The effect of tensile damage under unloading and reloading.
- The tensile stiffening
- The hysteretic response under cyclic loadings.

In this study the effects of the tensile stiffening and tensile damage are neglected in the analysis of the reinforced concrete structures. As a result, only the concrete material model without tensile stiffening is presented. However, the tensile stiffening is of great importance in predicting the monotonic response of reinforced concrete slab and beam strengthened with FRP or steel thin plates. As a result, only the behavior of concrete material under monotonic tensile loading is presented.

2.3.1 Concrete Stress-Strain Relation in Compression

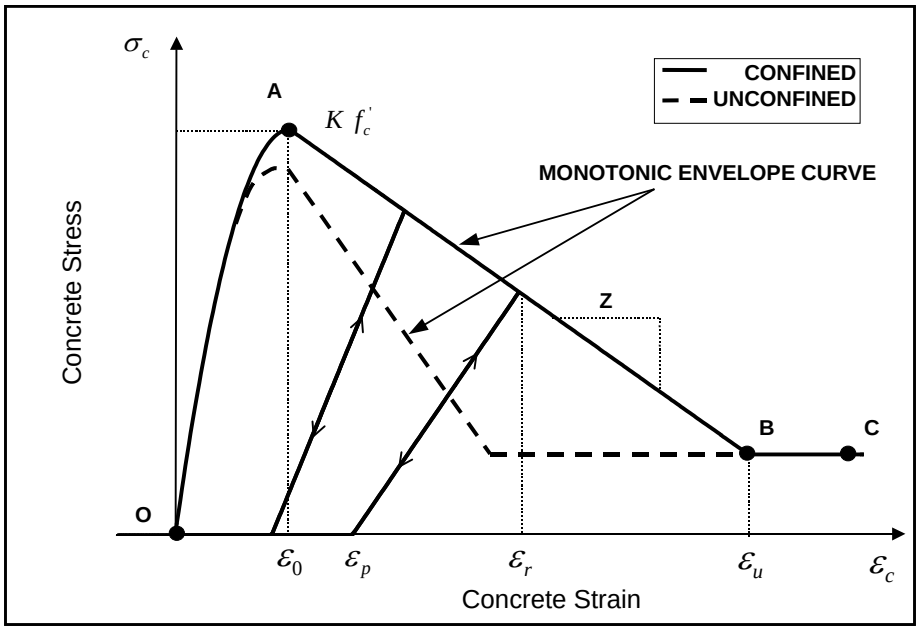

Figure 2-3 Concrete Material Model under Cyclic Loading in Compression

The monotonic envelope of the concrete model in compression is based on the Kent and Park (1971) model, which was later modified by Scott et al. (1982) to account for the confinement effect. Even though more precise and sophisticated concrete models based on the plasticity theory (for example Willam and Warnke, 1974) have been more recently proposed by the research community, the so-called *Kent and Park* model represents a good compromise between simplicity and accuracy. A number of experimental studies on the behavior of plain concrete under repetitions of compressive stress (Sinha et al., 1964 and Karsan et al., 1969) indicate that the envelope curve for cyclic loading is very close to the envelope curve for the monotonic loading. Consequently, in this present study, the cyclic damage of the compression envelope is not taken into account

In the modified Kent and Park concrete model of Figure 2-3 the three following regions are used to describe the monotonic concrete stress-strain relation:

$$\textbf{Region OA}: \quad \varepsilon_c \le \varepsilon_0 \qquad \sigma_c = K\, f_c^{'}\left[2\left(\frac{\varepsilon_c}{\varepsilon_0}\right)-\left(\frac{\varepsilon_c}{\varepsilon_0}\right)^2\right] \tag{2.7}$$

$$\textbf{Region AB}: \quad \varepsilon_c \le \varepsilon_0 \le \varepsilon_u \quad \sigma_c = K\, f_c^{'}\left[1-Z\left(\varepsilon_c-\varepsilon_0\right)\right] \tag{2.8}$$

$$\textbf{Region BC}: \quad \varepsilon_u \le \varepsilon_c \qquad \sigma_c = 0.2K\, f_c^{'} \tag{2.9}$$

The corresponding tangent stiffness E_t are given by the following expressions:

$$\textbf{Region OA}: \quad \varepsilon_c \le \varepsilon_0 \qquad E_t = \frac{K\, f_c^{'}}{\varepsilon_0}\left[1-\left(\frac{\varepsilon_c}{\varepsilon_0}\right)\right] \tag{2.10}$$

$$\textbf{Region AB}: \quad \varepsilon_0 \le \varepsilon_c \le \varepsilon_u \quad E_t = -ZK\, f_c^{'} \tag{2.11}$$

$$\textbf{Region BC}: \quad \varepsilon_u \le \varepsilon_c \qquad E_t = 0 \tag{2.12}$$

where

$$\varepsilon_0 = 0.002K \tag{2.13}$$

$$K = 1 + \frac{\rho_s f_{yh}}{f_c^{'}} \tag{2.14}$$

$$Z = \frac{0.5}{\frac{3 + 0.29 f_c^{'}}{145 f_c^{'} - 1000} + 0.75\rho_s \sqrt{\frac{h^{'}}{s_h}} - .002K} \tag{2.15}$$

In the above equations, ε_0 is the concrete strain at maximum stress, K is a factor which accounts for the strength increase due to confinement, Z is the slope of the softening branch, $f_c^{'}$ is the concrete compressive cylinder strength in MPa, f_{yh} is the yield strength of stirrups in MPa, ρ_s is the ratio of the volume of hoop reinforcement to the volume of concrete core measured to outside of stirrups, $h^{'}$ is the width of concrete core measured to outside of stirrups, and s_h is the center to center spacing of stirrups or hoop sets. The empirical expressions of K and Z in Eq. (2.14) and (2.15), respectively, are given by Scott et al. (1982).

If concrete is confined by stirrup-ties, Scott et al. (1982) suggest that ε_u be determined conservatively from the following expression:

$$\varepsilon_u = 0.004 + 0.9\rho_s \left(f_{yh} / 300 \right) \tag{2.16}$$

Crushing of concrete is accounted for by reducing the strength in concrete to $0.2 f_c^{'}$ once the compressive strains exceeds the values of ε_u. Figure 2-3 also shows the hysteretic behavior of the plain concrete stress-strain relation. The following rules are considered to define this behavior:

1. Unloading from a point on the envelope curve occurs along a straight line between the point ε_r at which unloading starts and the point ε_p on the strain axis given by the following equations:

$$\frac{\varepsilon_r}{\varepsilon_0} < 2: \qquad \frac{\varepsilon_p}{\varepsilon_0} = 0.145\left(\frac{\varepsilon_r}{\varepsilon_0}\right)^2 + 0.13\left(\frac{\varepsilon_r}{\varepsilon_0}\right) \tag{2.17}$$

$$\frac{\varepsilon_r}{\varepsilon_0} \geq 2: \qquad \frac{\varepsilon_p}{\varepsilon_0} = 0.707\left(\frac{\varepsilon_r}{\varepsilon_0} - 2\right) + 0.834 \tag{2.18}$$

where ε_0 is the concrete strain at maximum stress in compression. Eq. (2.17), which relates the normalized strain on the envelope with the strains at the completion of unloading through a quadratic formula, was proposed by Karsan and Jirsa (1969). This equation shows unrealistic behavior under high compressive strain conditions. Therefore, Eq. (2.18) is introduced to the model so that the unloading modulus of elasticity remains positive under high compressive strains.

2. As shown in Figure 2-3, the tensile resistance is ignored. Consequently, for concrete strains smaller than the concrete strain at complete unloading (crack opening). The concrete stress is equal to zero.

3. On reloading in compression, the concrete behavior is in tension as long as the strain is smaller than the strain at complete unloading (crack opening). Once the concrete strain exceeds that value, reloading follows the previous unloading path. In reality, unloading and reloading follow nonlinear paths, which together form a hysteretic loop. However, this phenomenon is neglected here for the sake of simplicity.

2.3.2 Concrete Stress-Strain Relation in Tension

The ability of the concrete between the cracks to resist the tensile stress and contribute to the member flexural stiffness is obtained by the concrete tension stiffening. Due to the discrete feature of the concrete cracks, concrete between cracks is still bonded to the reinforcing bars, hence contributing to the member stiffness. However, when the applied load is increased the crack intervals are closer and closer, hence limiting the contributions of concrete tension to the member stiffness. Beyond the post cracking state, the tensile stress decreases gradually when the applied load is increased. Past researches have considered the effect of tension stiffening by modifying the concrete tensile stress-strain relation such that, after the tensile strength (crack initiation), the tensile stress reduces gradually to zero as the tensile strain is increased. The descending path of the tensile stress-strain relation can be approximated as linear, multi-linear, or exponential decay functions. In this study the modified Kent and Park model developed by Yassin (1994) is adopted. In this modified model the linear descending path is used. The ultimate tensile strain ε_{tu} at which the tensile stress can no longer be resisted plays an important role in describing the tensile softening behavior. For this purpose, the fracture energy of concrete is considered so that the equivalent amount of energy can be dissipated by the concrete rupture between the nonlinear and linear branch model. The fracture energy G_f is defined as the amount of energy required to create one unit of area of a continuous crack and calculated by the area under the tensile stress-cracking opening softening diagram. Therefore, the fracture energy G_f can be expressed as

$$G_f = hg_f = h\int_0^{\varepsilon_{tu}} \sigma d\varepsilon_t \tag{2.19}$$

where g_f is the area under the tensile stress-strain diagram as shown in Figure 4-4. $\varepsilon_t^{'} = \frac{f_t^{'}}{E_c}$ and ε_{tu} is the ultimate strain beyond which stress can no longer transferred. The discrete crack model can be related to the smeared crack model by the relationship

$$w = h\varepsilon_1 \tag{2.20}$$

where *w* is crack opening displacement due to crack strain over the crack band width *h* in the direction of maximum tensile stress. Based on studies by Bazant and Oh (1983), the crack bandwidth is dependent on the aggregate size following the simplified equation.

$$h = 3d_a \tag{2.21}$$

where d_a is the maximum aggregate size. Based on the linear descending model, the tensile softening modulus E_{ts} can be defined as:

$$E_{ts} = -\frac{E_c}{\left(\frac{g_f}{r_0} - 1\right)} \tag{2.22}$$

where E_c is the initial stiffness of the concrete. r_0 is the elastic strain energy density, defined as:

$$r_0 = \frac{1}{2} f_t^{'} \varepsilon_t^{'} \tag{2.23}$$

The monotonic response of concrete under tensile strain is shown in Figure 4-5. The monotonic tensile stress-strain relation and tangential stiffness are defined by the following equations:

$$\begin{array}{lll} \varepsilon < \varepsilon_t^{'} & \sigma = E_c \varepsilon & E_t = E_c \\ \varepsilon_t^{'} \le \varepsilon \le \varepsilon_{tu} & \sigma = f_t^{'} + E_{ts}(\varepsilon - \varepsilon_t^{'}) & E_t = -E_{ts} \\ \varepsilon > \varepsilon_{tu} & \sigma = 0 & E_t = 0 \end{array} \qquad (2.24)$$

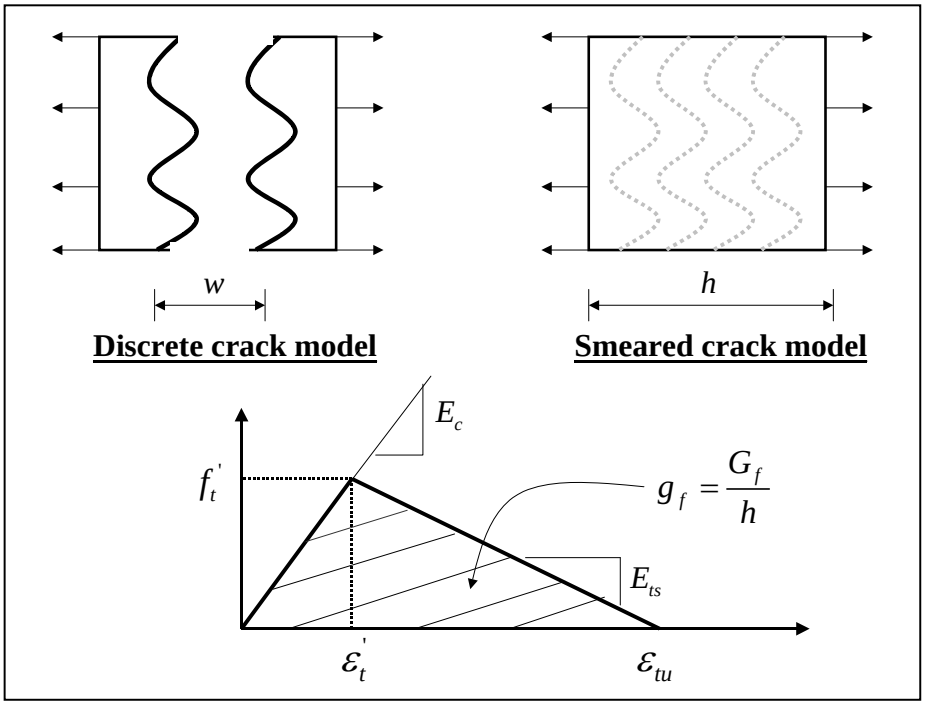

Figure 2-4 Crack Model and Definition of Fracture Energy of Concrete

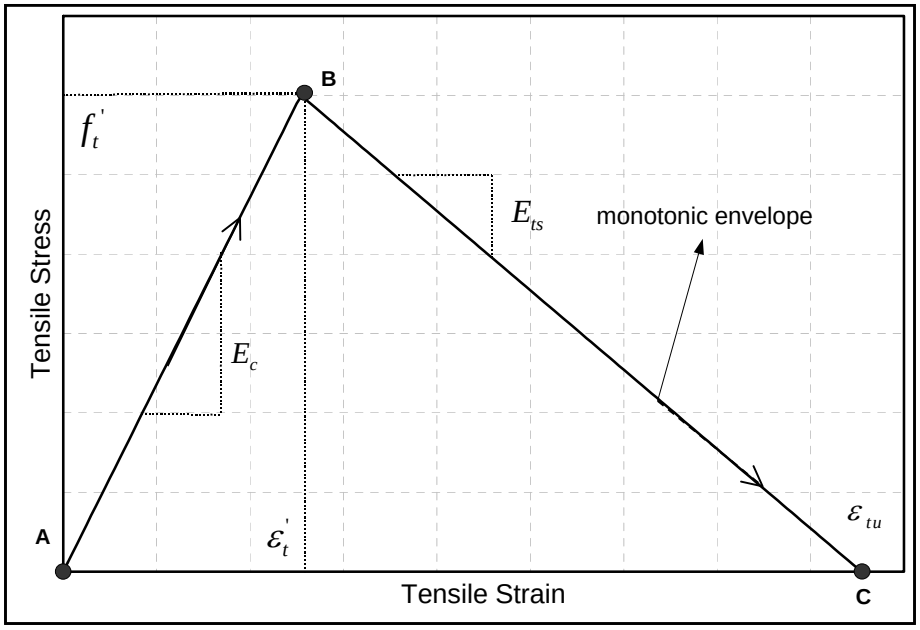

Figure 2-5 Monotonic Response of Concrete under Tensile Strain

Clearly, the sizes of member and maximum aggregate have a significant effect on the tension stiffening behavior of the member. However, the rigorous calibration of these parameters is beyond the scope of this study.

In this study the tensile behavior of model developed by Yassin (1994) takes into account the effects of tension stiffening. Typically, the maximum tensile strength of the concrete (modulus of rupture) is approximately:

$$f_t^{'} = 0.6228\sqrt{f_c^{'}} \tag{2.25}$$

where $f_c^{'}$ and $f_t^{'}$ are described in MPa.

CHAPTER 3
TOTAL LAGRANGIAN FORMULATION OF PLANAR BAR ELEMENT USING VECTORIAL KINEMATICAL DESCRIPTION

3.1 Introduction

In recent years, the Performance-Based Design and Assessment Methodology (ICC 2012) has been adopted in the structural engineering community. This forces structural engineers to rely on more advanced structural modeling techniques in order to understand and trace the structural responses to loading conditions ranging from service to collapse states. Therefore, a structural model capable of capturing the system nonlinearities is deemed essential in the Performance-Based Design and Assessment Methodology.

Large truss structures have been frequently used as structural systems for both civil and aerospace engineering structures. Bridges, offshore platforms, and large-span arch roofs are examples of truss structures for civil engineering structures. Solar power satellite platforms and supporting structures for antennae are examples of truss structures for aerospace engineering structures. Designers of such systems usually try to optimize the structural weights, thus rendering the systems highly flexible and prone to instability when subjected to loadings. Furthermore, the structural materials used nowadays could possess high strengths but light weights due to the drastic advance in material technology. The truss structures made of such materials become highly flexible and experience large displacements when subjected to loadings. Consequently, a geometrically nonlinear bar element is inevitably needed to model such truss systems.

Nonlinear behavior of truss structures has been investigated by several researchers since the late sixties. Berke and Mallet (1969) performed nonlinear analyses of trusses using the energy search approach (Mallet and Schmit 1967) to investigate the combined effects of geometric nonlinearity and member elastic buckling. Wolf (1971) incorporated member inelastic post-buckling with linear structural theory to predict the post-buckling strength of trusses using the initial stress method (Zienkiewicz, et al. 1969). The event-by-event method in which buckled or yielding members were removed from the model was used by Schmidt et al. (1976) to perform nonlinear analyses of trusses. Papadrakakis (1983) refined the model by Schmidt et al. (1976) by providing the post-buckling and post-yielding branches for buckled and yielding members, respectively. Kondoh and Atluri (1985) derived the bar element stiffness matrices for both pre-buckling and post-buckling states using the Euler elastica theory. The displacement-based Lagrangian bar model was developed by de Freitas and Ribeiro (1992). In this model, the bar-section constitutive relation was used to account for local elasto-plastic buckling effects. The geometrically nonlinear bar model with a bilinear sectional response was developed by Greco et al. (2006) using the nonlinear positional formulation. Recently, the updated Lagrangian bar model with a linear elastic section behavior was proposed by Torkamani and Shieh (2011).

In this chapter, a geometrically nonlinear bar element is developed within the total Lagrangian framework. Thus, the undeformed element state is used as the reference configuration. All statical and kinematical quantities of the current element state are measured with respect to this reference configuration. The vectorial form is conveniently used to describe the element kinematics and element strain as well as to eliminate the need of shape functions as required in a standard finite element formulation. The incremental equilibrium equations are obtained by linearization of

the nonlinear virtual displacement function. The generalized displacement control method proposed by Yang and Shieh (1990) is adopted as a nonlinear solution algorithm. Only linear elastic material law is of interest in this work. However, the model can naturally be extended to account for other more complex material behaviors (e.g. elastic-plastic, viscoelastic, etc.). Furthermore, it is worthwhile to emphasize that the total Lagrangian bar element developed in this chapter naturally complies with the material constitutive relation described in the total form (e.g. hyperelastic material, etc.). This kind of material law is widely used in modeling the behavior of nonlinear elastic materials (e.g. natural rubber, human muscle, etc.). The in-house structural analysis software is developed in which the proposed nonlinear bar element, as well as the adopted solution algorithm, are implemented in the MATLAB programming language (Chapman 2005). The validity and efficiency of the developed software are confirmed by analyzing five truss structures exhibiting several types of critical points and comparing these results with those available in the literature.

3.2 Total Lagrangian Formulation

Depending on the choice of reference configuration and method of kinematical description, there are two model formulations for geometrically nonlinear analyses of truss structures, namely: (*a*) Total Lagrangian (TL) formulation; and (*b*) Updated Lagrangian (UL) formulation. The schematic motion of a truss element shown in Figure 3-1 is used to convey the big picture of total Lagrangian and updated Lagrangian formulations. In the total Lagrangian formulation, the reference system is the original undeformed element configuration C_0. All statical and kinematical variables of the current element configuration C_t refer to this reference configuration.

In the updated Lagrangian formulation, the last computed equilibrium configuration C_{t-1} of the displaced element is used as the reference system. All statical and kinematical variables of the current element configuration C_t refer to this reference configuration. Due to its ease of model implementation and prevalent uses in research community, the geometrically nonlinear bar element developed in the present work is based on the total Lagrangian formulation.

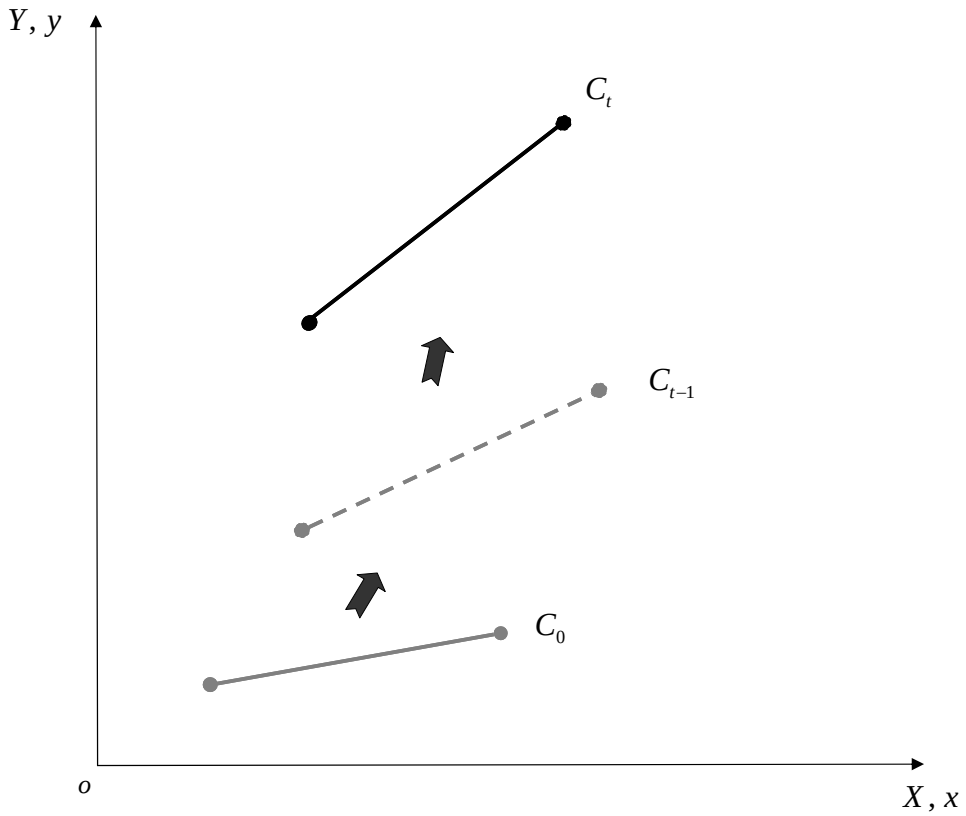

Figure 3-1: Schematic Motion of a Bar Element: Total Lagrangian vs. Updated Lagrangian Formulations.

3.2.1 Element Kinematics and Green-Lagrange Strain

The kinematics of a two-node bar element is shown in Figure 3-2. In the reference configuration C_0, the element has cross sectional area A_0 and length L_0. Under loading exertion, the element displaces from the reference configuration C_0 to the current configuration C_t and the element cross sectional area and element length become A_t and L_t, respectively. The first node moves from i_0 to i_t via horizontal and vertical displacements U_i and V_i, respectively while the second node moves from j_0 to j_t via horizontal and vertical displacements U_j and V_j, respectively. The vectorial approach is used to describe the element kinematics and element strain as shown in Figure 3-3. The positional vectors of nodes i and j in the configuration C_0 are:

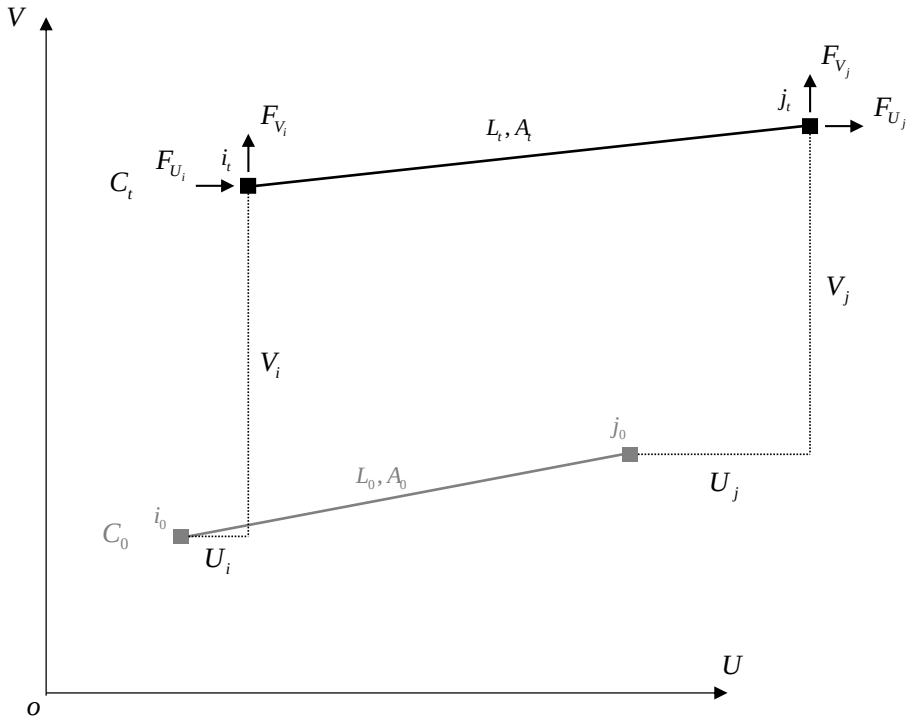

Figure 3-2. Element Kinematics.

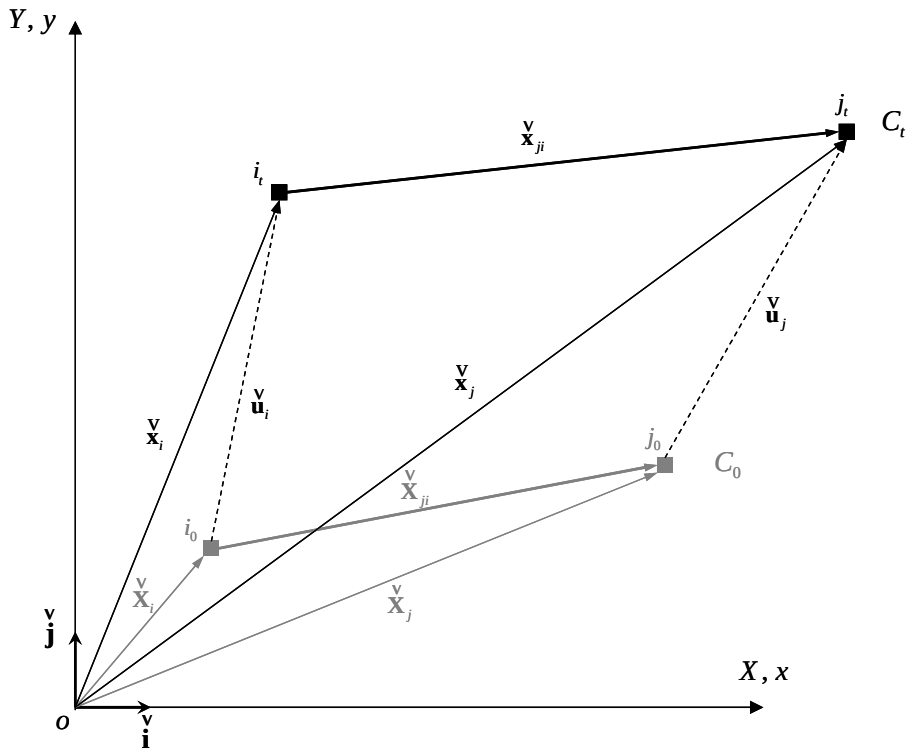

Figure 3-3. Vectorial Description of Element Kinematics and Strain.

$$\begin{aligned}\vec{\mathbf{X}}_i &= X_i\vec{\mathbf{i}} + Y_i\vec{\mathbf{j}} = \lfloor X_i \quad Y_i \rfloor^T \\ \vec{\mathbf{X}}_j &= X_j\vec{\mathbf{i}} + Y_j\vec{\mathbf{j}} = \lfloor X_j \quad Y_j \rfloor^T\end{aligned} \tag{3.1}$$

The direction and length of the element with respect to the configuration C_0 are contained in the element vector $\vec{\mathbf{X}}_{ji}$, defined as:

$$\vec{\mathbf{X}}_{ji} = \vec{\mathbf{X}}_j - \vec{\mathbf{X}}_i = \lfloor X_j - X_i \quad Y_j - Y_i \rfloor^T \tag{3.2}$$

Similarly, the positional vectors of nodes i and j in the configuration C_t are:

$$\begin{aligned}\vec{\mathbf{x}}_i &= x_i\vec{\mathbf{i}} + y_i\vec{\mathbf{j}} = \lfloor x_i \quad y_i \rfloor^T \\ \vec{\mathbf{x}}_j &= x_j\vec{\mathbf{i}} + y_j\vec{\mathbf{j}} = \lfloor x_j \quad y_j \rfloor^T\end{aligned} \tag{3.3}$$

The direction and length of the element with respect to the configuration C_t are contained in the element vector $\vec{\mathbf{x}}_{ji}$, defined as:

$$\vec{\mathbf{x}}_{ji} = \vec{\mathbf{x}}_j - \vec{\mathbf{x}}_i = \lfloor x_j - x_i \quad y_j - y_i \rfloor^T \tag{3.4}$$

The displacement vectors of nodes i and j moving from the configurations C_0 to C_t are:

$$\vec{\mathbf{u}}_i = U_i\vec{\mathbf{i}} + V_i\vec{\mathbf{j}} = \lfloor U_i \quad V_i \rfloor^T$$
$$\vec{\mathbf{u}}_j = U_j\vec{\mathbf{i}} + V_j\vec{\mathbf{j}} = \lfloor U_j \quad V_j \rfloor^T \tag{3.5}$$

From the geometrical analysis of vectors in Figure 3-3, the current element vector $\vec{\mathbf{x}}_{ji}$ can alternatively be written as:

$$\vec{\mathbf{x}}_{ji} = \vec{\mathbf{X}}_{ji} + \vec{\mathbf{u}}_{ji} \tag{3.6}$$

where $\vec{\mathbf{u}}_{ji} = \vec{\mathbf{u}}_j - \vec{\mathbf{u}}_i$ is the difference between displacement vectors of nodes i and j.

In the matrix relation, the relative vectors $\vec{\mathbf{X}}_{ji}$, $\vec{\mathbf{x}}_{ji}$, and $\vec{\mathbf{u}}_{ji}$ can be written in terms of their relevant nodal quantities as:

$$\vec{\mathbf{X}}_{ji} = \mathbf{hX};\ \vec{\mathbf{x}}_{ji} = \mathbf{hx};\ \text{and}\ \vec{\mathbf{u}}_{ji} = \mathbf{hU} \tag{3.7}$$

where $\mathbf{h} = \begin{bmatrix} -\mathbf{I} & \mathbf{I} \end{bmatrix}$ is the rectangular mapping matrix; $\mathbf{I}$ is the identity matrix; $\mathbf{X} = \lfloor X_i \quad Y_i \quad X_j \quad Y_j \rfloor^T$ is the reference nodal coordinate vector; $\mathbf{x} = \lfloor x_i \quad y_i \quad x_j \quad y_j \rfloor^T$ is the current nodal coordinate vector; and $\mathbf{U} = \lfloor U_i \quad V_i \quad U_j \quad V_j \rfloor^T$ is the nodal displacement vector.

In the total Lagrangian formulation, a consistent finite strain measure is the Green-Lagrange strains (Belytschko, et al. 2000). In a bar problem, only the axial strain component is present in the element formulation and is defined as:

$$\varepsilon_{XX}^{GL} = \frac{L_t^{\,2} - L_0^{\,2}}{2L_0^{\,2}} \tag{3.8}$$

The squares of reference and current element lengths can be expressed as scalar products of their relevant element vectors as:

$$L_0^{\,2} = \vec{\mathbf{X}}_{ji}^{\,T}\vec{\mathbf{X}}_{ji} \ \text{and}\ L_t^{\,2} = \vec{\mathbf{x}}_{ji}^{\,T}\vec{\mathbf{x}}_{ji} \tag{3.9}$$

Substituting Eqs. (3.6), (3.7), and (3.9) into (3.8), the axial strain component ε_{XX}^{GL} can

be expressed in terms of the reference nodal coordinate vector $\mathbf{X}$ and nodal displacement vector $\mathbf{U}$ as:

$$\varepsilon_{XX}^{GL} = \frac{1}{L_0^{\,2}}\mathbf{X}^T\mathbf{H}\mathbf{U} + \frac{1}{2L_0^{\,2}}\mathbf{U}^T\mathbf{H}\mathbf{U} \tag{3.10}$$

where $\mathbf{H} = \mathbf{h}^T\mathbf{h}$ is the square mapping matrix. It is noted that on the right-hand side of Eq. (3.10), the first term is a linear function of $\mathbf{U}$ while the second term is a quadratic function of $\mathbf{U}$. As a result, Eq. (3.10) represents the nonlinear compatibility relation between ε_{XX}^{GL} and $\mathbf{U}$.

3.2.2 Material Constitutive Law

In total Lagrangian formulation, the stress measure conjugate to the Green-Lagrange strain tensor is the 2nd Piola-Kirchhoff stress tensor (Holzapfel 2000). In a bar problem, only the axial stress component s_{XX}^{PK2} is present in the element formulation. Throughout this work, only a linear relation between axial stress and strain is of interest. Thus, the axial stress and strain are related through the following linear constitutive equation:

$$s_{XX}^{PK2} = E\varepsilon_{XX}^{GL} \tag{3.11}$$

where E is the elastic modulus. Based on this stress measure, the axial force is defined as:

$$N^{PK2} = A_0 s_{XX}^{PK2} \tag{3.12}$$

With Eqs. (3.10) and (3.11), N^{PK2} can be expressed in terms of $\mathbf{U}$ as:

$$N^{PK2} = \frac{A_0 E}{L_0^{\,2}}\left(\mathbf{X}^T + \frac{1}{2}\mathbf{U}^T\right)\mathbf{H}\mathbf{U} \tag{3.13}$$

3.2.3 Element Equilibrium: The Virtual Displacement Principle

As an alternative way to express the element equilibrium equations, the virtual displacement function is written in the general form as:

$$\delta W = \delta W_{int} + \delta W_{ext} \tag{3.14}$$

where δW is the system total virtual work; δW_{int} is the system internal virtual work; and δW_{ext} is the system external virtual work.

In the case of a bar element, δW_{int} and δW_{ext} can be expressed as:

$$\delta W_{int}\left[\mathbf{U}, \delta\mathbf{U}\right] = \int_{L_0} \delta\varepsilon_{XX}^{GL}\left[\mathbf{U}, \delta\mathbf{U}\right] N^{PK2}\, dX = L_0 \delta\varepsilon_{XX}^{GL}\left[\mathbf{U}, \delta\mathbf{U}\right] N^{PK2} \tag{3.15}$$

$$\delta W_{ext}\left[\delta\mathbf{U}\right] = -\delta\mathbf{U}^T\mathbf{F} \tag{3.16}$$

where the vector $\mathbf{F} = \begin{bmatrix} F_{U_i} & F_{V_i} & F_{U_j} & F_{V_j} \end{bmatrix}^T$ contains element nodal forces as shown in Figure 3-2; the vector $\delta\mathbf{U} = \begin{bmatrix} \delta U_i & \delta V_i & \delta U_j & \delta V_j \end{bmatrix}^T$ collects virtual nodal displacements; and $\delta\varepsilon_{XX}^{GL}$ is the virtual Green-Lagrange axial strain. Substituting Eqs. (3.15) and (3.16) into (3.14), the virtual displacement function becomes:

$$\delta W\left[\mathbf{U}, \delta\mathbf{U}\right] = L_0 \delta\varepsilon_{XX}^{GL}\left[\mathbf{U}, \delta\mathbf{U}\right] N^{PK2} - \delta\mathbf{U}^T\mathbf{F} \tag{3.17}$$

The directional derivative operator (Gâteaux operator) is used to obtain the virtual strain from the virtual nodal displacements as:

$$\delta\varepsilon_{XX}^{GL}\left[\mathbf{U}, \delta\mathbf{U}\right] = D\varepsilon_{XX}^{GL}\left[\mathbf{U}\right].\delta\mathbf{U} = \frac{d}{d\alpha}\left[\varepsilon_{XX}^{GL}\left(\mathbf{U} + \alpha\delta\mathbf{U}\right)\right]_{\alpha=0} = \frac{1}{L_0^{\,2}}\left(\mathbf{X}^T + \mathbf{U}^T\right)\mathbf{H}\delta\mathbf{U} \tag{3.18}$$

It is noted that $D\varepsilon_{XX}^{GL}\left[\mathbf{U}\right].\delta\mathbf{U}$ represents the directional derivative of the function $\varepsilon_{XX}^{GL}\left[\mathbf{U}\right]$ in the direction of $\delta\mathbf{U}$. Substitution of Eqs. (3.18) into (3.17) yields:

$$\delta W\left[\mathbf{U}, \delta\mathbf{U}\right] = \delta\mathbf{U}^T\left(\frac{N^{PK2}}{L_0}\mathbf{H}^T\left(\mathbf{X} + \mathbf{U}\right) - \mathbf{F}\right) \tag{3.19}$$

From the fundamental lemma of variational calculus (Washizu 1982), the equilibrated element configuration is obtained if $\delta W\left[\mathbf{U},\delta\mathbf{U}\right]$ vanishes for all choices of $\delta\mathbf{U}$. Thus, from the arbitrariness of $\delta\mathbf{U}$, the nonlinear relation between the internal axial force N^{PK2} and external applied nodal forces F is:

$$\frac{N^{PK2}}{L_0}\mathbf{H}^T\left(\mathbf{X}+\mathbf{U}\right)=\mathbf{F} \tag{3.20}$$

In summary, Eqs. (3.10), (3.13), and (3.20) represent the compatibility, constitutive, and equilibrium equations of the problem, respectively, and form the core of the displacement-based total Lagrangian bar element developed in this study. These three equations are conveniently represented in the so-called "Tonti's Diagram" (Tonti 1977) shown in Figure 3-4.

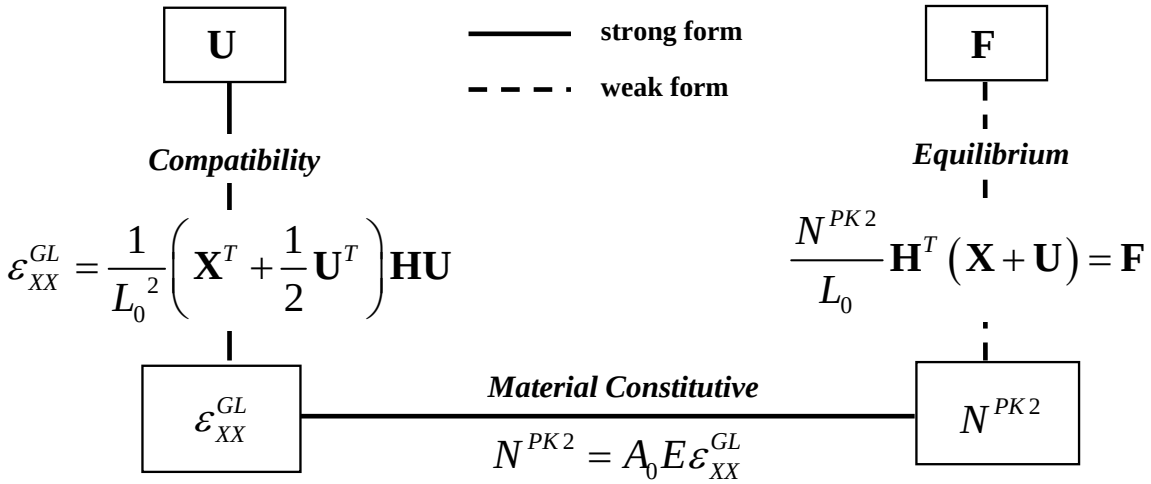

Figure 3-4. Tonti's Diagram for Displacement-Based Total Lagrangian Bar Element (Tonti 1977).

3.3 Incremental Equilibrium Equations

Due to the nonlinear nature of compatibility and equilibrium equations, an incremental-iterative structural analysis is used to trace an equilibrium path of a nonlinear truss system. In this type of structural analysis, the tangent element stiffness matrix and the internal element resisting forces are needed and can be derived from linearization of the virtual displacement function of Eq. (3.19). Let $\mathbf{U}_i$ represent the current bar configuration. It is noted that this bar configuration is not necessary in equilibrium. Consequently, Eq. (3.20) may not be satisfied. With respect to $\mathbf{U}_i$, Eq. (3.19) can be linearized as:

$$L\left[\delta W\right] = \left[\delta W\right]_{\mathbf{U}_i} + \Delta\left[\delta W\right]_{\mathbf{U}_i} \tag{3.21}$$

where

$$\left[\delta W\right]_{\mathbf{U}_i} = \delta\mathbf{U}^T \frac{N_i^{PK2}}{L_0}\mathbf{H}^T\left(\mathbf{X}+\mathbf{U}_i\right) - \delta\mathbf{U}^T\mathbf{F} \tag{22}$$

The incremental virtual displacement function $\Delta\left[\delta W\right]_{\mathbf{U}_i}$ can be determined using the directional derivative operator as:

$$\Delta\left[\delta W\right]_{\mathbf{U}_i} = D\left[\delta W\right]_{\mathbf{U}_i}.\delta\mathbf{U} = \frac{d}{d\alpha}\left[\delta W\left(\mathbf{U}+\alpha\Delta\mathbf{U},\delta\mathbf{U}\right)\right]_{\alpha=0}^{\mathbf{U}=\mathbf{U}_i} \tag{3.23}$$

It is noted that $D\left[\delta W\right]_{\mathbf{U}_i}.\delta\mathbf{U}$ implies the directional derivative of the function $\left[\delta W\right]_{\mathbf{U}_i}$ in the direction of $\delta\mathbf{U}$. Carrying out the above expression and substituting it into Eq. (3.21) yield:

$$L\left[\delta W\right] = \delta\mathbf{U}^T\left[\left(\mathbf{k}_0+\mathbf{k}_1+\mathbf{k}_1^{'}+\mathbf{k}_2+\mathbf{k}_G\right)\Delta\mathbf{U}_i - \mathbf{f}_{int} + \mathbf{F}\right] \tag{3.24}$$

where the element matrices are

$$\mathbf{k}_0 = \frac{EA_0}{L_0^3}\mathbf{H}\mathbf{X}\mathbf{X}^T\mathbf{H}$$
$$\mathbf{k}_1 = \frac{EA_0}{L_0^3}\mathbf{H}\mathbf{X}\mathbf{U}_i^T\mathbf{H}$$
$$\mathbf{k}_1^{'} = \frac{EA_0}{L_0^3}\mathbf{H}\mathbf{U}_i\mathbf{X}^T\mathbf{H} \tag{3.25}$$
$$\mathbf{k}_2 = \frac{EA_0}{L_0^3}\mathbf{H}\mathbf{U}_i\mathbf{U}_i^T\mathbf{H}$$
$$\mathbf{k}_G = \frac{N_i^{PK2}}{L_0}\mathbf{H}$$

and the element vector is:

$$\mathbf{f}_{int} = \frac{N_i^{PK2}}{L_0}\mathbf{H}^T\left(\mathbf{X} + \mathbf{U}_i\right) \tag{3.26}$$

It is noted that all element matrices and element vector are explicitly written in Appendix.

In the incremental-iterative solution technique, $L\left[\delta W\right]$ is forced to be zero regardless of $\delta\mathbf{U}$. Therefore, the incremental equilibrium equations are obtained as:

$$\mathbf{k}\Delta\mathbf{U}_i = \mathbf{r}_i \tag{3.27}$$

where

$$\mathbf{k} = \mathbf{k}_0 + \mathbf{k}_1 + \mathbf{k}_1^{'} + \mathbf{k}_2 + \mathbf{k}_G \text{ and } \mathbf{r}_i = \mathbf{F} - \mathbf{f}_{int} \tag{3.28}$$

The tangent element stiffness matrix consists of five matrices of Eq. (3.25). $\mathbf{k}_0$ is constant and corresponds to the stiffness matrix of a linear bar element; $\mathbf{k}_1$ and $\mathbf{k}_1^{'}$ are linear in current nodal displacements; $\mathbf{k}_2$ are quadratic in current nodal displacements; and $\mathbf{k}_G$ is linear in the current internal axial force. The vector $\mathbf{r}_i$ represents the unbalanced forces between external and internal nodal forces. This incremental equilibrium equations are used to estimate incremental nodal displacements $\Delta\mathbf{U}_i$. These incremental nodal displacements are used to improve the

current nodal displacements $\mathbf{U}_i$ in obtaining the equilibrated element configuration corresponding to the applied nodal forces **F**. More details on the solution technique are to be discussed in the next section.

3.4 INCREMENTAL-ITERATIVE SOLUTION PROCEDURE

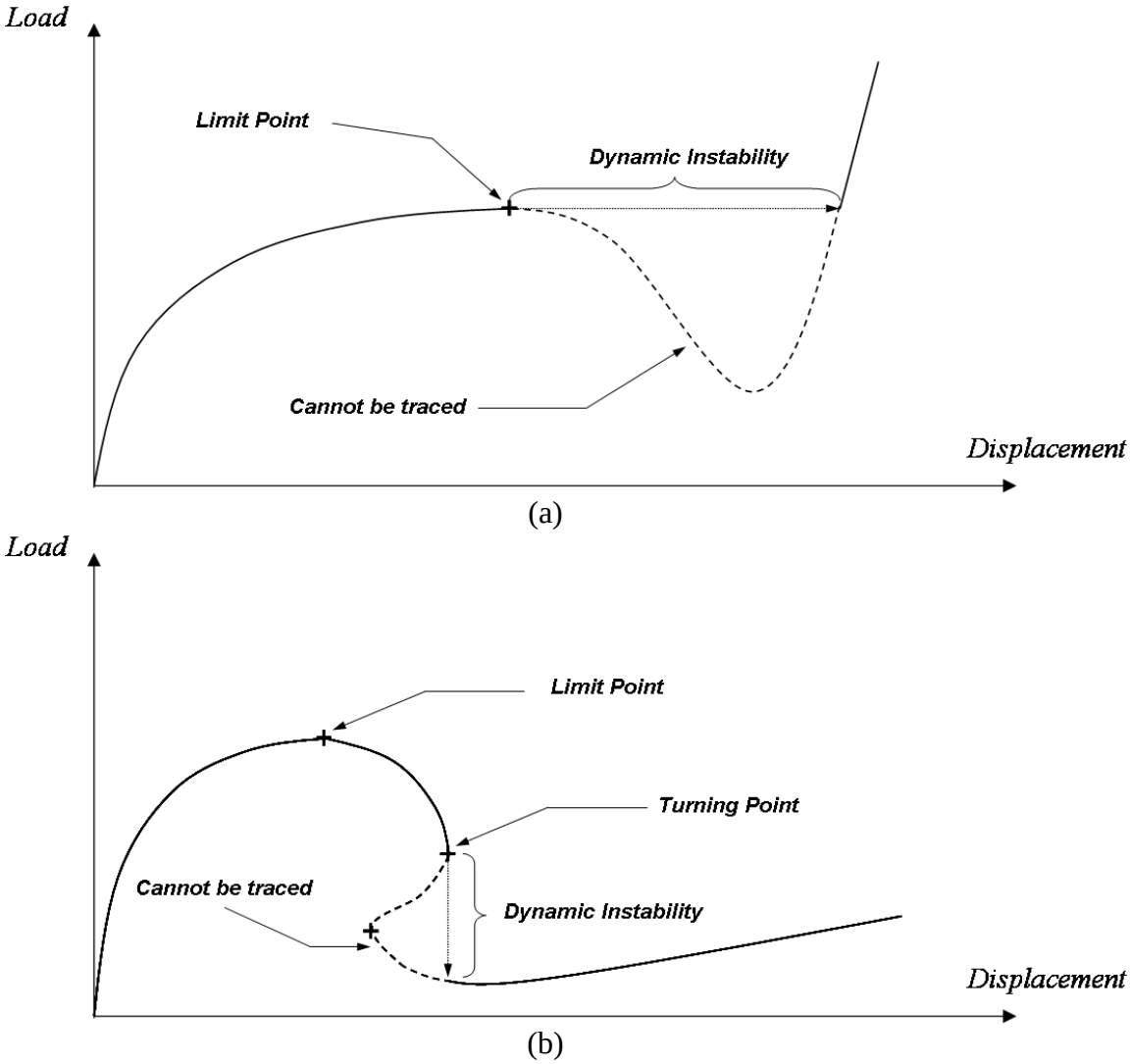

Figure 3-5. Breakdowns of Solution Procedures: (a) Load-Control Method; (b) Displacement-Control Method.

One of the main objectives in analyzing a structure is to trace its equilibrium path. This is usually represented in the form of a load-displacement diagram. In linear

structural analysis, the applied load can be imposed on the structure in a single step. However, in nonlinear structural analysis, the applied load has to be subdivided into several increments and each loading increment is imposed on the structure in a successive manner, with or without corrective steps (equilibrium check). Consequently, the incremental solution procedures used in nonlinear structural analysis can be categorized into two types, namely: (*a*) the pure incremental method; and (*b*) the incremental-iterative method. The pure incremental method is the earliest nonlinear solution method and is simplest to implement. However, in each incremental step, drift-off error is accumulated and the obtained equilibrium path may greatly deviate from the true one since no equilibrium check is performed. Thus, this nonlinear solution scheme becomes obsolete nowadays. The incremental-iterative method is more effective and free from the drift-off error since equilibrium check is performed to eliminate the unbalanced forces between applied and internal resistant forces. This solution scheme is employed in this work.

Two most widely used marching schemes in the incremental-iterative method are load-control and displacement-control methods. The concept of load-control method is very straightforward. The nodal force components are used as control variables. Unfortunately, this marching scheme becomes unstable after a limit point at which the tangent to the equilibrium path is horizontal as shown in Figure 3-5 (a). As a counterpart of load-control method, the nodal displacement components are used as marching variables in the displacement-control method. Even though the displacement-control method shows no difficulty in passing the limit point, it becomes unstable after a turning point at which the tangent to the equilibrium path is vertical, as shown in Figure 3-5 (b). Since both limit and turning points on equilibrium paths are of interest in this work, a more versatile marching scheme is

needed. Consequently, the so-called "*generalized displacement control*" method is employed herein to trace the equilibrium path since it can handle both limit and turning points. In addition to the generalized displacement control method, the so-called "*arc-length*" method proposed by Riks (1972) and modified by Crisfield (1981) is widely used to handle the snap-back instability phenomenon. However, in several aspects, the generalized displacement control method adopted here is superior to the arc-length method. The pros and cons of these two methods are thoroughly discussed in Yang and Kou (1994).

3.4.1 Generalized Displacement Control Method

In this study, the generalized displacement control method proposed by Yang and Shieh (1990) is adopted to solve for solution of nonlinear equilibrium equations. A brief description of the method is given as follows:

At the j^{th} iteration of the i^{th} incremental step, the incremental equilibrium equations of a structure are cast into the N+1 dimensional space as:

$$\mathbf{K}_i^{j-1}\Delta\mathbf{U}_i^j = \lambda_i^j\hat{\mathbf{F}} + \mathbf{R}_i^{j-1} \tag{3.29}$$

where $\mathbf{K}_i^{j-1}$ is the structural stiffness matrix assembling from element tangent stiffness matrices $\mathbf{k}_i^{j-1}$; $\Delta\mathbf{U}_i^j$ is the incremental displacement vector; λ_i^j is the incremental load factor and is determined from the constraint equation; $\hat{\mathbf{F}}$ is the reference load vector; $\mathbf{R}_i^{j-1} = \Lambda_i^{j-1}\hat{\mathbf{F}} - \mathbf{F}_{int,i}^{j-1}$ is the unbalanced force vector; $\Lambda_i^{j-1} = \sum_{k=1}^{j-1}\lambda_i^k$ is the cumulative load factor; and $\mathbf{F}_{int,i}^{j-1}$ is the internal resistant force vector assembling from element resistant force vector $\mathbf{f}_{int,i}^{j-1}$.

Based on the decomposition proposed by Batoz and Dhatt (1979), the incremental

solution of Eq. (29) can be written as:

$$\Delta \mathbf{U}_i^j = \lambda_i^j \Delta \bar{\mathbf{U}}_i^j + \Delta \bar{\bar{\mathbf{U}}}_i^j \tag{3.30}$$

where $\Delta \bar{\mathbf{U}}_i^j$ and $\Delta \bar{\bar{\mathbf{U}}}_i^j$ are determined from the following matrix equations:

$$\begin{aligned} \mathbf{K}_i^{j-1} \Delta \bar{\mathbf{U}}_i^j &= \hat{\mathbf{F}} \\ \mathbf{K}_i^{j-1} \Delta \bar{\bar{\mathbf{U}}}_i^j &= \mathbf{R}_i^{j-1} \end{aligned} \tag{3.31}$$

At the beginning ($j = 1$) of the i^{th} incremental step, the unbalanced force vector $\mathbf{R}_i^0$ is null and the initial incremental load factor λ_i^1 is calculated from:

$$\lambda_i^1 = \pm \lambda_1^1 \left| GSP \right|^{\frac{1}{2}} \tag{3.32}$$

where λ_1^1 is the very first incremental load factor and is defined beforehand; and GSP is the generalized stiffness parameter and is calculated from the following constraint equation:

$$GSP = \frac{\Delta \bar{\mathbf{U}}_1^{1^T} \Delta \bar{\mathbf{U}}_1^1}{\Delta \bar{\mathbf{U}}_{i-1}^{1^T} \Delta \bar{\mathbf{U}}_i^1} \tag{3.33}$$

The parameter GSP accounts for the variation in stiffness of a system. It increases as the system is stiffer and decreases as the system is softer. Based on Eq. (29), the first incremental displacement vector at each incremental load step can be computed from:

$$\mathbf{K}_i^0 \Delta \mathbf{U}_i^1 = \lambda_i^1 \hat{\mathbf{F}} \tag{3.34}$$

For subsequent iterative steps ($j \geq 2$), the initial incremental load factor λ_i^j is calculated from the following constraint equation:

$$\lambda_i^j = -\frac{\Delta \bar{\mathbf{U}}_1^{i-1^T} \Delta \bar{\bar{\mathbf{U}}}_j^i}{\Delta \bar{\mathbf{U}}_{i-1}^{1^T} \Delta \bar{\mathbf{U}}_j^i} \tag{3.35}$$

Eqs. (30) and (31) are employed to compute the incremental displacement vector $\Delta \mathbf{U}_i^j$ and the current displacement vector is updated accordingly:

$$\mathbf{U}_i^j = \mathbf{U}_{i-1}^{converged} + \sum_{k=1}^{j} \Delta\mathbf{U}_i^k \tag{3.36}$$

where $\mathbf{U}_{i-1}^{converged}$ is the converged displacement vector at the previous loading step.

Similarly, the current load factor Λ_i^j can be updated as:

$$\Lambda_i^j = \Lambda_i^{j-1} + \lambda_i^j \tag{3.37}$$

and the current applied load vector is:

$$\mathbf{F}_i^j = \Lambda_i^j \hat{\mathbf{F}} \tag{3.38}$$

In each incremental loading step, the iterative process is carried out until the following convergence criterion is satisfied:

$$\left| \frac{\Delta\bar{\bar{\mathbf{U}}}_i^{j^T} \mathbf{R}_i^j}{\left(\lambda_i^1 \Delta\bar{\mathbf{U}}_i^1\right)^T \left(\lambda_i^1 \hat{\mathbf{F}}\right)} \right| \leq \varepsilon \tag{3.39}$$

where ε is the convergence tolerance and is specified beforehand. In this work, $\varepsilon = 10^{-12}$ is used in all analyses.

3.4.2 Step-by-step Algorithm for Generalized Displacement Control Method

The generalized displacement control method previously discussed is implemented in the in-house nonlinear structural analysis program and is incorporated into the proposed nonlinear bar element. The step-by-step procedure of the generalized displacement control method is presented as follows:

1: Set the reference load vector $\hat{\mathbf{F}}$ and the very first incremental load factor λ_1^1.

2: At the beginning ($j = 1$) of the i^{th} incremental step,

(i) Retrieve $\mathbf{K}_i^0$ from the last converged step.

(ii) Compute $\Delta\bar{\mathbf{U}}_i^1$ from Eq. (3.31)

(a) For the very first incremental loading step ($i = 1$), set GSP = 1.

(b) For subsequent loading steps ($i \geq 2$), use Eqs. (3.33) and (3.32) to determine GSP and λ_i^1, respectively.

(c) Check if $GSP < 0$, if yes, reverse the sign of λ_i^1.

(d) Use Eq. (3.30) to compute $\Delta \mathbf{U}_i^1$.

3: For subsequent iteration steps ($j \geq 2$) of the i^{th} incremental step,

(i) Retrieve $\mathbf{K}_i^{j-1}$ and $\mathbf{R}_i^{j-1}$ from the last iterative step.

(ii) Compute $\Delta \bar{\mathbf{U}}_i^1$ and $\Delta \bar{\bar{\mathbf{U}}}_i^1$ from Eq. (3.31).

(iii) Compute λ_i^j from Eq. (3.35).

(iv) Use Eq. (3.30) to compute $\Delta \mathbf{U}_i^j$.

4: Use Eqs. (3.36), (3.37), and (3.38) to compute $\mathbf{U}_i^j$, Λ_i^j, and $\mathbf{F}_i^j$, respectively.

5: For each element, perform the state determination to compute the current element stiffness matrix and element resistant force vector. It is noted that both statical and kinematical quantities required in the element state determination are measured with respect to the undeformed element configuration within the total Lagrangian framework.

Based on $\mathbf{U}_i^j$:

(i) Compute $N_i^{PK2,j}$ from Eq. (3.13).

(ii) Compute $\mathbf{k}_i^j$ from Eq. (3.25).

(iii) Compute $\mathbf{f}_{int,i}^{j-1}$ from Eq. (3.26).

6: Assemble $\mathbf{K}_i^j$ from $\mathbf{k}_i^j$ and $\mathbf{F}_{int,i}^{j-1}$ from $\mathbf{f}_{int,i}^{j-1}$.

7: Compute $\mathbf{R}_i^j = \mathbf{F}_i^j - \mathbf{F}_{int,i}^j$.

8: Check if the convergence criterion of Eq. (3.39) is satisfied.

(i) If no, set $j = j + 1$ and go to step 3.

(ii) If yes, go to step 9.

9: Check if Λ_i^j and $\mathbf{U}_i^j$ are larger than target values.

(i) If no, set $i = i + 1$ and go to step 2.

(ii) If yes, stop the analysis.

3.5 NUMERICAL EXAMPLES

Five numerical examples are used to verify the accuracy and show the efficiency of the proposed geometrically nonlinear bar element as well as the implemented solution procedure. The correlation studies are performed by comparing the obtained numerical results with the analytical results (if obtainable) or with other numerical results published in the literature.

3.5.1 Example I: Shallow von Mises Truss

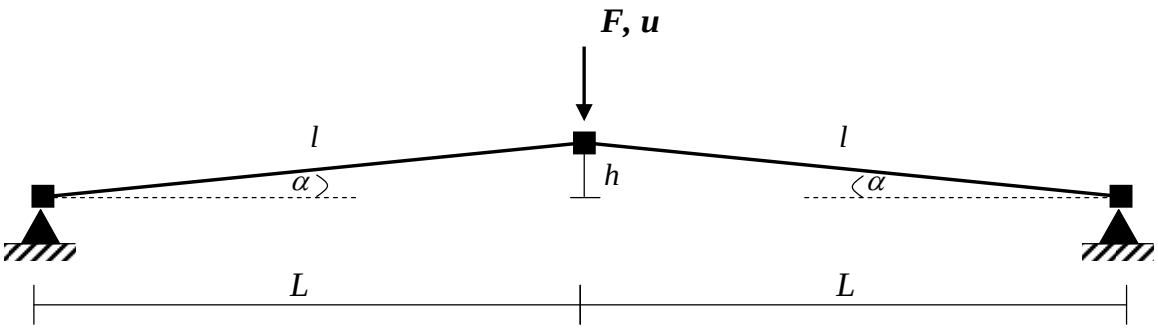

Figure 3-6. Example I: Shallow von Mises Truss.

The shallow von Mises truss of Figure 3-6 is used to show the ability of the proposed model as well as the implemented solution procedure to handle a snap-through instability phenomenon. This truss structure is considered a "*classic*" benchmark since it has been widely used by several researchers to evaluate their nonlinear bar models (e.g. Papadrakakis 1983, Kondoh and Atluri 1985, Greco et al. 2006,

Torkamani and Shieh 2011, etc.). It consists of two identical bar members with cross section area $A = 1.69 \times 10^{-2}\ m^2$, length $l = 11\,m$, and elastic modulus $E = 206\,GPa$. The rise angle α is 3.62^0 and is corresponding to the aspect ratio $h/2L$ of 0.032. Since the aspect ratio is low, this truss structure is considered shallow.

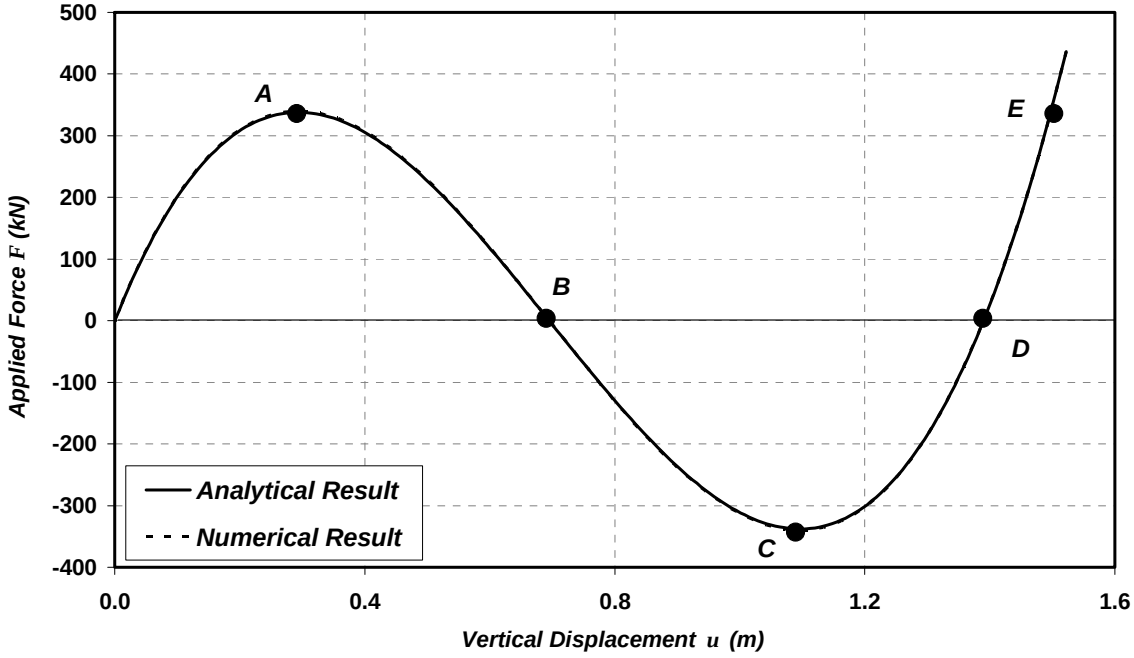

Figure 3-7. Midspan Load-Displacement Response for Shallow von Mises Truss.

Figure 3-7 compares the numerical result obtained by the proposed model with the analytical result for the mid-span load and mid-span displacement. The snap-through phenomenon is clearly observed. The analytical result for this problem was given by Greco et al. (2006). Clearly, there is a good agreement between analytical and numerical results. From this plot, the first limit point occurs at point *A* and corresponds to the mid-span load of 339.6 *kN* and the mid-span displacement of 0.287 *m.* This value of applied load is the maximum load that the system can sustain before experiencing the snap-through instability. The second limit point occurs at point *C* and corresponds to the mid-span load of -339.6 *kN* (upward) and the mid-span displacement of 1.1 *m.* After this point, the system becomes stable as indicated by the

positive slope of the equilibrium path. At points *B* and *D*, the structure is flat with a zero applied load and the corresponding displacements are 0.7 and 1.4 *m*, respectively. It is noted that when the load-control marching scheme is used for the solution procedure, the portion *A-B-C-D-E* of the equilibrium path cannot be traced and the structure suddenly snaps from points *A* to *E*.

3.5.2 Example II: Crisfield Bar-Spring System

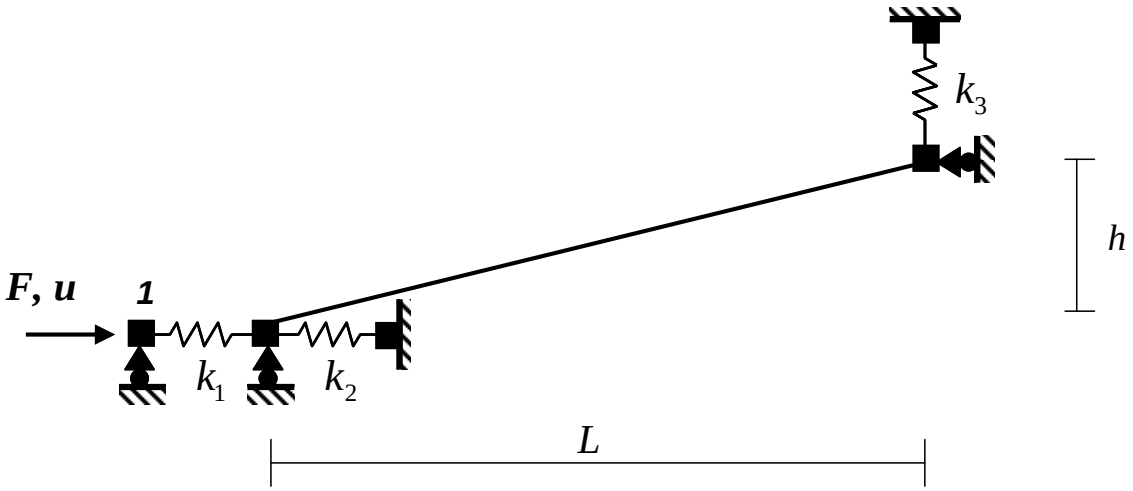

Figure 3-8. Example II: Crisfield Bar-Spring System.

The Crisfield bar-spring system of Figure 3-8 is analyzed to show the ability of the proposed model as well as the implemented solution procedure to cope with a snap-back instability phenomenon. It consists of a bar member with three linear springs. The aspect ratio h/L of the system is 0.01. The bar has its axial rigidity EA_0 of 50×10^6 and its three spring stiffnesses k_1, k_2, and k_3 are 1.0, 0.25, and 1.5, respectively. Numerically, the snap-back instability phenomenon is one of the most challenging problems in nonlinear structural analysis. A good explanation of this kind of elastic instability can be found in the textbook by Bazant and Cedolin (1991). It is noted that both load and displacement control marching schemes fail to completely trace the equilibrium path of a snap-back structure.

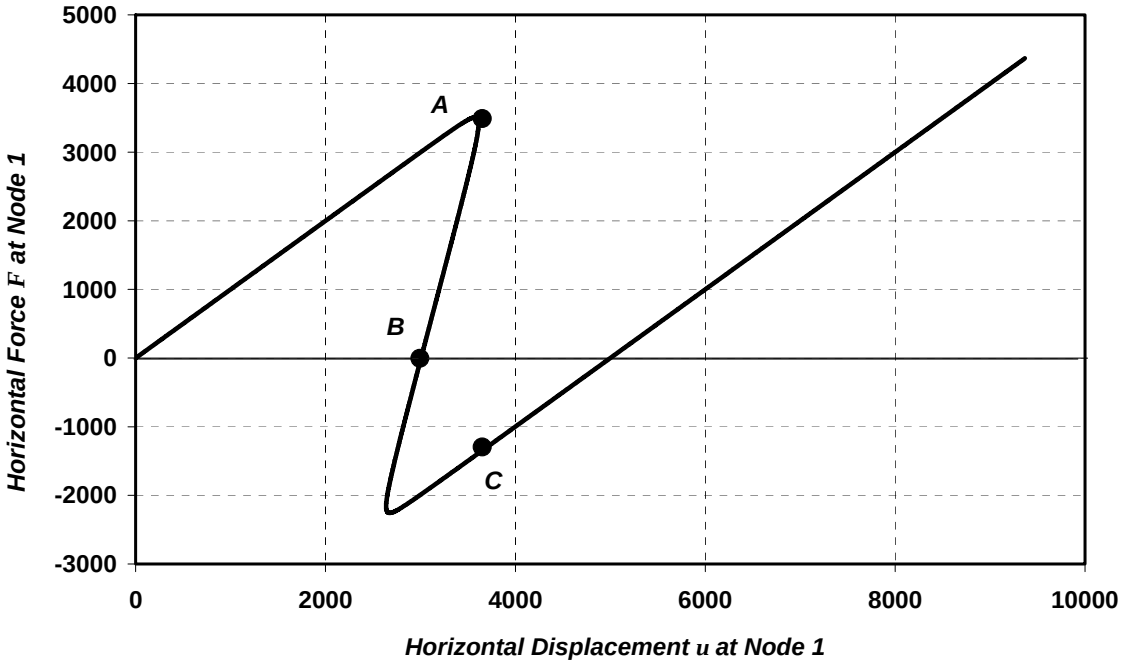

Figure 3-9. Load-Displacement Response of Node *1* for Crisfield Bar-Spring System.

Figure 3-9 shows the load-displacement response curve of node *1* and exhibits the snap-back instability phenomenon. At point *A*, the system buckles and the corresponding applied load is 3507. This value agrees reasonably well with that determined by Crisfield (1991). The buckling load computed by Crisfield (1991) is approximately 3750. It is noted that when the displacement-control marching scheme is used for the solution procedure, the portion *A*-*B*-*C* of the equilibrium path cannot be traced and the structure suddenly snaps from points *A* to *C*.

3.5.3 Example III: Thompson-Hunt Strut

A strut structure of Figure 3-10 was first studied by Thompson and Hunt (1973) to show the effects of local and global imperfections on the global buckling behavior. Kondoh and Atluri (1983) and Torkamani and Shieh (2011) also used this strut to evaluate the ability of their nonlinear bar models to represent the global buckling behavior. This strut is adopted as a benchmarking problem in the present work to assess the model capability to handle the global buckling phenomenon. As shown in

Figure 3-10, the strut consists of 35 circular cross-section members with an identical elastic modulus of $69\,GPa$. Two sizes of circular cross sections are used. Members 1-21 has a sectional area of $5.484\times10^{-3}\ m^2$ while members 22-35 has a sectional area of $5.161\times10^{-3}\ m^2$.

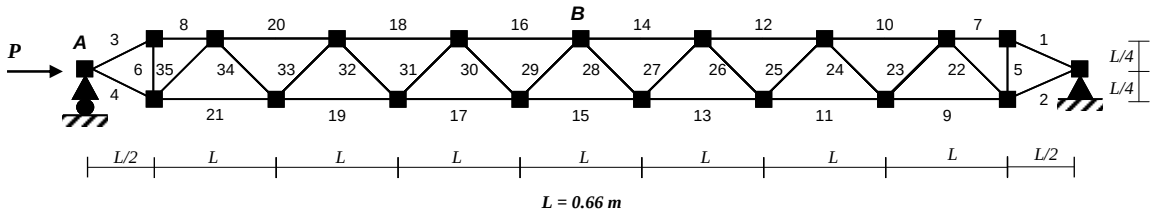

Figure 3-10. Example III: Thompson-Hunt Strut.

Figures 3-11 and 3-12 compare the numerical results obtained by the present model with those obtained by the bar models of Kondoh and Atluri (1983) and Torkamani and Shieh (2011). Figure 3-11 shows the load-displacement response of node A while Figure 3-12 shows the response curve between the applied load at node A and the vertical displacement at node B. Generally, there are good agreements between the present results and the results obtained by Kondoh and Atluri (1983) and Torkamani and Shieh (2011). At a load of approximately 7000 *kN*, the structure buckles globally. It is noted that the buckling loads reported by Kondoh and Atluri (1983) and Torkamani and Shieh (2011) are 7063 and 6916 *kN*, respectively. After this load level, the tangent of the equilibrium path becomes flat but the system can still maintain its loading capacity.

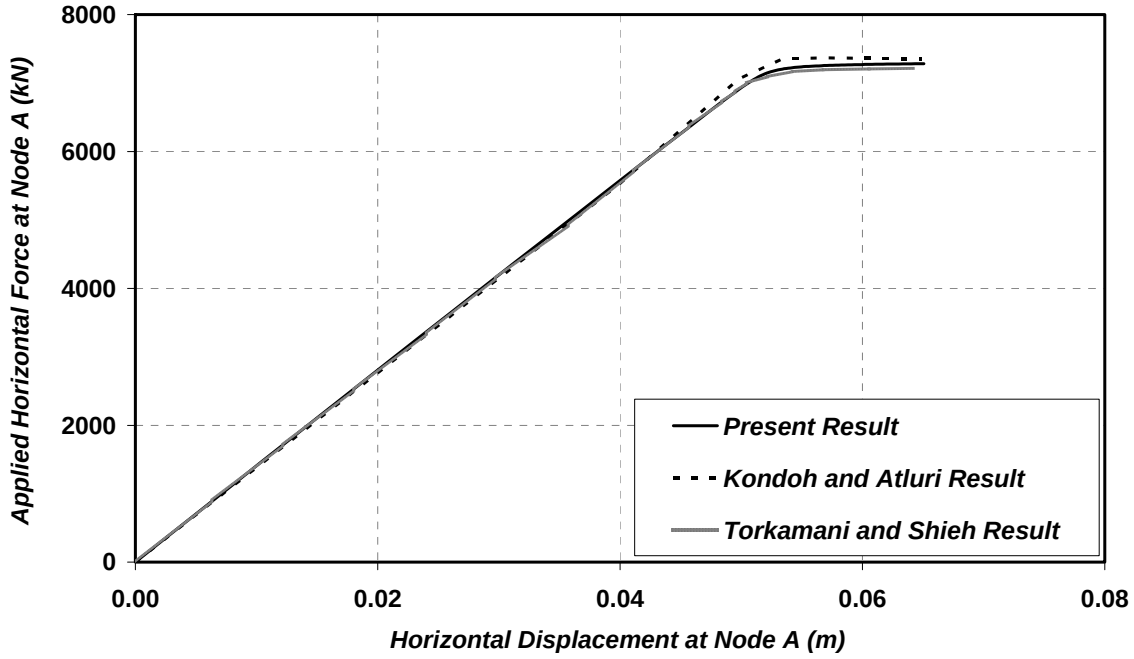

Figure 3-11. Load-Displacement Response at Node *A* for Thompson-Hunt Strut.

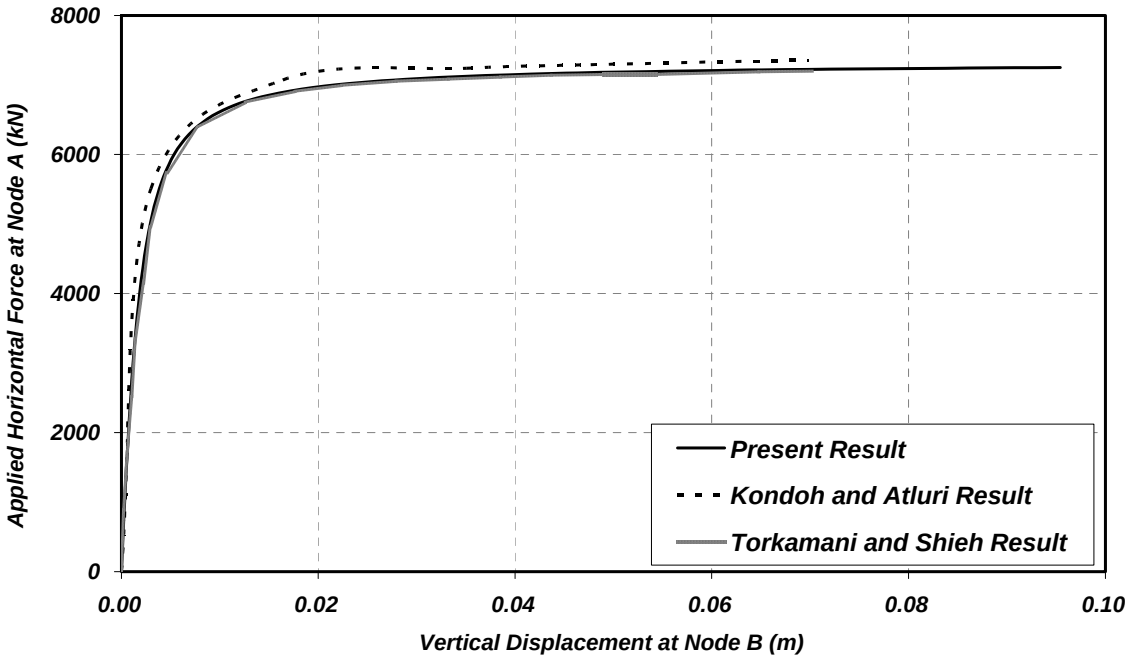

Figure 3-12. Load-Displacement Response at Node *B* for Thompson-Hunt Strut.

3.5.4 Example IV: Shallow Arch Truss

The shallow arch truss of Figure 3-13 is analyzed to show the global limit point of the system. Kondoh and Atluri (1983) and Torkamani and Shieh (2011) also used this structure to evaluate the ability of their nonlinear bar models. It consists of 35 members with an identical elastic modulus of $69\,GPa$ and is subjected to a concentrated load at node A. The cross-section areas of all members are summarized in Table 3-1.

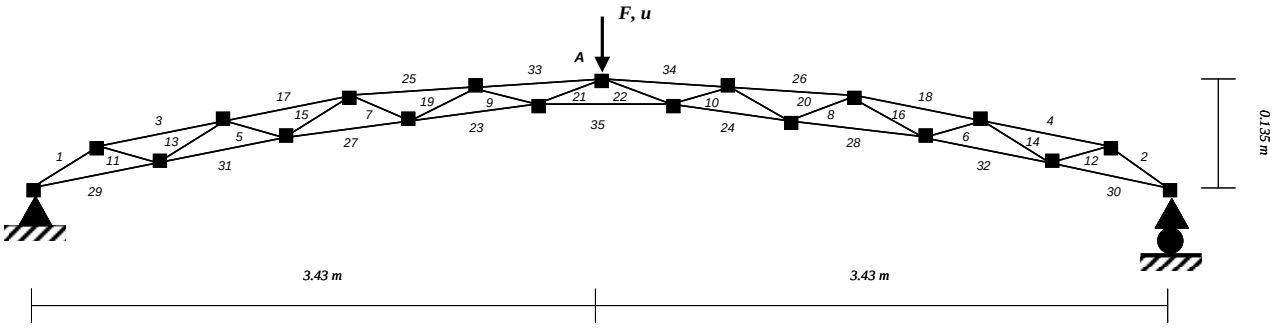

Figure 3-13. Example IV: Shallow Arch Truss.

Table 3-1: Cross Section Areas of the Members of the Shallow Arch Truss

Member	Area (m^2)
1-10 and 35	5.161×10^{-3}
11-12	6.452×10^{-3}
13-16	8.387×10^{-3}
17-18	9.677×10^{-3}
19-22	10.323×10^{-3}
23-24	16.129×10^{-3}
25-26	19.355×10^{-3}
27-28	25.806×10^{-3}
29-32	29.032×10^{-3}
33-34	30.968×10^{-3}

Figure 3-14 compares the numerical results obtained by the present model with those obtained by the models of Kondoh and Atluri (1983) and Torkamani and Shieh (2011). It represents the vertical load-displacement response curves of node A. In general, they are all in a good agreement. The applied load corresponding to the limit

point is 25.6 *kN* as predicted by the proposed model while the models of Kondoh and Atluri (1983) and Torkamani and Shieh (2011) indicate that the limit point is reached at applied loads of 25.87 and 25.11 *kN*, respectively. It is noted that the response curve of Torkamani and Shieh (2011) shows a drastic loss of the system loading capacity after the limit point. As reported by Torkamani and Shieh (2011), this is due to some divergence that their model experiences after reaching the limit point. Unlike the updated Lagrangian bar element by Torkamani and Shieh (2011), the total Lagrangian bar element presented herein does not experience such a divergence.

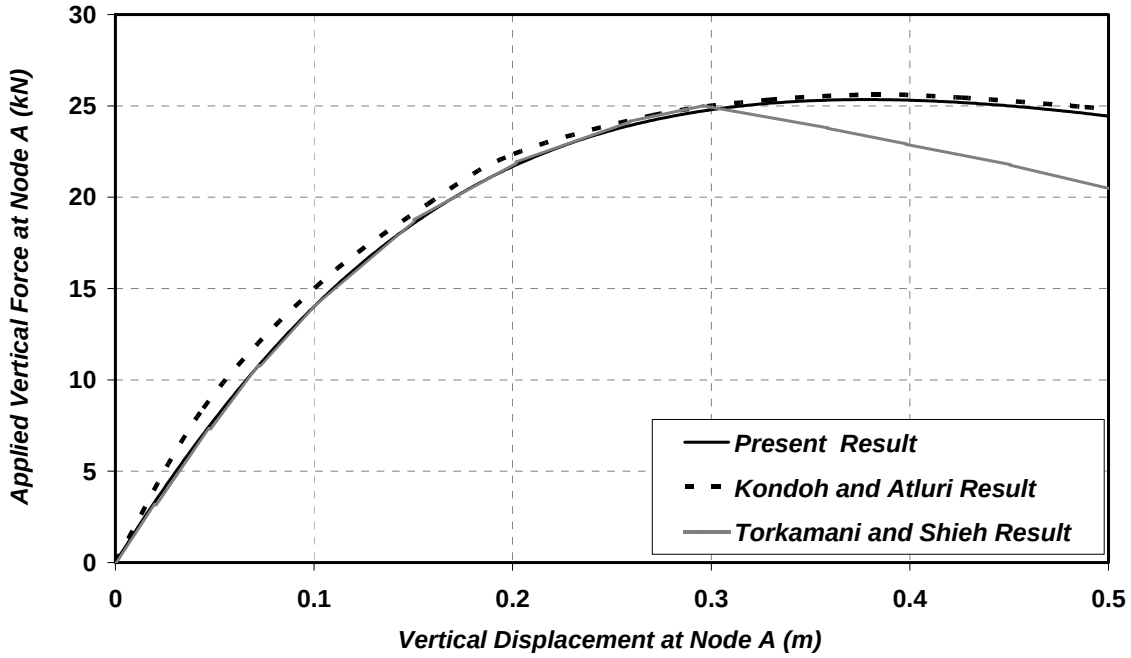

Figure 3-14. Load-Displacement Response at Node *A* for Shallow Arch Truss.

3.5.5 Example V: Cantilever Truss

The cantilever truss of Figure 3-15 is employed to assess the model capability to resemble the response of an elastic beam under large displacement. It is composed of 41 members with an identical elastic modulus of $100\,GPa$ and an identical sectional area of $0.03\,m^2$. The system is subjected to an applied load at its free end.

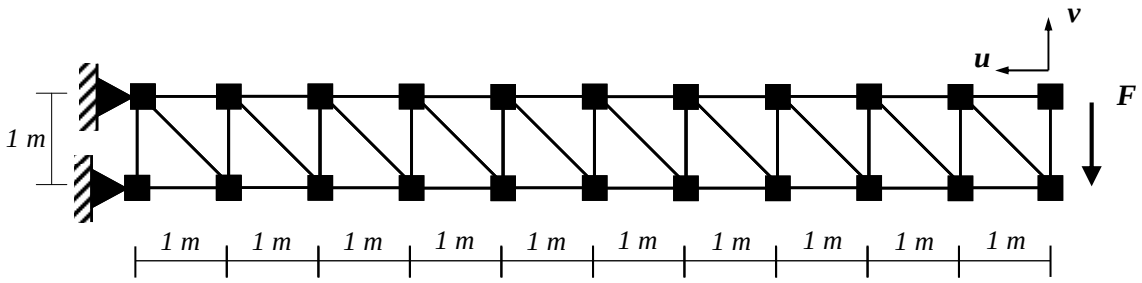

Figure 3-15. Example V: Cantilever Truss.

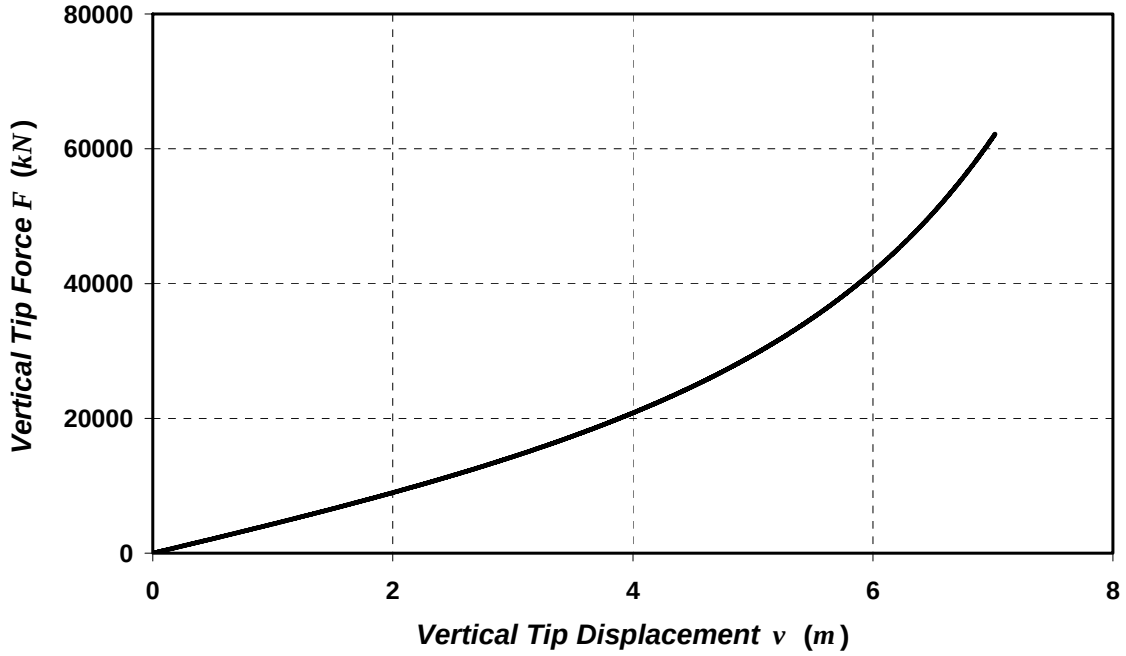

Figure 3-16. Vertical Load-Displacement Response at the Free End.

Figure 3-16 shows the vertical load-displacement response at the free end. It is observed that the structure behaves linearly at small loads. As the load increases, the system becomes stiffer and behaves nonlinearly. This is due to tension stiffening of the system in its deformed configuration. Figure 3-17 shows the response curve between the vertical applied load and the horizontal displacement at the free end. It is observed that at small loads, the tangential slope of the response curve decreases. This is due to the compression forces in the bottom chord members at small loads. However, this phenomenon diminishes drastically as the applied load increases. The

response characteristics of Figures 16 and 17 are similar to those of a cantilever beam under large displacement (Nanakorn and Vu 2006).

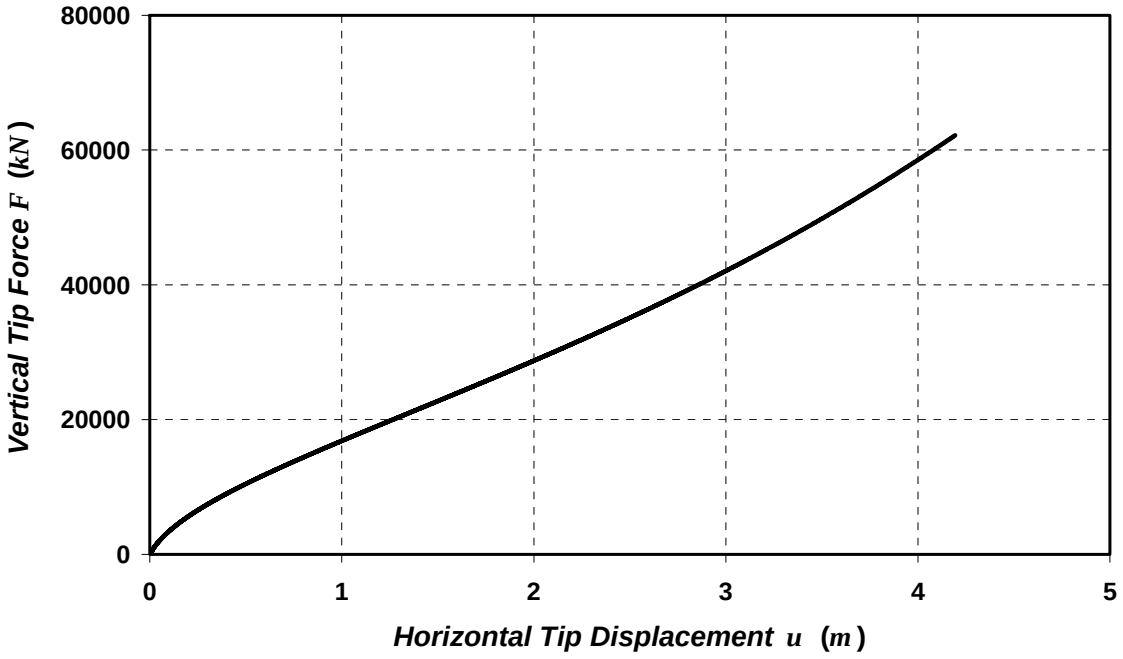

Figure 3-17. Vertical Load-Horizontal Displacement Response at the Free End.

APPENDIX: TANGENT STIFFNESS MATRICES AND ELEMENT VECTOR

The stiffness matrix $\mathbf{k}_0$:

$$\mathbf{k}_0 = \frac{EA_0}{L_0^{\,3}} \begin{bmatrix} X_{ij}^{\,2} & X_{ij}Y_{ij} & -X_{ij}^{\,2} & -X_{ij}Y_{ij} \\ X_{ij}Y_{ij} & Y_{ij}^{\,2} & -X_{ij}Y_{ij} & -Y_{ij}^{\,2} \\ -X_{ij}^{\,2} & -X_{ij}Y_{ij} & X_{ij}^{\,2} & X_{ij}Y_{ij} \\ -X_{ij}Y_{ij} & -Y_{ij}^{\,2} & X_{ij}Y_{ij} & Y_{ij}^{\,2} \end{bmatrix}$$

The stiffness matrices $\mathbf{k}_1$ and $\mathbf{k}_1^{'}$:

$$\mathbf{k}_1 = \frac{EA_0}{L_0^{\,3}} \begin{bmatrix} X_{ij}U_{ij} & X_{ij}V_{ij} & -X_{ij}U_{ij} & -X_{ij}V_{ij} \\ Y_{ij}U_{ij} & Y_{ij}V_{ij} & -Y_{ij}U_{ij} & -Y_{ij}V_{ij} \\ -X_{ij}U_{ij} & -X_{ij}V_{ij} & X_{ij}U_{ij} & X_{ij}V_{ij} \\ -Y_{ij}U_{ij} & -Y_{ij}V_{ij} & Y_{ij}U_{ij} & Y_{ij}V_{ij} \end{bmatrix} = \mathbf{k}_1^{'T}$$

The stiffness matrix $\mathbf{k}_2$:

$$\mathbf{k}_2 = \frac{EA_0}{L_0^{\,3}} \begin{bmatrix} U_{ij}^{\,2} & U_{ij}V_{ij} & -U_{ij}^{\,2} & -U_{ij}V_{ij} \\ U_{ij}V_{ij} & V_{ij}^{\,2} & -U_{ij}V_{ij} & -V_{ij}^{\,2} \\ -U_{ij}^{\,2} & -U_{ij}V_{ij} & U_{ij}^{\,2} & U_{ij}V_{ij} \\ -U_{ij}V_{ij} & -V_{ij}^{\,2} & U_{ij}V_{ij} & V_{ij}^{\,2} \end{bmatrix}$$

The stiffness matrix $\mathbf{k}_G$:

$$\mathbf{k}_G = \frac{N^{PK2}}{L_0} \begin{bmatrix} 1 & 0 & -1 & 0 \\ 0 & 1 & 0 & -1 \\ -1 & 0 & 1 & 0 \\ 0 & -1 & 0 & 1 \end{bmatrix}$$

The element vector $\mathbf{f}_{int}$:

$$\mathbf{f}_{int} = \frac{N^{PK2}}{L_0} \begin{Bmatrix} U_{ij} + X_{ij} \\ V_{ij} + Y_{ij} \\ -U_{ij} - X_{ij} \\ -V_{ij} - Y_{ij} \end{Bmatrix}$$

where

$$X_{ij} = X_i - X_j;\ Y_{ij} = Y_i - Y_j;\ U_{ij} = U_i - U_j;\ \text{and}\ V_{ij} = V_i - V_j$$

CHAPTER 4

FINITE FRAME ELEMENT FOR LARGE DISPLACEMENT ELASTIC AND INELASTIC ANALYSES OF FRAME STRUCTURES

4.1 Introduction

Frame members are commonly used in engineering structures (e.g. aerospace structures, marine vessels, innovative structural buildings, etc.). Due to drastic advance in material technology and economic reasons, designers of such structures usually try to optimize the structural weights, thus rendering the systems highly flexible. Such structures often fail by losses of their stability and may behave elastically well into the post-buckling regime. During the post-buckling regime, these structures generally experience large displacements and rotations. Furthermore, the Performance-Based Design and Assessment Methodology (ICBO 2000) has recently been adopted in the structural engineering community. In this design and assessment methodology, it urges structural engineers to understand and trace the structural responses to loading conditions ranging from service to collapse states. Thus, the frame model used to analyze highly flexible frame structures and employed in accordance with the Performance-Based Design and Assessment Methodology needs to be more sophisticated and capable of capturing the system nonlinearities (geometric and material nonlinearities).

Several nonlinear frame models have been proposed in literatures. Depending on the

choice of reference configuration and the complexity of the embedded beam theory, these frame models can be classified into three groups, namely: (*a*) Total Lagrangian model; (*b*) Updated Lagrangian model; and (*c*) Corotational model.

Several nonlinear frame models based on the total Lagrangian description have been proposed by several researchers (e.g. Milner 1981; Cichon 1984; Saje 1990; Pai et al. 2000; Nanakorn and Vu 2006, etc.). Within the total Lagrangian framework, a highly nonlinear beam theory (Reissner 1972) is usually required to simulate the frame motion even if the relative deformations of the frame experiencing the finite rigid displacements are small. Using the standard Hermite frame interpolation functions leads to the problem of field inconsistency (Nanakorn and Vu 2006), thus degrading the model accuracy. This is due to the fact that for large displacement/rotation problems, the longitudinal displacement field, the transverse displacement field, and the sectional rotation field are complicatedly dependent on each other. Several researchers have proposed several approaches to overcome this difficulty. For example, Saje (1990) and Nanakorn and Vu (2006) proposed the semi-analytical approaches to obtain the field-consistency interpolation functions.

A number of updated Lagrangian frame elements for large displacement/rotation problems have been proposed by several researchers in the research community (e.g. Bathe and Bolourchi 1979; Yang and McGuire 1986; Gattass and Abel 1987; Chan 1988; etc.). Due to the updating nature of the reference configuration, the standard Hermite interpolation functions could be used if the displacement increment from the reference element configuration to the current element configuration is sufficiently small. If this is not to be the case, the use of the standard Hermite interpolation

functions may lead to the field-inconsistency problem (Nanakorn and Vu 2006).

Besides total Lagrangian and updated Lagrangian formulations used to derive geometrically nonlinear frame elements, the corotational concept is an alternative to formulate the numerical model for large displacement and large rotation analyses of frame structures and has become extremely popular. The corotational concept has employed the polar decomposition principle used in continuum mechanics in its rudimentary form. Following the polar decomposition principle (Reddy 2008), the deformational motions of a solid body can be separated from its rigid body motions (translations and rotations). In other words, the total motion of a solid body can be decomposed into two parts: rigid-body part and deformational part. In the finite frame element formulation, the corotational frame is introduced to split the element motion into rigid-body part and deformation part. With respect to the corotational frame, the small displacement/rotation assumption could be made. Thus, the linear beam theory or any lower-order beam theory can be applied to the large displacement/rotation problems.

Ancestors of the corotational approach date back to the "*natural"* approach presented by Argyris et al. (1964) and the "*convected-coordinate*" approach proposed by Belytschko and Hsieh (1973). It is worth noting that Oran (1973) also recognized that the element formulation could be done locally within the corotational frame and realized the importance of accounting for the variation between local and global transformation matrices in order to derive a consistent tangent stiffness matrix. The Eulerian reference frame was referred to the corotational frame in works by Oran (1973) and Wen and Rahimzadeh (1983). In a subsequent work by Belytschko and

Glaum (1979), the word "*corotational*" was coined to unify the rigid-body-motion/deformation decomposition concept and has been commonly adopted. Up to date, the corotational concept has been widely employed by several researchers to formulate geometrically nonlinear frame elements (e.g. Crisfield 1990; Iura 1994; Jiang and Olson 1994; Lee 1997; Urthaler and Reddy 2005; Rungamornrat and Tangnovarad 2011, etc.).

In this chapter, an efficient frame element for large displacement and large rotation analyses of planar frame structures is proposed. The element formulation is based on the marriage of the corotational concept and the Euler-Bernoulli-von Karman beam theory. In other words, the global geometric nonlinearity (e.g. $P-\Delta$ effect) is introduced into the element via the corotational approach while the local geometric nonlinearity ($P-\delta$ effect) is accounted for using the Euler-Bernoulli-von Karman beam theory. The enhancement of the Euler-Bernoulli-von Karman beam theory over the linear Euler-Bernoulli beam theory is the inclusion of the rotational-related quadratic term in the axial strain-displacement equation, thus resulting in the membrane axial strain. However, this membrane axial strain might have an adverse effect on the element performance when the standard displacement-based finite element is employed. This adverse effect is known as the "*membrane locking*" phenomenon (Reddy 2004). Several approaches have been proposed to remedy this locking problem for example: reduced integration (Geyer and Groenwold 2003), use of enhanced strain field (Perego 2000), mixed and force-based formulations (Hjelmstad and Taciroglu 2003), etc. This study employs the Hellinger-Reissner mixed functional to formulate the locking-free Euler-Bernoulli-von Karman frame

element within the system without rigid-body modes (basic system). It is noted that the Hellinger-Reissner mixed functional has been used by the authors to formulate the mixed frame element with bond-interfaces presented in Limkatanyu and Spacone (2002a) and the mixed Winkler foundation element presented in Limkatanyu and Spacone (2006).

The organization of the present chapter is set as follows. The kinematics and kinetics of the corotational framework as well as the transformation relation for the stiffness matrices are first discussed. Then, the derivation of the governing differential equations for the Euler-Bernoulli-von Karman beam theory is given. These governing equations consist of compatibility, equilibrium, and constitutive relations. It can be shown that the axial strain in the Euler-Bernoulli-von Karman beam theory is simply a degenerated Green-Lagrange strain in continuum mechanics. A set of governing differential equilibrium equations are derived in a direct manner. The virtual displacement principle is used to demonstrate the variational consistency between the derived governing differential equilibrium equations and the compatibility equations. Next, the Hellinger-Reissner mixed functional is employed to formulate the Euler-Bernoulli-von Karman frame element with respect to the basic system. The directional derivative operator or Gâteaux operator (Hughes and Pister 1978) is used to linearize the Hellinger-Reissner mixed functional, thus leading to the incremental element equations. The derivation of the displacement and force interpolation functions and element state determination process are also briefly discussed. Finally, the validity of the proposed nonlinear frame element is confirmed by analyzing seven benchmark examples exhibiting several types of critical points and comparing these

results with analytical and experimental results available in literatures. The efficiency of the proposed nonlinear frame element is assessed by comparing the numerical results obtained with the proposed model to those obtained with other nonlinear frame models. The general-purpose finite element platform FEAP (Taylor 2000) is used to host the proposed element and its available solution marching schemes are employed to obtain the numerical results.

4.2 Corotational Formulation of Planar Frames

4.2.1 Frame Kinematics and Kinetics

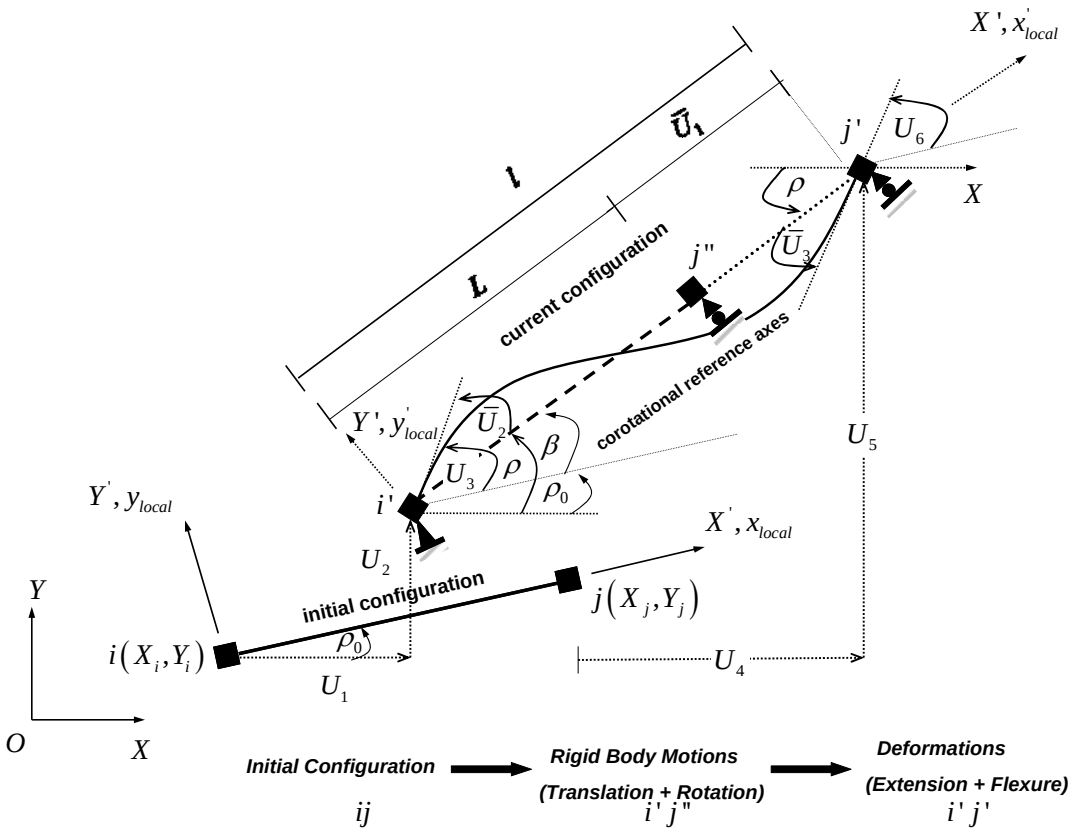

Figure 4-1 Corotational Framework of Planar Frame Element

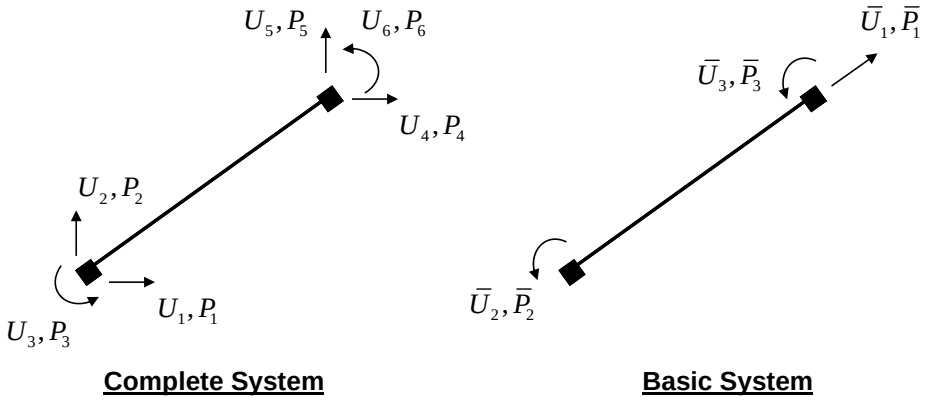

Figure 4-2 Element Systems: Complete and Basic Systems

The frame element shown in Figure 4-1 is taken as a generic frame element to convey the corotational concept. The kinematics of this generic element moving from its initial to current configurations is described by its nodal displacements in the global reference system $(X\text{-}Y)$. These nodal displacements and their corresponding nodal forces are grouped in the vectors $\mathbf{U}$ and $\mathbf{P}$, respectively:

$$\begin{aligned} \mathbf{U} &= \lfloor U_1 \quad U_2 \quad U_3 \quad U_4 \quad U_5 \quad U_6 \rfloor^T \\ \mathbf{P} &= \lfloor P_1 \quad P_2 \quad P_3 \quad P_4 \quad P_5 \quad P_6 \rfloor^T \end{aligned} \tag{4.1}$$

Six components of $\mathbf{U}$ and six components of $\mathbf{P}$ form the element complete system as shown in Figure 4-2. Eliminating three rigid-body motions leaves three basic element deformations and forms the element basic system as shown in Figure 4-2. Three basic element deformations and their corresponding basic forces are grouped in the vectors $\bar{\mathbf{U}}$ and $\bar{\mathbf{P}}$, respectively:

$$\begin{aligned} \bar{\mathbf{U}} &= \lfloor \bar{U}_1 \quad \bar{U}_2 \quad \bar{U}_3 \rfloor^T \\ \bar{\mathbf{P}} &= \lfloor \bar{P}_1 \quad \bar{P}_2 \quad \bar{P}_3 \rfloor^T \end{aligned} \tag{4.2}$$

The objective of this section is to derive the statical and kinematical relations between the element basic and complete systems using the corotational concept. In the finite

element frame formulation, the corotational reference axes ($X'-Y'$) are rigidly bounded to the cross section at node i in the initial configuration and at node i' in the current configuration. If the element displaces as a rigid body, the corotational reference axes are carried with it and no element deformations are induced. As shown in Figure 4-1, the basic element deformations are defined as displacements relative to the corotational reference axes. Relative to this reference system, the element can be visualized as a beam simply supported with a pin at node i' and with a roller at nodes j' and j''. This virtual supporting system simply helps us to suppress the rigid body modes. The basic element deformations of this basic system are defined as: the relative displacement $\bar{U}_1$ at node j' along the chord connecting nodes i' and j'; the rotational deformation $\bar{U}_2$ at node i' relative to the chord $i'j'$; and the rotational deformation $\bar{U}_3$ at node j' relative to the chord $i'j'$. Thus, these three basic element deformations are computed as:

$$\begin{aligned} \bar{U}_1 &= l - L \\ \bar{U}_2 &= U_3 - \beta = U_3 - \rho + \rho_0 \\ \bar{U}_3 &= U_6 - \beta = U_6 - \rho + \rho_0 \end{aligned} \tag{4.3}$$

where L and l are the initial and current lengths of element chords, respectively and are computed as:

$$\begin{aligned} L &= \sqrt{\left(X_j - X_i\right)^2 + \left(Y_j - Y_i\right)^2} \\ l &= \sqrt{\left(X_j + U_4 - X_i - U_1\right)^2 + \left(Y_j + U_5 - Y_i - U_2\right)^2} \end{aligned} \tag{4.4}$$

ρ_0 and ρ denote the orientation angles of initial and current element chords, respectively, and are expressed as:

$$\cos\rho_0 = \frac{X_j - X_i}{L} \text{ and } \sin\rho_0 = \frac{Y_j - Y_i}{L} \tag{4.5}$$

$$\cos\rho = \frac{X_j + U_4 - X_i - U_1}{l} \text{ and } \sin\rho = \frac{Y_j + U_5 - Y_i - U_2}{l} \tag{4.6}$$

The compatibility relation between the element basic and complete systems can be derived by establishing the kinematical relation between the virtual basic element deformations $\delta\bar{\mathbf{U}}$ and virtual nodal displacements $\delta\mathbf{U}$. This can be done by first taking the variation of Eq. (4.3):

$$\begin{aligned} \delta\bar{U}_1 &= \delta l \\ \delta\bar{U}_2 &= \delta U_3 - \delta\beta = \delta U_3 - \delta\rho \\ \delta\bar{U}_3 &= \delta U_6 - \delta\beta = \delta U_6 - \delta\rho \end{aligned} \tag{4.7}$$

The virtual axial deformation $\delta\bar{U}_1$ can be expressed in terms of $\delta\mathbf{U}$ by taking the variation of the second relation in Eq. (4.4):

$$\delta\bar{U}_1 = \delta l = -\cos\rho\delta U_1 - \sin\rho\delta U_2 + \cos\rho\delta U_4 + \sin\rho\delta U_5 \tag{4.8}$$

The virtual element-chord orientation angle $\delta\rho$ can be expressed in terms of $\delta\mathbf{U}$ by taking the variation of Eq. (4.6):

$$\delta\rho = \frac{1}{l}\left(\sin\rho\delta U_1 - \cos\rho\delta U_2 - \sin\rho\delta U_4 + \cos\rho\delta U_5\right) \tag{4.9}$$

Substituting Eqs. (4.8) and (4.9) into (4.7) leads to the following matrix compatibility relation:

$$\delta\bar{\mathbf{U}} = \mathbf{T}_{RBM}\delta\mathbf{U} \tag{4.10}$$

where $\mathbf{T}_{RBM}$ is the compatibility matrix and filters out the rigid body modes from $\delta\mathbf{U}$.

$$\mathbf{T}_{RBM} = \begin{bmatrix} -\cos\rho & -\sin\rho & 0 & \cos\rho & \sin\rho & 0 \\ -\sin\rho/l & \cos\rho/l & 1 & \sin\rho/l & -\cos\rho/l & 0 \\ -\sin\rho/l & \cos\rho/l & 0 & \sin\rho/l & -\cos\rho/l & 1 \end{bmatrix} \quad (4.11)$$

The statical relation between the nodal forces in the element complete and basic systems can be established by accounting for the invariant property of the virtual work with respect to either the element complete or basic system:

$$\delta W = \delta\bar{\mathbf{U}}^T\bar{\mathbf{P}} = \delta\mathbf{U}^T\mathbf{P} = \delta\mathbf{U}^T\mathbf{T}_{RBM}^T\bar{\mathbf{P}} \quad (4.12)$$

Due to arbitrariness of $\delta\mathbf{U}$, the statical relation between the nodal force vectors $\mathbf{P}$ and $\bar{\mathbf{P}}$ is:

$$\mathbf{P} = \mathbf{T}_{RBM}^T\bar{\mathbf{P}} \quad (4.13)$$

The contragradient nature between Eqs. (4.10) and (4.13) confirms the conjugate-work pairs of nodal forces and displacements in both element basic and complete systems.

4.2.2 Global and Basic Element Stiffness Matrices

The transformation relation between the complete and basic element stiffness matrices can be obtained by taking the variation of Eq. (4.13) as:

$$\delta\mathbf{P} = \mathbf{T}_{RBM}^T\delta\bar{\mathbf{P}} + \delta\mathbf{T}_{RBM}^T\bar{\mathbf{P}} \quad (4.14)$$

The first term in Eq. (4.14) can be alternatively expressed by accounting for the compatibility relation of Eq. (4.10) and introducing the basic element stiffness equation $\delta\bar{\mathbf{P}} = \bar{\mathbf{K}}\delta\bar{\mathbf{U}}$:

$$\mathbf{T}_{RBM}^T\delta\bar{\mathbf{P}} = \mathbf{T}_{RBM}^T\bar{\mathbf{K}}\delta\bar{\mathbf{U}} = \mathbf{T}_{RBM}^T\bar{\mathbf{K}}\mathbf{T}_{RBM}\delta\mathbf{U} \quad (4.15)$$

where $\bar{\mathbf{K}}$ is the basic element stiffness matrix.

The second term in Eq. (4.14) can be explicitly written as:

$$\delta \mathbf{T}_{RBM}^{T} \bar{\mathbf{P}} = \delta \mathbf{t}_{RBM1} \bar{P}_1 + \delta \mathbf{t}_{RBM2} \bar{P}_2 + \delta \mathbf{t}_{RBM3} \bar{P}_3 \tag{4.16}$$

where $\delta \mathbf{t}_{RBM1}$, $\delta \mathbf{t}_{RBM2}$, and $\delta \mathbf{t}_{RBM3}$ represent the first, second, and third columns of $\delta \mathbf{T}_{RBM}^{T}$, respectively. Taking the first variation of $\mathbf{T}_{RBM}^{T}$, the row matrices $\delta \mathbf{t}_{RBM1}$, $\delta \mathbf{t}_{RBM2}$, and $\delta \mathbf{t}_{RBM3}$ are expressed as:

$$\delta \mathbf{t}_{RBM1} = \frac{\mathbf{g}_1^{\,T} \mathbf{g}_1}{l} \delta \mathbf{U} \text{ and } \delta \mathbf{t}_{RBM2} = \delta \mathbf{t}_{RBM3} = \frac{\mathbf{g}_2^{\,T} \mathbf{g}_1 + \mathbf{g}_1^{\,T} \mathbf{g}_2}{l^2} \delta \mathbf{U} \tag{4.17}$$

where the row matrices $\mathbf{g}_1$ and $\mathbf{g}_2$ are defined as:

$$\begin{aligned} \mathbf{g}_1 &= \lfloor \sin\rho \quad -\cos\rho \quad 0 \quad -\sin\rho \quad \cos\rho \quad 0 \rfloor \\ \mathbf{g}_2 &= \lfloor -\cos\rho \quad -\sin\rho \quad 0 \quad \cos\rho \quad \sin\rho \quad 0 \rfloor \end{aligned} \tag{4.18}$$

Substituting Eqs. (4.15-4.17) into (4.14) leads to the global stiffness equation:

$$\delta \mathbf{P} = \mathbf{K} \delta \mathbf{U} \tag{4.19}$$

where $\mathbf{K}$ represents the global element stiffness defined as:

$$\mathbf{K} = \mathbf{K}_M + \mathbf{K}_G \tag{4.20}$$

In Eq. (4.20), the material and global geometric stiffness contributions to the global element stiffness matrix $\mathbf{K}$ are denoted by the matrices $\mathbf{K}_M$ and $\mathbf{K}_G$, respectively, and are computed as:

$$\mathbf{K}_M = \mathbf{T}_{RBM}^{T} \bar{\mathbf{K}} \mathbf{T}_{RBM} \tag{4.21}$$

$$\mathbf{K}_G = \bar{P}_1 \frac{\mathbf{g}_1^{\,T} \mathbf{g}_1}{l} + \left(\bar{P}_2 + \bar{P}_3 \right) \frac{\mathbf{g}_2^{\,T} \mathbf{g}_1 + \mathbf{g}_1^{\,T} \mathbf{g}_2}{l^2} \tag{4.22}$$

The elegant outcome of the corotational formulation is the natural separation of model nonlinearities. The geometric nonlinearity at the global level (large displacements and rotations) is taken into account in the global geometric stiffness matrix $\mathbf{K}_G$. The nonlinearity within the element basic system is accounted for in the

material stiffness matrix $\mathbf{K}_M$. This source of nonlinearities may have come from material nonlinearity (e.g. elastic-plastic, nonlinear elastic, etc.) or local geometrical nonlinearity (e.g. $P-\delta$ effect, etc.).

4.3 Basic (Local) Beam System: Euler-Bernoulli-von Karman Beam Theory

4.3.1 Compatibility: Motion, Deformation, and Strain

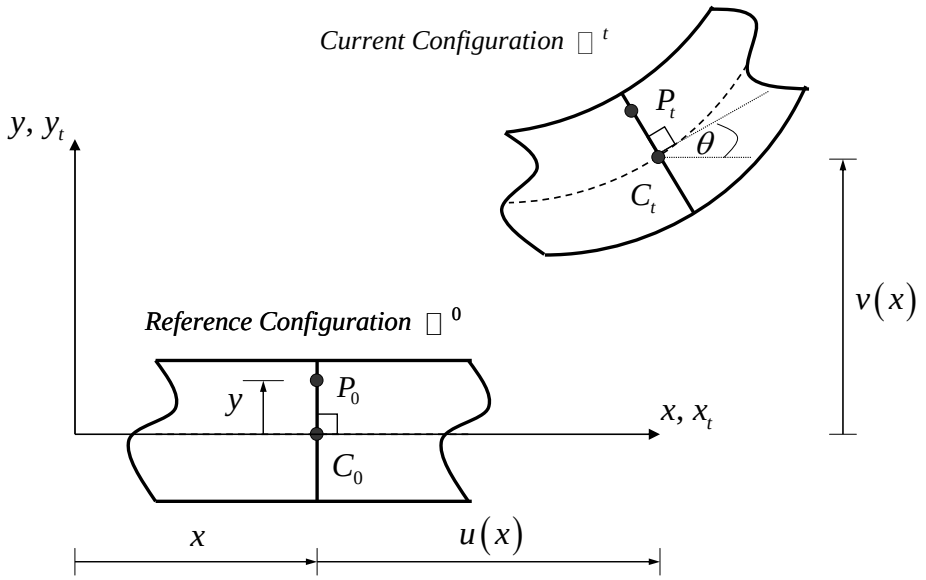

Figure 4-3 Lagrangian Kinematical Description of Beam Section

Let us consider a portion of an initially straight prismatic beam as shown in Figure 4-3. The Lagrangian kinematical description is used to study the motion of a generic particle P_0 originally located at the Lagrangian coordinates (x, y). Under loading exertion, the particle P_0 in the reference configuration Ω^0 displaces to the particle P_t currently located at the Eulerian coordinates (x_t, y_t) in the current configuration Ω^t.

Following the Euler-Bernoulli beam-section hypothesis, the mapping between the Lagrangian and Eulerian coordinates is written as:

$$\begin{aligned} x_t(x,y) &= x + u(x) - y\sin\theta(x) \\ y_t(x,y) &= v(x) + y\cos\theta(x) \end{aligned} \tag{4.23}$$

where $u(x)$ and $v(x)$ are horizontal and vertical displacements of the centroidal point moving from its reference position $C_0[x,0]$ to its current position $C_t[x,v(x)]$; and $\theta(x)$ is the sectional rotation angle.

The deformation gradient matrix of the motion of the particle P_0 is:

$$\mathbf{F} = \begin{bmatrix} \dfrac{\partial x_t}{\partial x} & \dfrac{\partial x_t}{\partial y} \\ \dfrac{\partial y_t}{\partial x} & \dfrac{\partial y_t}{\partial y} \end{bmatrix} = \begin{bmatrix} 1 + \dfrac{\partial u}{\partial x} - y\cos\theta\dfrac{\partial\theta}{\partial x} & -\sin\theta \\ \dfrac{\partial v}{\partial x} - y\sin\theta\dfrac{\partial\theta}{\partial x} & \cos\theta \end{bmatrix} \tag{4.24}$$

Accordingly, the Green-Lagrange strain matrix is:

$$\mathbf{E}^{GL} = \begin{bmatrix} E_{xx}^{GL} & E_{xy}^{GL} \\ E_{yx}^{GL} & E_{yy}^{GL} \end{bmatrix} = \frac{1}{2}\left(\mathbf{F}^T\mathbf{F} - \mathbf{I}\right) \tag{4.25}$$

Explicitly, each Green-Lagrange strain component is expressed as:

$$\begin{aligned} E_{xx}^{GL} &= \frac{1}{2}\left(1 + \frac{\partial u}{\partial x} - y\cos\theta\frac{\partial\theta}{\partial x}\right)^2 + \frac{1}{2}\left(\frac{\partial v}{\partial x} - y\sin\theta\frac{\partial\theta}{\partial x}\right)^2 \\ 2E_{xy}^{GL} &= 2E_{yx}^{GL} = -\left(1 + \frac{\partial u}{\partial x} - y\cos\theta\frac{\partial\theta}{\partial x}\right)\sin\theta + \left(\frac{\partial v}{\partial x} - y\sin\theta\frac{\partial\theta}{\partial x}\right)\cos\theta \\ E_{yy}^{GL} &= 0 \end{aligned} \tag{4.26}$$

As expected, the transverse normal strain E_{yy}^{GL} vanishes since the cross section is assumed to be transversely rigid. Considering small strains, the first-order approximation $\mathbf{e}^{GL}$ to the Green-Lagrange strain matrix $\mathbf{E}^{GL}$ can be written as:

$$\mathbf{e}^{GL} = \begin{bmatrix} e_{xx}^{GL} & e_{xy}^{GL} \\ e_{yx}^{GL} & e_{yy}^{GL} \end{bmatrix} \tag{4.27}$$

where

$$\begin{aligned} e_{xx}^{GL} &= \frac{\partial u}{\partial x} + \frac{1}{2}\left(\frac{\partial u}{\partial x}\right)^2 + \frac{1}{2}\left(\frac{\partial v}{\partial x}\right)^2 - y\cos\theta\frac{\partial \theta}{\partial x}; \\ 2e_{xy}^{GL} &= 2e_{yx}^{GL} = -\left(1+\frac{\partial u}{\partial x}\right)\sin\theta + \frac{\partial v}{\partial x}\cos\theta; \\ e_{yy}^{GL} &= 0; \end{aligned} \tag{4.28}$$

Ensuring that the shear strain e_{xy}^{GL} vanishes, three sectional displacement fields $u(x)$, $v(x)$, and $\theta(x)$ must be inter-dependent and need to satisfy the following kinematical constraint:

$$\left(1+\frac{\partial u}{\partial x}\right)\sin\theta = \frac{\partial v}{\partial x}\cos\theta \tag{4.29}$$

The beam theory based Eqs. (4.28) and (4.29) is referred to as the "*Euler-Bernoulli-Reissner*" or "*refined*" beam theory (Reissner 1972). Considering small rotations with respect to the corotational angle ($\sin\theta \cong \tan\theta \cong \theta = \partial v/\partial x$ and $\cos\theta \cong 1$) and neglecting high-order terms ($(\partial u/\partial x)\sin\theta$ and $(\partial u/\partial x)^2$), the second-order approximation $\boldsymbol{\varepsilon}^{GL}$ to the Green-Lagrange strain matrix $\mathbf{E}^{GL}$ can be written as:

$$\boldsymbol{\varepsilon}^{GL} = \begin{bmatrix} \varepsilon_{xx}^{GL} & \varepsilon_{xy}^{GL} \\ \varepsilon_{yx}^{GL} & \varepsilon_{yy}^{GL} \end{bmatrix} = \begin{bmatrix} \dfrac{\partial u}{\partial x} + \dfrac{1}{2}\left(\dfrac{\partial v}{\partial x}\right)^2 - y\dfrac{\partial^2 v}{\partial x^2} & 0 \\ 0 & 0 \end{bmatrix} \tag{4.30}$$

It is noted that the vanishing condition of the shear strain ε_{xy}^{GL} is satisfied only in the approximate sense. The only non-zero strain is ε_{xx}^{GL} and can be alternatively expressed in terms of sectional deformations ε_0^{GL} and κ as:

$$\varepsilon_{xx}^{GL} = \varepsilon_0^{GL} - y\kappa \tag{4.31}$$

where the membrane axial strain ε_0^{GL} at the centroidal axis and the bending strain (material measure of curvature) κ are expressed as:

$$\varepsilon_0^{GL} = \frac{\partial u}{\partial x} + \frac{1}{2}\left(\frac{\partial v}{\partial x}\right)^2 \text{ and } \kappa = \frac{\partial \theta}{\partial x} = \frac{\partial^2 v}{\partial x^2} \tag{4.32}$$

The beam theory based on the strain definition of Eq. (4.32) is often referred to as the *Euler-Bernoulli-von Karman* or "*technical*" beam theory (Pignataro et al. 1991). Two sectional deformations of Eq. (4.32) can be grouped in the following array:

$$\mathbf{d}\left[\mathbf{u}(x)\right] = \mathbf{d}(x) = \begin{bmatrix} \varepsilon_0^{GL} & \kappa \end{bmatrix}^T = \begin{bmatrix} \dfrac{\partial u}{\partial x} + \dfrac{1}{2}\left(\dfrac{\partial v}{\partial x}\right)^2 & \dfrac{\partial^2 v}{\partial x^2} \end{bmatrix}^T \tag{4.33}$$

where $\mathbf{u}(x) = \begin{bmatrix} u(x) & v(x) \end{bmatrix}^T$ is the array containing section displacements. On the left-hand side of Eq. (4.33), the presence of the centroidal displacement vector $\mathbf{u}(x)$ emphasizes that the section deformation vector $\mathbf{d}(x)$ is related to the section displacement vector $\mathbf{u}(x)$ through the compatibility condition. In other words, the variable $\mathbf{d}(x)$ is a slave to the variable $\mathbf{u}(x)$.

4.3.2 Equilibrium: Direct Approach vs. Variational Approach

The governing differential equilibrium equations of the Euler-Bernoulli-von Karman beam shown in Figure 4-4 (a) are derived in a direct manner. A differential element dx taken from the beam is shown in Figure 4-4 (b). Considering horizontal and vertical equilibriums of the infinitesimal segment *dx* lead to:

$$\frac{\partial N(x)}{\partial x} + w_x(x) = 0 \tag{4.34}$$

$$\frac{\partial V(x)}{\partial x} + w_y(x) = 0 \tag{4.35}$$

where $N(x)$ and $V(x)$ are the section axial and shear forces, respectively; and $w_x(x)$ and $w_y(x)$ are the horizontal and transverse distributed loads, respectively.

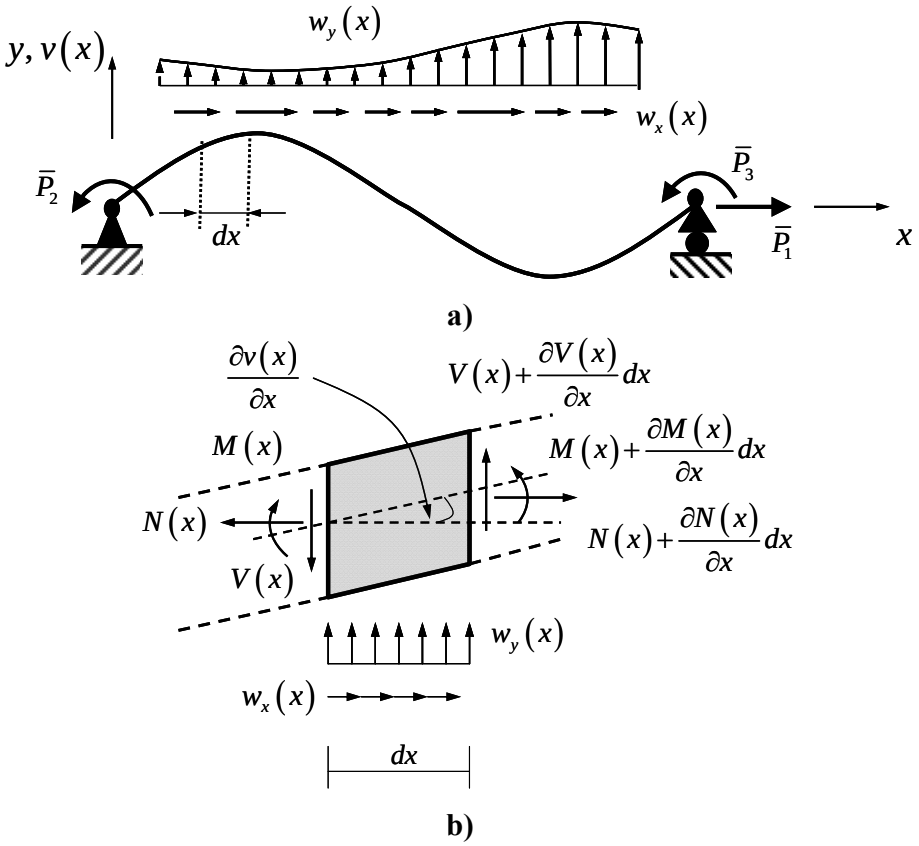

Figure 4-4 Equilibrium of Element Basic System: a) Deformed Basic System; b) An Infinitesimal Frame Segment

Considering the moment equilibrium and neglecting higher-order terms lead to:

$$\frac{\partial M(x)}{\partial x} + V(x) - N(x)\frac{\partial v(x)}{\partial x} = 0 \tag{4.36}$$

where $M(x)$ is the section bending moment.

Differentiating Eq. (4.36) with respect to x and eliminating the section shear force

$V(x)$ through Eq. (4.35) yield:

$$\frac{\partial^2 M(x)}{\partial x^2} - w_y(x) - \frac{\partial\left(N(x)\dfrac{\partial v(x)}{\partial x}\right)}{\partial x} = 0 \tag{4.37}$$

Eqs. (4.34) and (4.37) form a set of governing differential equilibrium equations of the Euler-Bernoulli-von Karman beam theory. To validate the variational consistency between the derived governing differential equilibrium equations and compatibility equations obtained earlier, the virtual displacement principle is employed as follows. For the basic system of Figure 4-4 (a), the virtual work equation can be written as:

$$\begin{aligned}\delta W = &\int_L \left(\delta\varepsilon_0^{GL} N + \delta\kappa M\right) dx - \int_L \left(\delta u w_x + \delta v w_x\right) dx \\ &- \delta\bar{U}_1\bar{P}_1 - \delta\bar{U}_2\bar{P}_2 - \delta\bar{U}_3\bar{P}_3 = 0\end{aligned} \tag{4.38}$$

The directional derivative operator (Gâteaux operator) is used to obtain the virtual sectional deformations $\delta\varepsilon_0^{GL}$ and $\delta\kappa$ from the virtual section displacements δu and δv as:

$$\delta\mathbf{d}[\mathbf{u}, \delta\mathbf{u}] = \begin{bmatrix} \delta\varepsilon_0^{GL} & \delta\kappa \end{bmatrix}^T = D\mathbf{d}[\mathbf{u}].\delta\mathbf{u} = \begin{bmatrix} \dfrac{\partial\delta u}{\partial x} + \dfrac{\partial v}{\partial x}\dfrac{\partial\delta v}{\partial x} & \dfrac{\partial^2\delta v}{\partial x^2} \end{bmatrix}^T \tag{4.39}$$

The matrix form of Eq. (4.39) can be written as:

$$\delta\mathbf{d} = \boldsymbol{\Theta}\partial\delta\mathbf{u} \tag{4.40}$$

where the differential matrices $\boldsymbol{\Theta}$ and ∂ are defined as:

$$\boldsymbol{\Theta} = \begin{bmatrix} 1 & \dfrac{\partial v}{\partial x} & 0 \\ 0 & 0 & 1 \end{bmatrix} \text{ and } \partial = \begin{bmatrix} \dfrac{\partial}{\partial x} & 0 \\ 0 & \dfrac{\partial}{\partial x} \\ 0 & \dfrac{\partial^2}{\partial x^2} \end{bmatrix} \tag{4.41}$$

Substituting Eqs. (4.39) into (4.38), applying integration by parts, and imposing essential boundary conditions for δu and δv yield the weighted residual form of equilibrium equations:

$$\int_L \delta u\left(\frac{\partial N}{\partial x}+w_x\right)dx+\int_L \delta v\left(\frac{\partial^2 M}{\partial x^2}-w_y-\frac{\partial\left(N\dfrac{\partial v}{\partial x}\right)}{\partial x}\right)dx+ \\ \delta\bar{U}_1\left(\bar{P}_1-N_{x=L}\right)+\delta\bar{U}_2\left(\bar{P}_2+M_{x=0}\right)+\delta\bar{U}_3\left(\bar{P}_3-M_{x=L}\right)=0 \tag{4.42}$$

Accounting for the arbitrariness of all virtual quantities yields the governing differential equilibrium equations of Eqs. (4.34) and (4.37) as well as three natural boundary conditions. Therefore, it confirms that the equilibrium and compatibility equations derived earlier are variationally consistent.

4.3.3 Sectional Deformation-Force Relations

Throughout this work, both linear and nonlinear material responses are of interest. For a linearly elastic material, the sectional deformations are related to their conjugate-work sectional forces as follows:

$$\varepsilon_{xx}^{GL}(x)=\frac{N(x)}{EA} \text{ and } \kappa(x)=\frac{M(x)}{IE} \tag{4.43}$$

where *EA* and *IE* are the axial and flexural rigidities, respectively. The matrix form of Eq. (4.43) can be written as:

$$\mathbf{d}(x)=\mathbf{f}\mathbf{D}(x) \tag{4.44}$$

where $\mathbf{D}(x)$ is the array containing sectional forces $N(x)$ and $M(x)$; and $\mathbf{f}$ is the diagonal matrix containing sectional compliances 1/*EA* and 1/*IE*.

For a nonlinear material, the fiber section model is used to derive the beam-section constitutive law $\mathbf{D} = \mathbf{D}(\mathbf{d})$. The fiber model automatically accounts for the interaction between axial and bending responses and can be used to model reinforced concrete, steel and other kinds of composite sections. The explicit expression for the fiber beam-section force-deformation relation is given in Spacone et al (1996). The section nonlinear law is linearized according to the following forms:

$$\mathbf{D}(x) = \mathbf{D}^0(x) + \Delta\mathbf{D}(x) = \mathbf{D}^0(x) + \mathbf{k}^0(x)\Delta\mathbf{d}(x) \tag{4.45}$$

where $\mathbf{k}(x)$ is the section matrix. The consistent inverse of Eq. (4.45) can be expressed in the following form:

$$\mathbf{d}(x) = \mathbf{d}^0(x) + \Delta\mathbf{d}(x) = \mathbf{d}^0(x) + \mathbf{f}^0(x)\Delta\mathbf{D}(x) \tag{4.46}$$

where $\mathbf{f}^0(x)$ is the section flexibility matrices, respectively. In the above equation, the superscript 0 indicates the value of a vector or matrix at the initial point of a linearized nonlinear scheme.

4.4 Local Euler-Bernoulli-von Karman Finite Beam Formulation

4.4.1 Hellinger-Reissner Mixed Functional

In the two-field mixed formulation (Reddy 2002), both section forces and section deformations are approximated by interpolation functions. The section forces $\mathbf{D}(x)$ are expressed in terms of the nodal force degrees of freedom **R** (to be defined later in the paper) through force interpolation functions, and the section deformations $\mathbf{d}(x)$ are expressed as functions of the basic nodal displacements $\bar{\mathbf{U}}$ via displacement

interpolation functions. The nodal force degrees of freedom **R** and basic nodal displacements $\bar{\mathbf{U}}$ serve as the primary element variables. For the sake of simplicity, it is assumed that horizontal and vertical element loads $w_x(x)$ and $w_y(x)$ vanish along the element.

Based on the virtual displacement principle, the integral form of the equilibrium equations is expressed as:

$$\delta\Pi_{\mathbf{u}}^{HR} = \int_L \delta\mathbf{d}(x)^T \mathbf{D}(x)\,dx - \delta\bar{\mathbf{U}}^T\bar{\mathbf{P}} \tag{4.47}$$

where $\delta\mathbf{d}(x)$ are the virtual section deformations compatible with the virtual section displacements $\delta\mathbf{u}(x)$ through Eq. (4.40).

Based on the virtual force principle, the integral form of the compatibility equations can be written as:

$$\delta\Pi_{\mathbf{D}}^{HR} = \int_L \delta\mathbf{D}(x)^T \left[\mathbf{d}(x) - \hat{\mathbf{d}}(x)\right] dx \tag{4.48}$$

where $\delta\mathbf{D}(x)$ are the virtual section forces; and $\hat{\mathbf{d}}(x)$ are the section deformations determined from the section forces $\mathbf{D}(x)$.

Combining Eqs. (4.47) and (4.48), the first variation of the Hellinger-Reissner mixed functional can be written as:

$$\begin{aligned}\delta\Pi^{HR}[\mathbf{u},\mathbf{D},\delta\mathbf{u},\delta\mathbf{D}] &= \delta\Pi_{\mathbf{u}}^{HR} + \delta\Pi_{\mathbf{D}}^{HR} \\ &= \int_L \left(\delta\mathbf{d}(x)^T \mathbf{D}(x) + \delta\mathbf{D}(x)^T \left[\mathbf{d}(x) - \hat{\mathbf{d}}(x)\right]\right) dx - \delta\bar{\mathbf{U}}^T\bar{\mathbf{P}}\end{aligned} \tag{4.49}$$

According to the fundamental lemma of variational calculus (Washizu 1982), the compatible equilibrium configuration is obtained when $\delta\Pi^{HR}[\mathbf{u},\mathbf{D},\delta\mathbf{u},\delta\mathbf{D}]$ vanishes

for all choices of $\delta\mathbf{u}(x)$ and $\delta\mathbf{D}(x)$.

4.4.2 Incremental Element Equations

Due to the nonlinear nature of compatibility and equilibrium equations, an incremental-iterative structural analysis is used to trace an equilibrium path of a system. In this type of structural analysis, the tangent element stiffness matrix and the internal element resisting forces are needed and can be derived from linearization of Eq. (4.49). Let $\mathbf{u}_i(x)$ and $\mathbf{D}_i(x)$ represent the current element state. It is noted that this element state is not necessary in equilibrium and compatibility. Consequently, $\delta\Pi^{HR}$ may not necessarily vanish. With respect to $\mathbf{u}_i(x)$ and $\mathbf{D}_i(x)$, Eq. (4.49) can be linearized as:

$$L\left[\delta\Pi^{HR}\right] = \delta\Pi^{HR}\Big|_{\mathbf{u}_i,\mathbf{D}_i} + \Delta\left[\delta\Pi^{HR}\right]_{\mathbf{u}_i,\mathbf{D}_i} \tag{4.50}$$

where

$$\delta\Pi^{HR}\Big|_{\mathbf{u}_i,\mathbf{D}_i} = \int_L \left(\delta\mathbf{d}(x)^T\,\mathbf{D}_i(x) + \delta\mathbf{D}(x)^T\left[\mathbf{d}_i(x) - \hat{\mathbf{d}}_i(x)\right]\right)dx - \delta\overline{\mathbf{U}}^T\overline{\mathbf{P}}_i \tag{4.51}$$

The increment of the first variational Hellinger-Reissner mixed functional can be determined using the directional derivative operator as:

$$\Delta\left[\delta\Pi^{HR}\right]_{\mathbf{u}_i,\mathbf{D}_i} = \frac{d}{d\alpha}\left[\delta\Pi^{HR}\left(\mathbf{u}+\alpha\Delta\mathbf{u},\mathbf{D}+\alpha\Delta\mathbf{D},\delta\mathbf{u},\delta\mathbf{D}\right)\right]_{\mathbf{u}_i,\mathbf{D}_i}^{\alpha=0} \tag{4.52}$$

Carrying out the above expression yields:

$$\Delta\left[\delta\Pi^{HR}\right]_{\mathbf{u}_i,\mathbf{D}_i} = \int_L \left(\delta\mathbf{u}^T\partial^T\left[\boldsymbol{\Theta}_i^T\Delta\mathbf{D} + \mathbf{N}_i\partial\Delta\mathbf{u}\right] + \delta\mathbf{D}^T\left[\boldsymbol{\Theta}_i\partial\Delta\mathbf{u} - \mathbf{f}_i\Delta\mathbf{D}\right]\right)dx \tag{4.53}$$

where the axial-force matrix $\mathbf{N}_i$ is defined as:

$$\mathbf{N}_i = \begin{bmatrix} 0 & 0 & 0 \\ 0 & N_i(x) & 0 \\ 0 & 0 & 0 \end{bmatrix} \tag{4.54}$$

It is noted that $\mathbf{f}_i$ and $\mathbf{N}_i$ are computed with respect to $\mathbf{D}_i(x)$ while $\mathbf{\Theta}_i$ is evaluated with respect to $\mathbf{u}_i(x)$.

To obtain the discrete form of Eq. (4.50), the section forces and section displacements are expressed in terms of the nodal force degrees of freedom $\mathbf{R}$ and basic nodal displacements $\bar{\mathbf{U}}$ through the force and displacement interpolation functions, respectively:

$$\mathbf{D}_i(x) = \mathbf{N}_{\mathbf{R}1_i}^{HR}(x)\mathbf{R}_i \text{ and } \delta\mathbf{D}(x) = \mathbf{N}_{\mathbf{R}1_i}^{HR}(x)\delta\mathbf{R} + \mathbf{N}_{\mathbf{R}2_i}^{HR}(x)\delta\bar{\mathbf{U}} \tag{4.55}$$

$$\mathbf{u}(x) = \mathbf{N}_{\mathbf{u}}^{HR}(x)\bar{\mathbf{U}} \text{ and } \delta\mathbf{u}(x) = \mathbf{N}_{\mathbf{u}}^{HR}(x)\delta\bar{\mathbf{U}} \tag{4.56}$$

where $\mathbf{N}_{\mathbf{R}1_i}^{HR}(x)$ and $\mathbf{N}_{\mathbf{R}2_i}^{HR}(x)$ are the vertical displacement-dependent and axial force-dependent force interpolation functions, respectively for the beam-section forces; and $\mathbf{N}_{\mathbf{u}}^{HR}(x)$ are the displacement interpolation functions for the beam-section displacements. It is noted that $\mathbf{N}_{\mathbf{R}1_i}^{HR}(x)$ and $\mathbf{N}_{\mathbf{R}2_i}^{HR}(x)$ are evaluated with respect to $\mathbf{u}_i(x)$ and $\mathbf{R}_i$, respectively. Detailed derivations of these interpolation functions are to be discussed later in the paper.

Substituting Eqs. (4.55) and (4.56) into (4.50) and enforcing that $L\left[\delta\Pi^{HR}\right]$ vanishes for all choices of $\delta\mathbf{R}$ and $\delta\bar{\mathbf{U}}$ yield the following mixed matrix equations:

$$\begin{aligned} &\mathbf{T}_i^T\Delta\mathbf{R} + \left[\mathbf{G}_{1i} + \mathbf{K}_{N_i}\right]\Delta\bar{\mathbf{U}} + \mathbf{r}_{\bar{\mathbf{U}}_i} = \mathbf{0} \\ &-\mathbf{F}_i\Delta\mathbf{R} + \mathbf{T}_i\Delta\bar{\mathbf{U}} + \mathbf{r}_{\mathbf{R}_i} = \mathbf{0} \end{aligned} \tag{4.57}$$

where $\mathbf{T}_i$ serves as the transformation matrix between the force degrees of freedom and the displacement degrees of freedom, and is defined as:

$$\mathbf{T}_i = \int_L \mathbf{N}_{\mathbf{R}1_i}^{HR\,T} \boldsymbol{\Theta}_i \mathbf{B}_{\mathbf{u}}^{HR} dx - \int_L \mathbf{N}_{\mathbf{R}1_i}^{HR\,T} \mathbf{f}_i \mathbf{N}_{\mathbf{R}2_i}^{HR} dx \tag{4.58}$$

with $\mathbf{B}_{\mathbf{u}}^{HR}(x) = \partial \mathbf{N}_{\mathbf{u}}^{HR}(x)$.

The local geometric stiffness matrix $\mathbf{G}_i$ accounts for the coupling between axial force and transverse displacement, and is defined as:

$$\mathbf{G}_i = \int_L \mathbf{B}_{\mathbf{u}}^{HR\,T} \boldsymbol{\Theta}_i^T \mathbf{N}_{\mathbf{R}2_i}^{HR} dx + \int_L \mathbf{N}_{\mathbf{R}2_i}^{HR\,T} \boldsymbol{\Theta}_i \mathbf{B}_{\mathbf{u}}^{HR} dx - \int_L \mathbf{N}_{\mathbf{R}2_i}^{HR\,T} \mathbf{f}_i \mathbf{N}_{\mathbf{R}2_i}^{HR} dx \tag{4.59}$$

The axial-force matrix $\mathbf{K}_{N_i}$ takes into account the effects of the axial force, and is defined as:

$$\mathbf{K}_{N_i} = \int_L \mathbf{B}_{\mathbf{u}}^{HR\,T} \mathbf{N}_i \mathbf{B}_{\mathbf{u}}^{HR} dx \tag{4.60}$$

$\mathbf{F}_i$ is the flexibility matrix, and is defined as:

$$\mathbf{F}_i = \int_L \mathbf{N}_{\mathbf{R}1_i}^{HR\,T} \mathbf{f}_i \mathbf{N}_{\mathbf{R}1_i}^{HR} dx \tag{4.61}$$

$\mathbf{r}_{\bar{\mathbf{U}}_i}$ and $\mathbf{r}_{\mathbf{R}_i}$ represent the force and displacement residuals corresponding to the weighted integral forms of equilibrium and of compatibility, respectively, and are defined as:

$$\begin{aligned} \mathbf{r}_{\bar{\mathbf{U}}_i} &= \int_L \mathbf{B}_{\mathbf{u}}^{HR\,T} \boldsymbol{\Theta}_i^T \mathbf{D}_i \, dx + \int_L \mathbf{N}_{\mathbf{R}2_i}^{HR\,T} \left(\mathbf{d}_i - \hat{\mathbf{d}}_i \right) dx - \bar{\mathbf{P}}_i \\ \mathbf{r}_{\mathbf{R}_i} &= \int_L \mathbf{N}_{\mathbf{R}1_i}^{HR\,T} \left(\mathbf{d}_i - \hat{\mathbf{d}}_i \right) dx \end{aligned} \tag{4.62}$$

In view of the element implementation into a general-purpose finite element program, the force degrees of freedom in Eq. (4.57) are eliminated using static condensation.

Consequently, solving the second relation in Eq. (4.57) yields:

$$\Delta\mathbf{R} = \mathbf{F}_i^{-1}\left(\mathbf{r}_{\mathbf{R}_i} + \mathbf{T}_i\,\Delta\bar{\mathbf{U}}\right) \tag{4.63}$$

Substitution of Eq. (4.63) into the first relation in Eq. (4.57) leads to the mixed stiffness equation:

$$\bar{\mathbf{K}}_i\,\Delta\bar{\mathbf{U}} = \bar{\mathbf{P}}_i - \bar{\mathbf{F}}_i \tag{4.64}$$

where $\bar{\mathbf{K}}_i$ and $\bar{\mathbf{F}}_i$ represent the basic element stiffness matrix and basic element resisting force vector, respectively, and are defined as:

$$\begin{aligned}\bar{\mathbf{K}}_i &= \mathbf{T}_i^T\mathbf{F}_i^{-1}\mathbf{T}_i + \mathbf{G}_{1i} + \mathbf{K}_{N_i}\\ \bar{\mathbf{F}}_i &= \int_L \mathbf{B}_{\mathbf{u}}^{HR\,T}\boldsymbol{\Theta}_i^T\mathbf{D}_i\,dx + \int_L \mathbf{N}_{\mathbf{R}2_i}^{HR\;T}\left(\mathbf{d}_i - \hat{\mathbf{d}}_i\right)dx - \mathbf{T}_i^T\mathbf{F}_i^{-1}\mathbf{r}_{\mathbf{R}_i}\end{aligned} \tag{4.65}$$

4.4.3 Displacement and Force Interpolation Functions

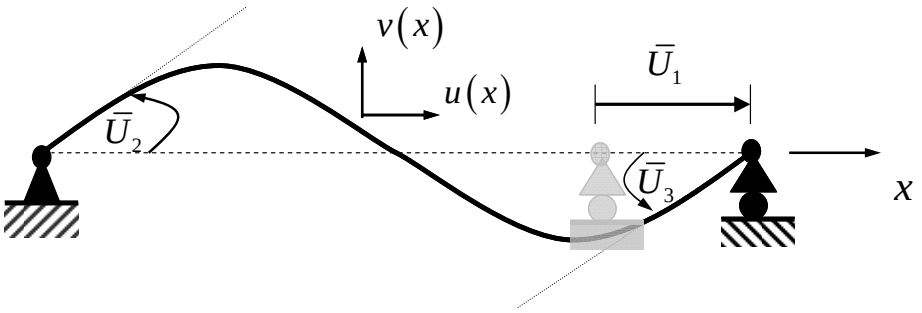

Figure 4-5 Displacement Interpolation Functions

Following the first derivative of the axial displacement and the second derivative of the transverse displacement, C^0 and C^1 continuous functions are used respectively for the axial and transverse displacements for the basic system shown in Figure 4-5. As a result, linear Lagrangian and cubic Hermitian polynomials are used for the axial and transverse displacements, respectively. Therefore, the displacement- interpolation

matrix $\mathbf{N}_{\mathbf{u}}^{HR}(x)$ is defined as:

$$\mathbf{N}_{\mathbf{u}}^{HR}(x)=\begin{bmatrix} 1-\frac{x}{L} & 0 & 0 \\ 0 & x\left(1-\frac{x}{L}\right)^2 & \frac{x^2}{L}\left(\frac{x}{L}-1\right) \end{bmatrix} \tag{4.66}$$

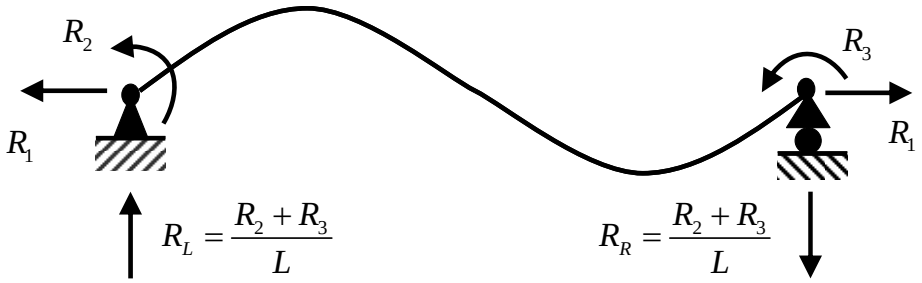

A)

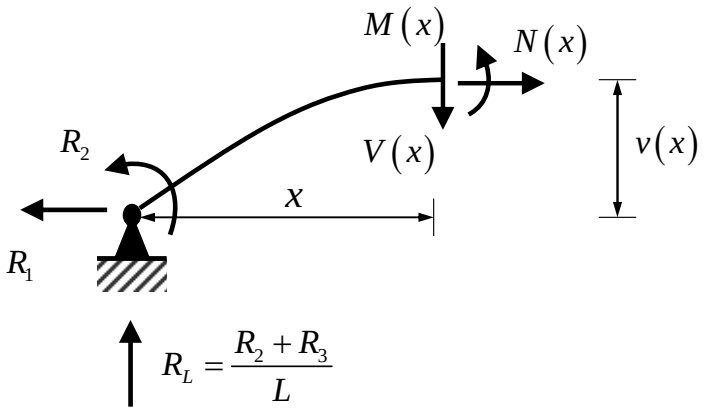

B)

Figure 4-6 Force Interpolation Functions

Considering equilibriums of the basic system shown in Figure 4-6 with respect to its deformed configuration, the displacement-dependent and axial force-dependent force interpolation functions are:

$$\mathbf{N}_{\mathbf{R}1_i}^{HR}(x)=\begin{bmatrix} 1 & 0 & 0 \\ v_i(x) & \dfrac{x}{L}-1 & \dfrac{x}{L} \end{bmatrix} \tag{4.67}$$

$$\mathbf{N}_{\mathbf{R}2_i}^{HR}(x)=\begin{bmatrix} 0 & 0 & 0 \\ 0 & x\left(1-\dfrac{x}{L}\right)^2 N_i(x) & \dfrac{x^2}{L}\left(\dfrac{x}{L}-1\right)N_i(x) \end{bmatrix} \tag{4.68}$$

It is noted that with assumed transverse displacement, the displacement-dependent force interpolation functions in $\mathbf{N}_{\mathbf{R}1_i}^{HR}(x)$ satisfy the axial and moment equilibrium of Eqs. (4.34) and (4.37). The axial force-dependent force interpolation matrix $\mathbf{N}_{\mathbf{R}2_i}^{HR}(x)$ accounts for the dependence of the virtual section forces $\delta\mathbf{D}(x)$ on the virtual basic nodal displacements $\delta\bar{\mathbf{U}}$.

4.5 Element State Determination

The element state determination procedure for the mixed frame element proposed in this study follows the one presented by Limkatanyu and Spacone (2002b). A similar procedure is also proposed by Hjelmstad and Taciroglu (2003). The adopted state determination procedure is briefly explained as follows:

Solving the incremental stiffness equation yields the incremental nodal displacements $\Delta\mathbf{U}$ and the incremental basic element deformations $\Delta\bar{\mathbf{U}}$ through the rigid-body-mode transformation matrix $\mathbf{T}_{RBM}$. The incremental nodal forces $\Delta\mathbf{R}$ can be computed from Eq. (4.63). The current nodal forces, current nodal displacements, and current basic element deformations are updated as:

$$\begin{aligned} \mathbf{R}_{i+1} &= \mathbf{R}_i + \Delta\mathbf{R} \\ \mathbf{U}_{i+1} &= \mathbf{U}_i + \Delta\mathbf{U} \\ \bar{\mathbf{U}}_{i+1} &= \bar{\mathbf{U}}_i + \Delta\bar{\mathbf{U}} \end{aligned} \tag{4.69}$$

With this element state determination procedure, all residuals at element level are sent to the global structure level. Therefore, iterations are conducted only at the global level, thus easing the model implementation. A more refined element state determination procedure in which iterations are also performed at element level is proposed by several researchers (e.g. Simo et al. 1993; Spacone et al. 1996; etc.).

4.6 Model Evaluation by Benchmark Examples

Seven numerical examples are used to verify the accuracy and show the efficiency of the proposed geometrically nonlinear frame element as well as the solution marching schemes available in FEAP (Taylor 2000). The correlation studies are performed by comparing the obtained numerical results with the analytical and experimental results. For the first two examples, the numerical results obtained with the proposed model are also compared with those obtained with two different frame models. For the sake of brevity, the proposed frame model is abbreviated as the *CR-HR-EBvK* model while other two frame models are abbreviated as the *CR-DB-EB* and the *CR-DB-EBvK* models. For the *CR-DB-EB* model, the element formulation within the basic system is based on the displacement-based Euler-Bernoulli frame element and the corotational framework is used to describe the global element kinematics. Detailed formulation of the *CR-DB-EB* model is presented in Urthaler and Reddy (2005). For the *CR-DB-EBvK* model, the element formulation within the basic system is based on the displacement-based Euler-Bernoulli-von Karman frame element as given by

Hjelmstad and Taciroglu (2003) and the corotational framework is used to describe the global element kinematics.

4.6.1 Example I: Cantilever Beam Subjected to an End-Point Load

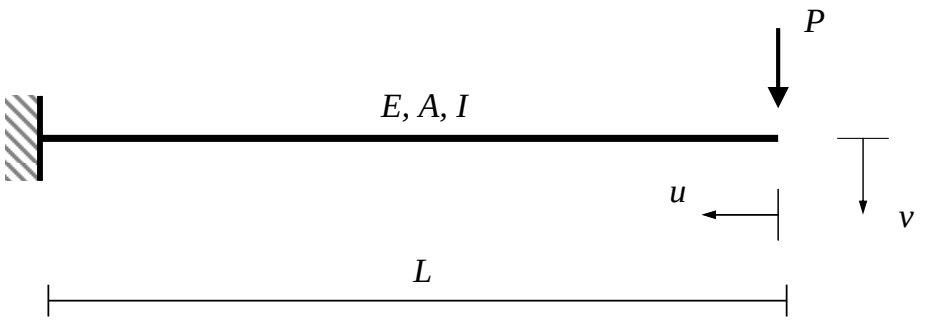

Figure 4-7 Example I: Cantilever Beam Subjected to an End-Point Load

A cantilever beam subjected to an end-point load shown in Figure 4-7 is employed to illustrate the ability and accuracy of the proposed element to model a beam experiencing considerable large displacements compared to its initial length and showing unlimited hardening behavior. This beam system is considered a "*classic*" benchmark since it has been widely used by several researchers to evaluate their nonlinear frame models (Iura 1994; Jiang and Olson 1994; Urthaler and Reedy 2005). It consists of an prismatic beam with cross section area $A = 1.27 \times 10^{-2}\ m^2$, moment of inertia $I = 3.66 \times 10^{-6}\ m^4$, length $L = 4\,m$, and elastic modulus $E = 200\,GPa$. The displacement-control method is used to trace the equilibrium path of the system. The target value of the vertical displacement v is 3.2 m corresponding to approximately 80 % of the beam initial length.

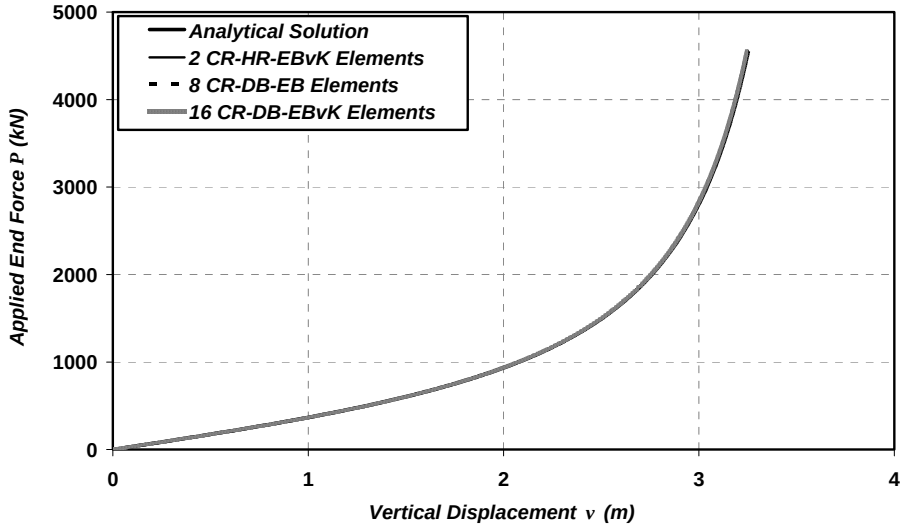

(a)

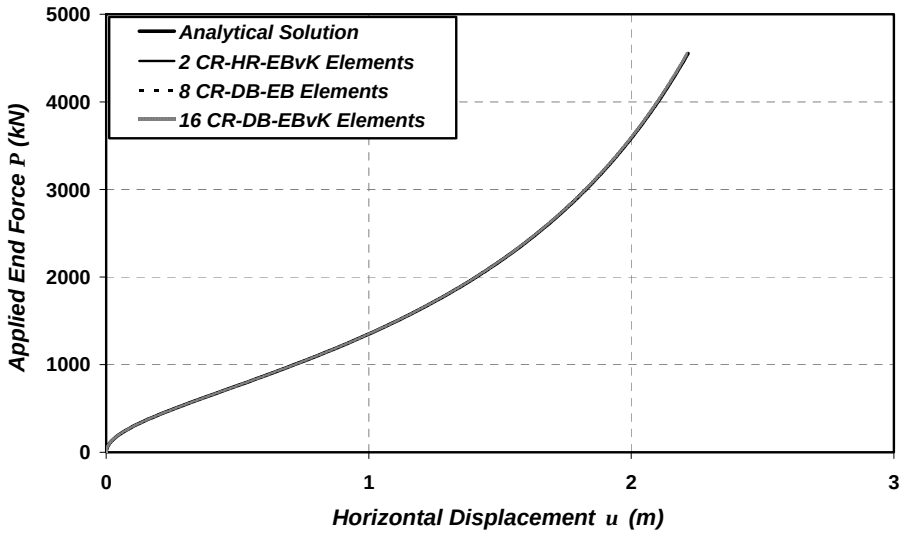

(b)

Figure 4-8 Load-Displacement Responses for Example I: (a) End Point Load-Vertical Displacement Diagram; B) End Point Load-Horizontal Displacement Diagram

Figures 4-8 (a) and (b) compare the numerical results obtained by three models with the analytical results for the end point load-vertical displacement and end point load-horizontal displacement responses, respectively. The analytical results for this problem were given by Bisshop and Drucker (1945) based on elliptical integrals. These plots indicate that only 2 *CR-HR-EBvK* elements are needed to match the analytical responses while 8 *CR-DB-EB* and 16 *CR-DB-EBvK* elements are required to obtain the same degree of accuracy. It is noted that even though the local beam theory of the *CR-DB-EBvK* model is more refined than that of the *CR-DB-EB* model, its accuracy is hampered by the membrane locking phenomenon (Reddy 2004). Comparing between the *CR-HR-EBvK* and *CR-DB-EB* models, it is confirmed that the local geometrical nonlinearity embedded in the *CR-HR-EBvK* model greatly enhance the element accuracy.

4.6.2 Example II: Cantilever Beam Subjected to an End Moment

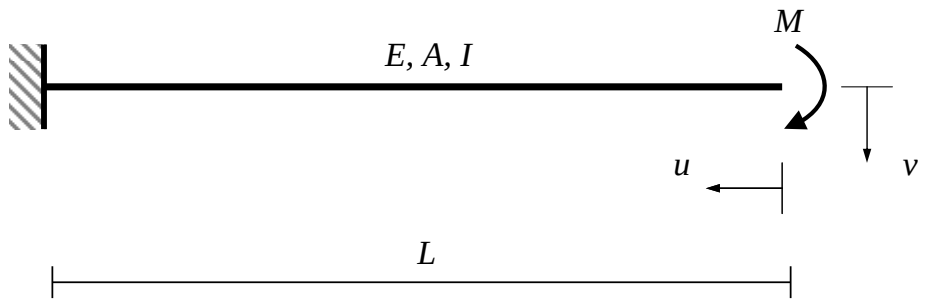

Figure 4-9 Example II: Cantilever Beam Subjected to an End Moment

The same cantilever beam of Figure 4-7 is subjected to an end moment as shown in Figure 9. This beam system is used to demonstrate the large-rotational capability and accuracy of the proposed element under extreme inextensible bending action. This

beam system is also considered a "*classic*" benchmark since it has been widely used by several researchers to evaluate their nonlinear frame models (Saje 1990; Lee 1997; Urthaler and Reedy 2005). Under an applied end moment M_{end}, this cantilever is rolled up one time into a circle when $M_{end} = M_{circle} = 2\pi\left(IE/L\right)$, two times into two circles when $M_{end} = 2M_{circle}$, and so on. The load-control marching scheme is used to trace the equilibrium path of the system. To show the robustness of the proposed element under arbitrarily large rotations, the target value of the end moment M is set to $3M_{circle} = 3450\ kN-m$, thus curling the beam around the fixed end three times.

Figures 4-10 (a) and (b) show the correlation studies between the numerical results obtained by the three models and the analytical results, respectively for the end moment-horizontal displacement and the end moment-vertical displacement responses. The analytical results for this problem were given by Saje and Srpčič (1985) based on the integral solution to the nonlinear differential equations. From these plots, it is shown that only 8 *CR-HR-EBvK* elements are needed to match the analytical responses while 16 *CR-DB-EB* and 32 *CR-DB-EBvK* elements are required to obtain the same degree of accuracy. During the convergence study, it is found that only 2 and 4 *CR-HR-EBvK* elements are sufficient to trace the equilibrium paths for the cases of the beam rolled up one-time and two-times, respectively. Comparing these three frame models, it is found that the accuracy of the *CR-DB-EBvK* model is degraded by the membrane locking and the superiority of the *CR-HR-EBvK* model is due to the local geometrical nonlinearity.

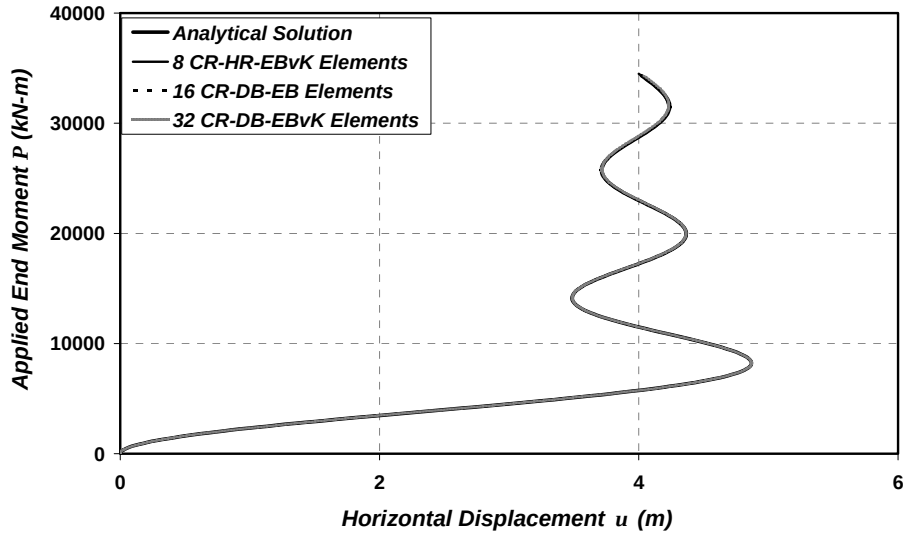

(a)

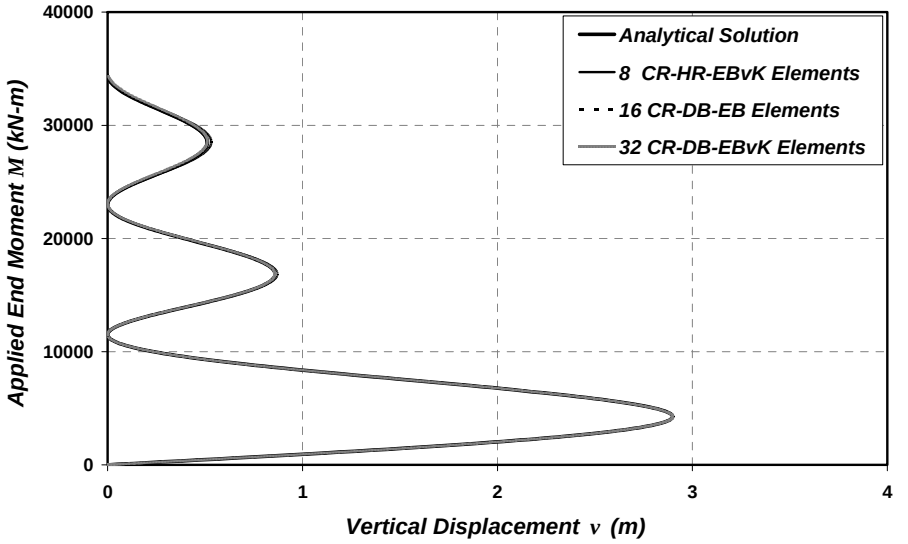

(b)

Figure 4-10 Load-Displacement Responses for Example II: (a) End Moment-Horizontal Displacement Diagram; (b) End Moment-Vertical Displacement Diagram

4.6.3 Example III: Williams' Toggle Frame

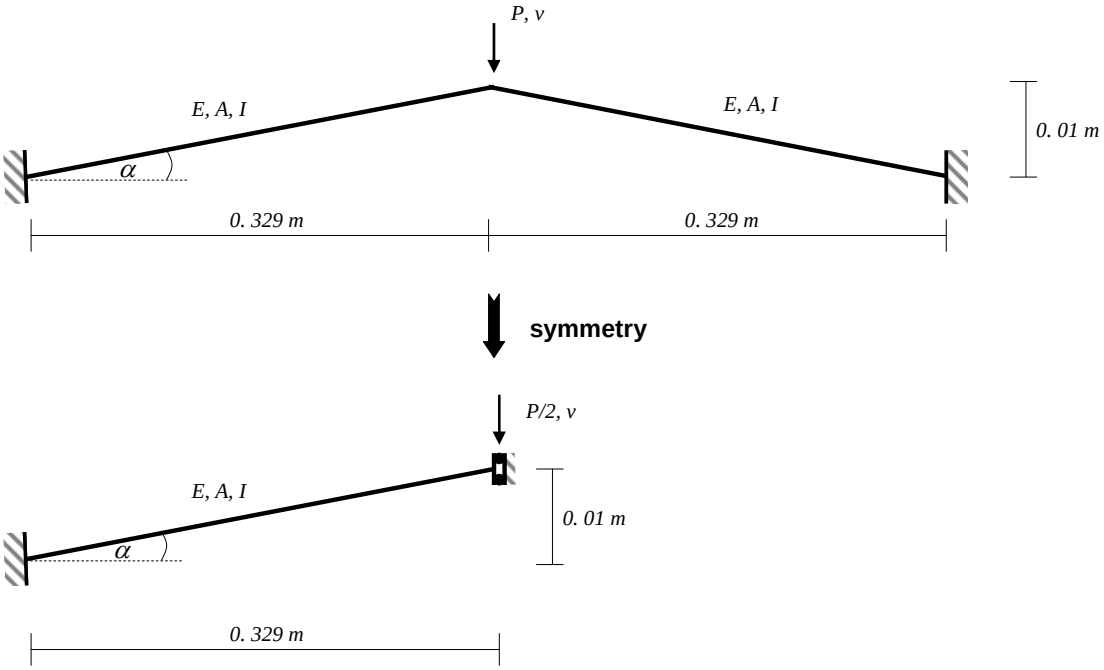

Figure 4-11 Example III: Williams' Toggle Frame [50]

The toggle frame shown in Figure 4-11 was analytically and experimentally studied by Williams (1964). This frame serves as a benchmark example to show the ability and efficiency of the proposed model to handle a snap-through instability phenomenon and has been investigated by several researchers (Powell 1969; Yang and Chiou 1987; Nanakorn and Vu 2006). It consists of two identical frame members with cross section area $A = 1.14 \times 10^{-4}\ m^2$, moment of inertia $I = 3.42 \times 10^{-10}\ m^4$, length $l = 0.3292\ m$, and elastic modulus $E = 71\ GPa$. The rise angle α is 1.74^0 and is corresponding to an aspect ratio of 0.0304. Since the aspect ratio is low, this toggle frame structure is considered shallow. Due to symmetry, only one-half of the toggle is modeled. To overcome the limit point, the displacement-control marching scheme is used to trace the equilibrium path of the system. The target vertical

displacement v_{target} is 0.018 *m*.

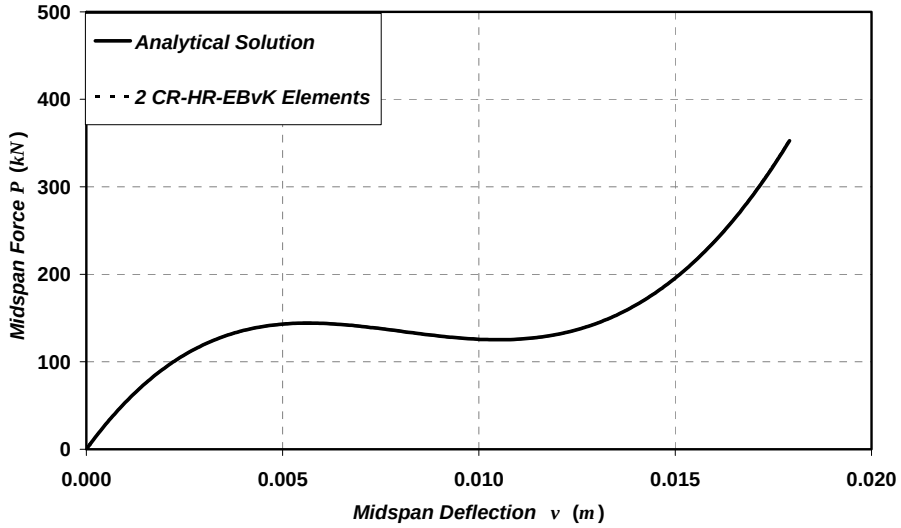

Figure 4-12 Equilibrium Path for Example III

Figure 12 compares the numerical results obtained by the proposed model with the analytical result for the midspan load-vertical displacement response. The analytical result for this problem was given by Williams (1964). From Figure 12, it is observed that only 2 *CR-HR-EBvK* elements are needed to match the analytical response.

4.6.4 Example IV: Jenkins et al.'s Diamond Frame

A pinned-fixed diamond frame shown in Figure 4-13 was analytically and experimentally investigated by Jenkins et al. (1966). Several researches (Mattiasson 1981; Coda and Greco 2004; Rungamornrat and Tangnovarad 2011) have used this frame as a caliber to evaluate their proposed frame models. It consists of four identical frame members with cross section area $A = 1000$, moment of inertia $I = 1$, length $L = 1$, and elastic modulus $E = 1$ and is subjected to tension and compression as shown in Figures 13 (a) and (b), respectively. Due to symmetry, only one-half of the frame is considered. The load-control marching scheme is used to trace the

equilibrium path of the system. The target value of the point load P is 10.

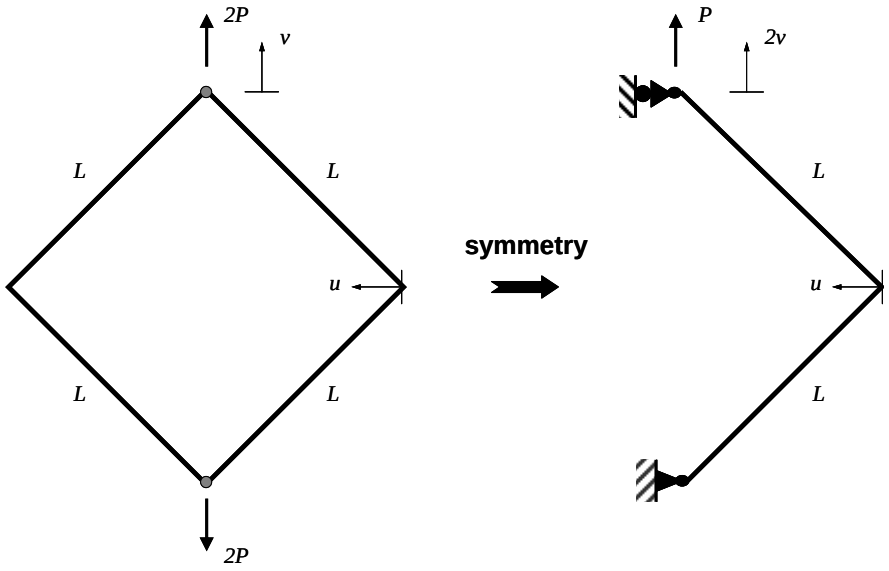

A)

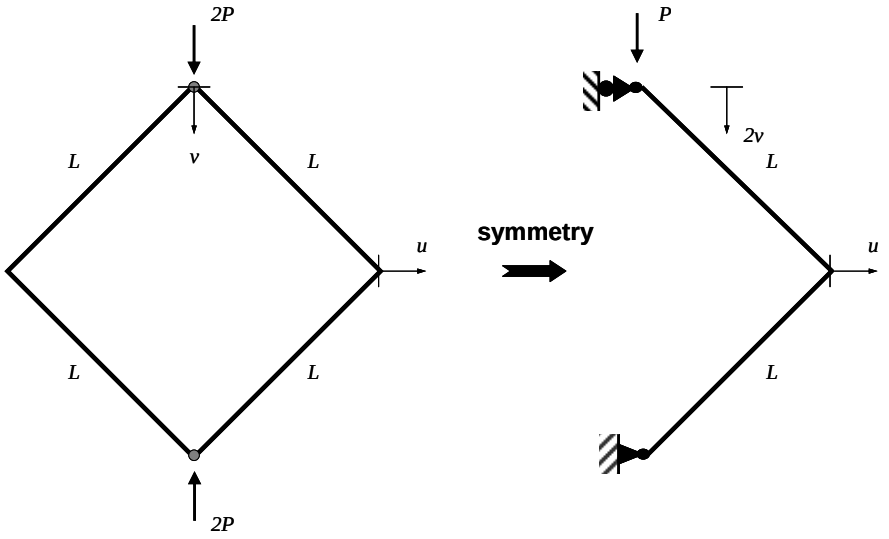

B)

Figure 4-13 Example IV: Jenkins et al.'s Diamond Frame [53]: (a) Tension; (b) Compression

Figures 4-14 (a) and (b) compare the numerical results obtained by the proposed model with the analytical results for the case of the diamond frame under tension. The

analytical results were given by Jenkins et al. (1966) using elliptic integrals. These plots show the point load-vertical displacement and point load-horizontal displacement. Only 2 *CR-HR-EBvK* elements per frame member are needed to resemble the analytical responses.

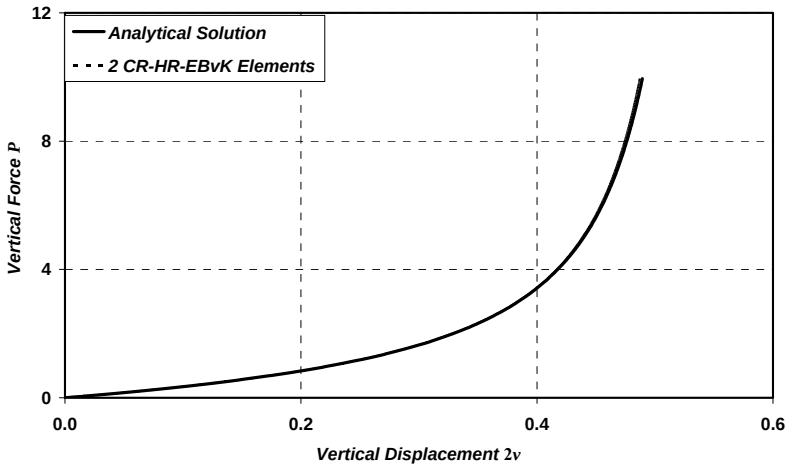

A)

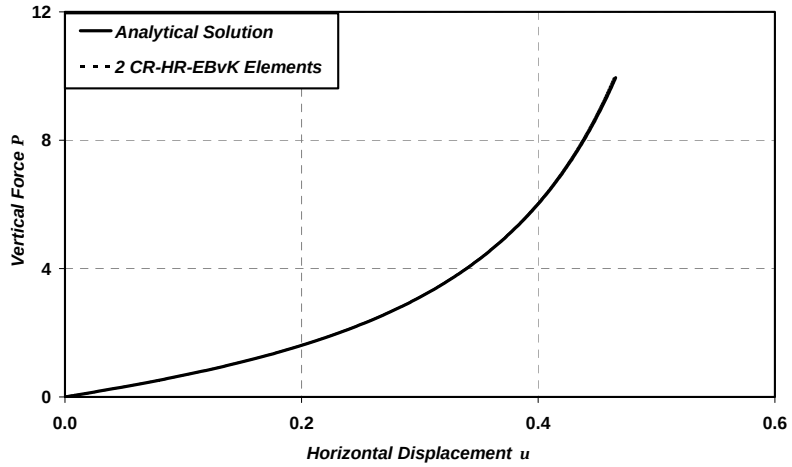

B)

Figure 4-14 Load-Displacement Responses for Example IV under Tension: (a) Load-Vertical Displacement Diagram; (b) Load-Horizontal Displacement Diagram

Figures 4-15 (a) and (b) superimpose the numerical results obtained by the proposed model with the analytical results for the case of the diamond frame under compression. These plots show the point load-vertical displacement and point load-horizontal displacement responses. Only 2 *CR-HR-EBvK* elements per frame member are sufficient to match the analytical responses.

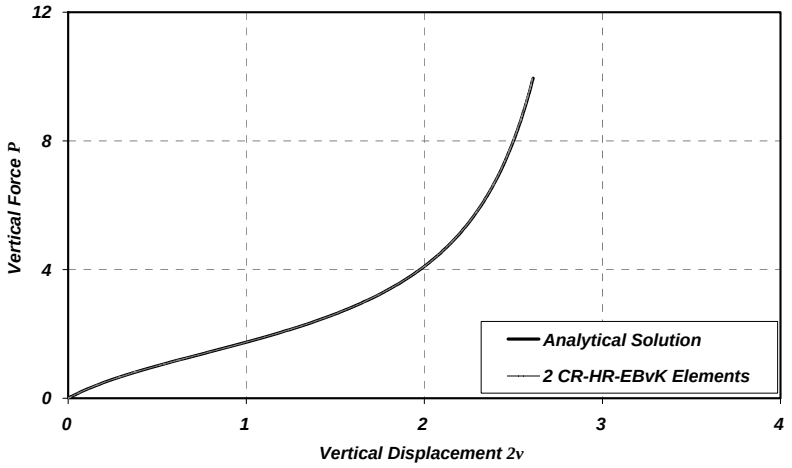

(a)

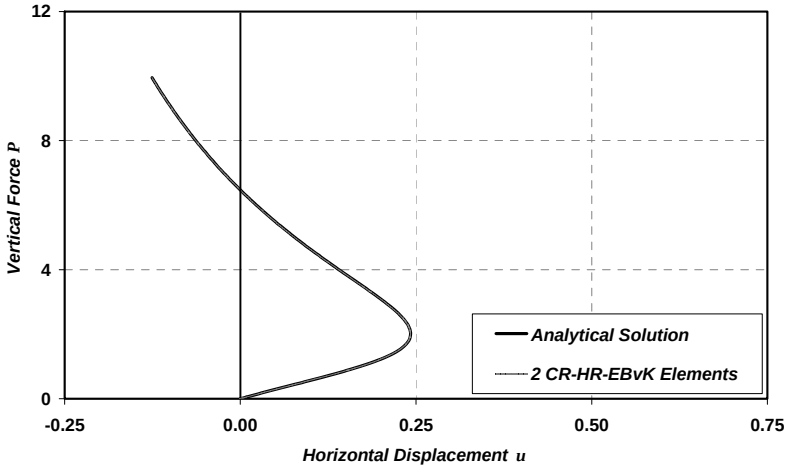

(b)

Figure 15 Load-Displacement Responses for Example IV under Compression: A) Load-Vertical Displacement Diagram; B) Load-Horizontal Displacement Diagram

4.6.5 Example V: Lee et al.'s Frame

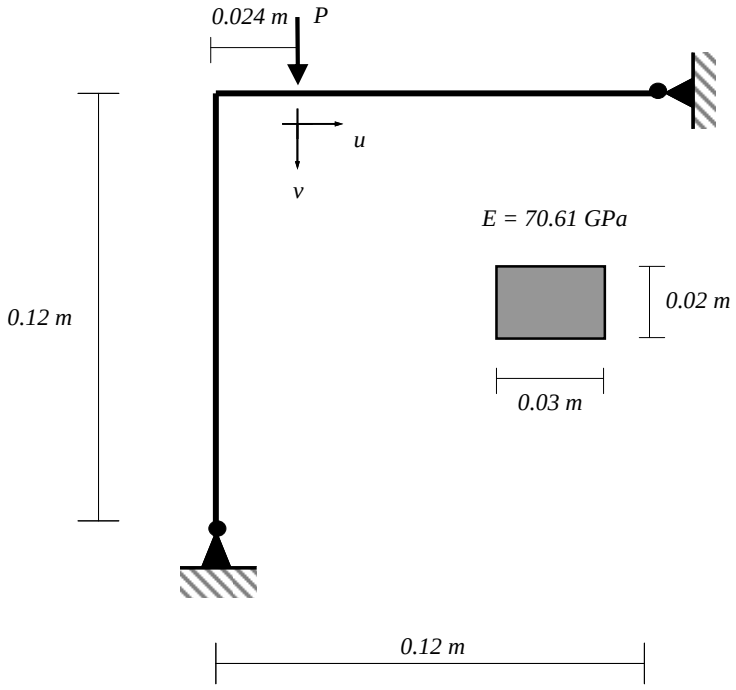

Figure 4-16 Example V: Lee et al.'s Frame

The analytical solution to the frame problem shown in Figure 4-16 was given by Lee et al. (1968). Numerous researchers (Waszczyszyn and Janus-Michalska 1998) have employed this frame example to assess their model capability to handle a snap-back instability phenomenon. Numerically, the snap-back instability phenomenon is one of the most challenging problems in nonlinear structural analysis. A good explanation of this kind of elastic instability can be found in the textbook by Bazant and Cedolin (1991). The geometric and material properties of the frame are given in Figure 4-16. To cope with the snap-back instability phenomenon, the arc-length control marching scheme is used to trace the equilibrium path of the system.

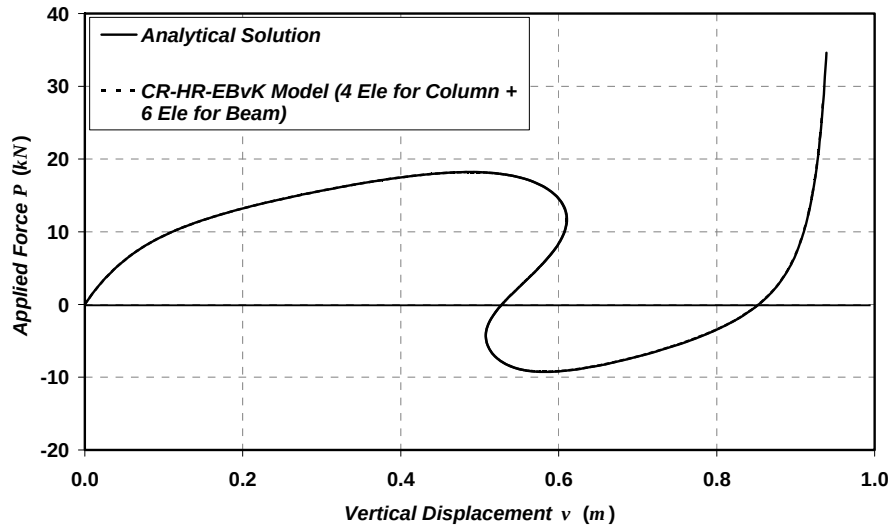

(a)

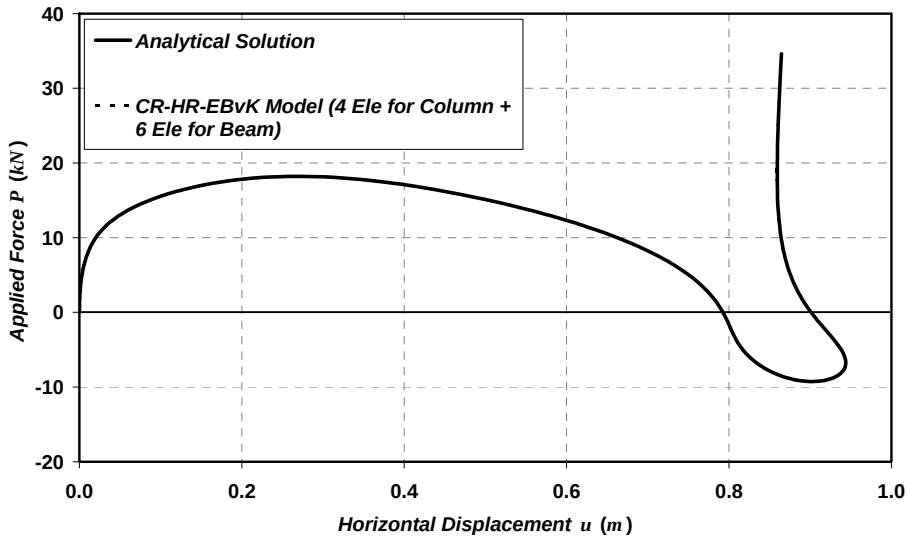

(b)

Figure 4-17 Load-Displacement Responses for Example V under Compression: (a) Load-Vertical Displacement Diagram; (b) Load-Horizontal Displacement Diagram

Comparison between the analytical and the numerical responses is shown in Figures 4-17 (a) and (b) for the point load-vertical displacement and point load-horizontal

displacement responses. The column is modeled with 4 *CR-HR-EBvK* elements while the beam is discretized by 6 *CR-HR-EBvK* elements with 2 elements to the left of the point load and 4 elements to the right of the point load. Good agreement between the analytical and the numerical responses is clearly observed.

4.6.6 Example VI: El Zanaty's Portal Frame with Stiffness Softening

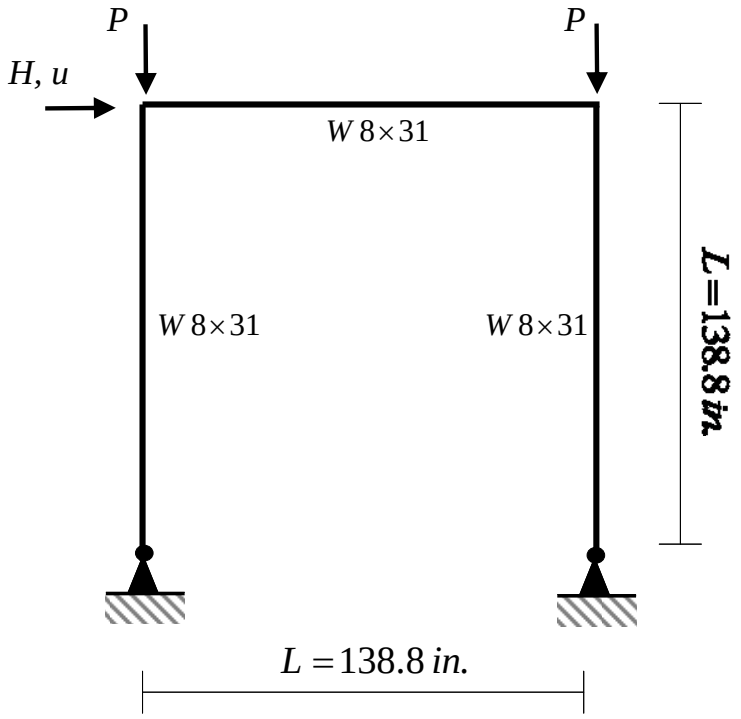

Figure 4-18 El Zanaty's Portal Frame Test Set Up

The steel portal frame shown in Figure 4-18 was first employed by El Zanaty et al. (1980) as a test case for 2^{nd} -order analysis simulations. Subsequently, this frame has served as a benchmark example to show the ability and efficiency of the proposed model to handle a frame structure with softening stiffness and has been investigated by several researchers (e.g. White, 1985; King et al., 1992; Attalla et al., 1994; Chen

and Chan, 1995). The frame is consists of three steel wide flange members $W\,8\times31$ (two columns and one beam) with length $L=138.8\,in.$, elastic modulus $E=29\times10^{3}\,ksi$, and yield stress $\sigma_y=36$ ksi. The resulting column slenderness ratio L/r_x is 40. To account for the residual-stress effects, a linear distribution pattern with a peak tensile residual stress σ_{rt} of 6.78 ksi and a peak compressive residual stress σ_{rc} of 10.8 ksi is assumed as suggested by Ketter et al. (1955). The fiber-section model is employed to account for the sectional nonlinear response as well as the residual-stress effects. Thus, the wide-flange section of a frame member is subdivided into three regions, namely; web, top flange, and bottom flange. Ten steel fibers are used to discretize each flange region while twenty steel fibers are employed to discretize the web region. As shown in Figure 4-18, the frame is first loaded by two constant gravity loads *P*, Subsequently, an applied lateral load *H* exerts monotonically. To investigate the effects of column axial forces on the frame response, three values of gravity loads *P* are considered: $0.2P_y$, $0.4P_y$, and $0.6P_y$.

Figure 4-19 shows the lateral load-displacement response curves under different values of gravity loads ($0.2P_y$, $0.4P_y$, and $0.6P_y$). On the same diagram, the responses obtained with the stiffness-based model proposed by King et al. (1992) are also superimposed. Obviously, only 2 CR-HR-EBvK elements per frame member are sufficient to model the system responses.

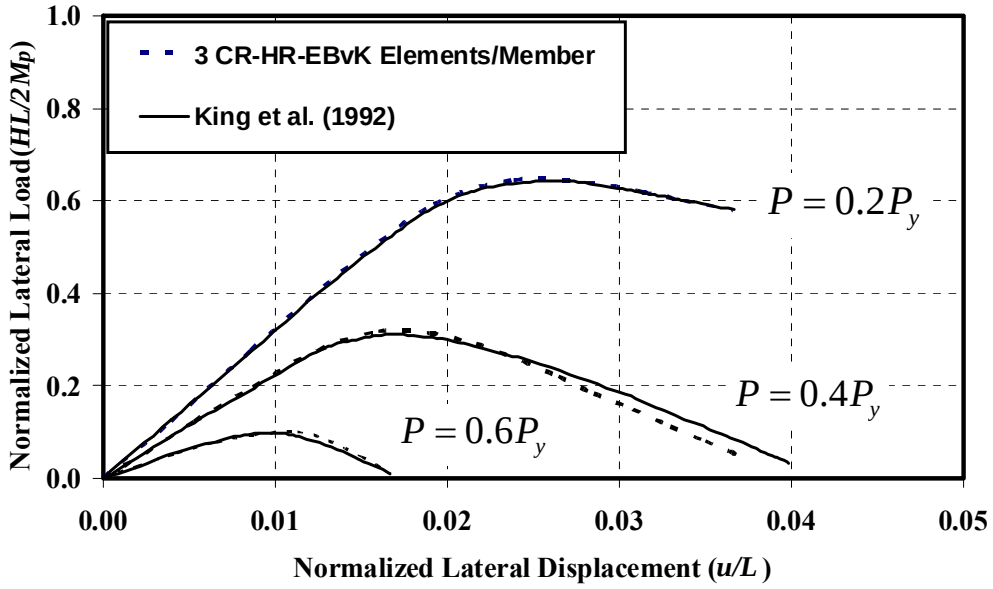

Figure 4-19 Lateral Load-Displacement Response Curves for El Zanaty's Portal Frame

4.6.7 Example VII: Bazan' s Two-Span Beam Specimen

Figures 4-20 and 4-21 show a 3/8th scaled model of a continuous two-span reinforced concrete beam specimen tested by Bazan (2008). This specimen is a part of the exterior frame of an RC building where an exterior column underlying the upper beam is lost. The correlation study between experimental and numerical results of this beam is performed to assess the model capability to simulate the catenary actions in reinforced concrete beams when subjected to large displacements. This capability is an essential feature of the proposed frame model in studying the progressive collapse resistance of a reinforced concrete frame. Figure 4-22 shows the reinforcement detail of the 3/8th scaled continuous two-span reinforced concrete beam specimen.

Figure 4-20 Bazan' s 3/8th Scaled Two-Span Beam Specimen (Bazan, 2008)

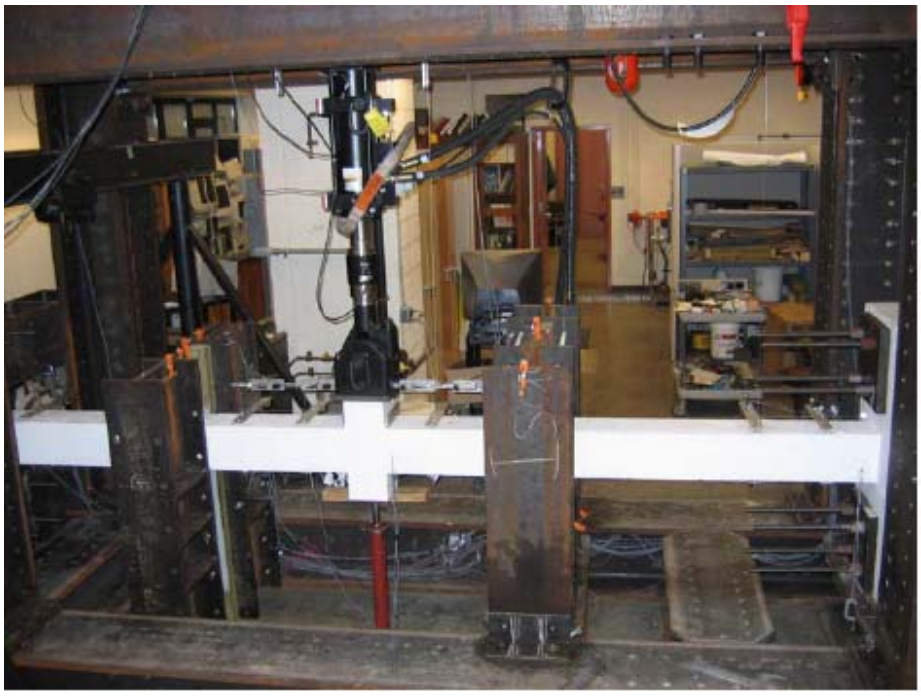

Figure 4-21 Bazan' s Two-Span Beam Specimen Installed on Steel Reaction Frame (Bazan, 2008)

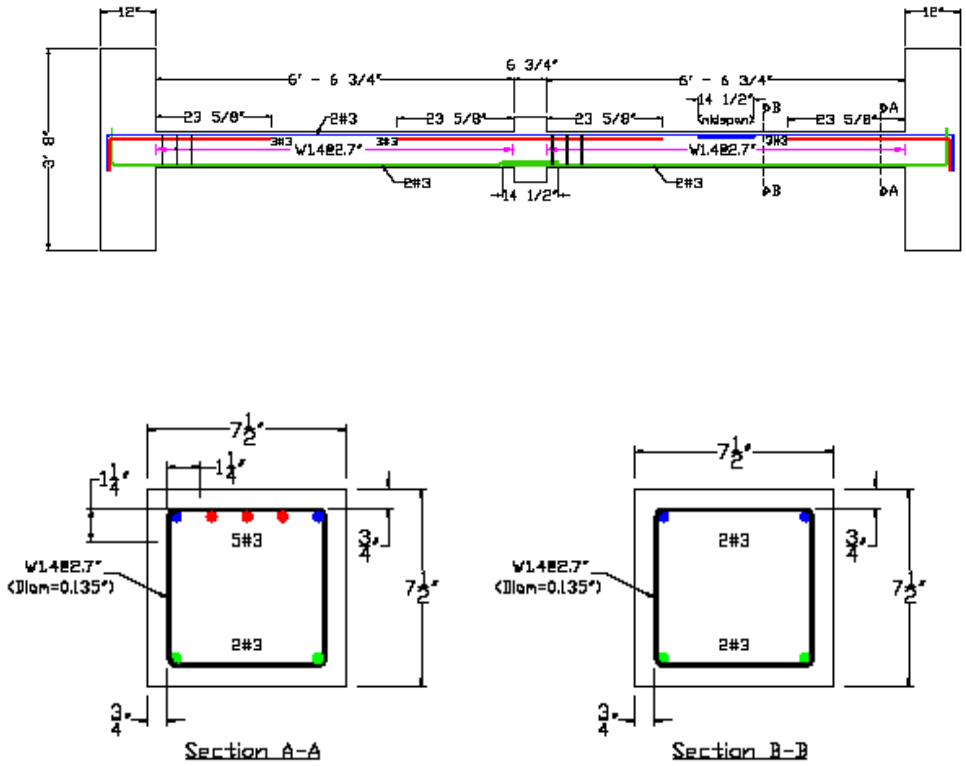

Figure 4-22 Reinforcement Detail of Bazan' s Two-Span Beam Specimen (Bazan, 2008)

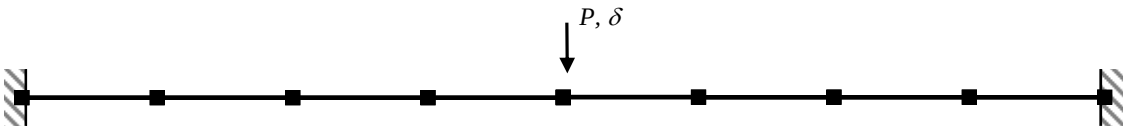

Figure 4-23 Finite Frame Element Discretization of Bazan's Two-Span Beam Specimen

Figure 4-23 shows the finite-element mesh of Bazan's two-span beam specimen. Each beam span is modeled by four proposed frame elements. The fiber section and

material constitutive laws for concrete and steel discussed in Chapter 2 are used to represent the beam sectional response.

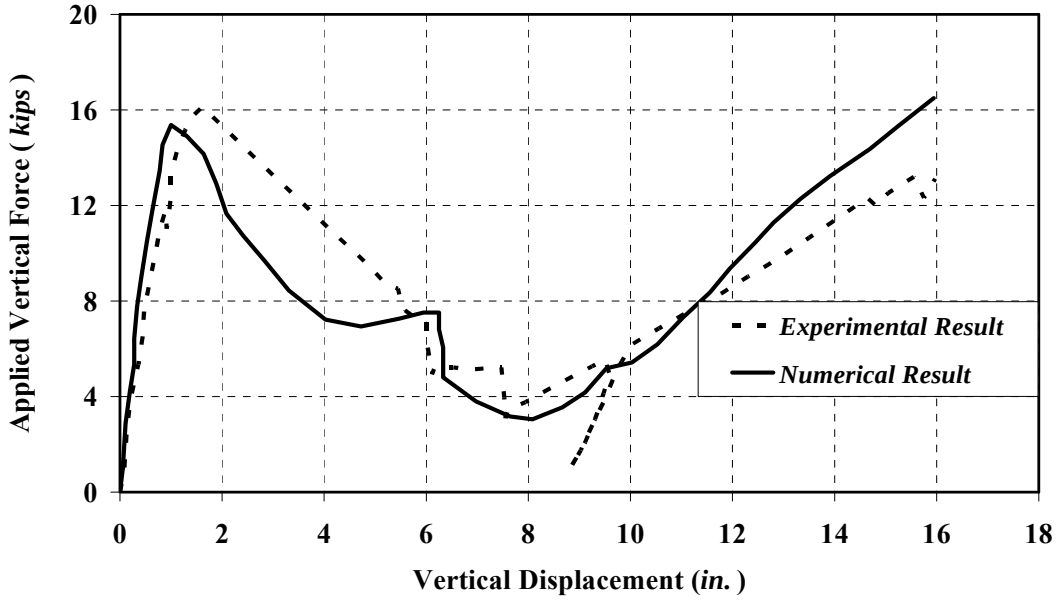

Figure 4-24 Comparison between Experimental and Numerical Results

Comparison between the analytical and the numerical responses is shown in Figure 4-24. These plots show the point load-vertical displacement responses. Generally, the proposed model can match well the experimental response. The sudden drops are associated with the fracture of the two bottom reinforcing bars.

CHAPTER 5
SUMMARY AND CONCLUSIONS

5.1 Total Lagrangian Formulation of Planar Bar Element Using Vectorial Kinematical Description

Based on the total Lagrangian formulation, a geometrically nonlinear bar element is developed. This bar model is suitable to analyze large displacement problems of plane truss structures. The vectorial form is used to describe the element kinematics. Within the total Lagrangian framework, the Green-Lagrange axial strain is employed to measure the element strain while the 2^{nd} Piola-Kirchhoff axial stress is employed to measure the element stress. Only linear elastic material law is of interest in this work. However, the model can naturally be extended to account for other more complex material behaviors (e.g. elastic-plastic, nonlinear elastic, etc.). The element equilibrium is expressed in the weak form through the nonlinear virtual displacement function. The tangent element stiffness matrix and the element resistant force vector are consistently derived by linearization of the virtual displacement function using the directional derivative operator (Gâteaux operator). In the solution process of solving nonlinear equilibrium equations, the generalized displacement control method is adopted and implemented into the in-house nonlinear structural analysis program.

Five numerical examples presented prove the accuracy of the proposed bar element and the efficiency of the implemented solution algorithm. Examples I and II are small truss systems. They are analyzed to show that the proposed model as well as the implemented solution procedure can cope with the snap-through and snap-back instability phenomena, respectively. Examples III and IV are larger truss systems and

are composed of 35 members. Both Kondoh and Atluri (1983) and Torkamani and Shieh (2011) used these two examples to assess their models, as well as the adopted solution procedures. The ability of the proposed model to predict the global pre-buckling and post-buckling responses of truss systems is verified in Examples III and IV. The obtained results are in good agreements with those obtained by Kondoh and Atluri (1983) and Torkamani and Shieh (2011). Example V shows the ability of the proposed model to resemble the response of a cantilever beam subjected to large displacements at its free end.

In summary, the development of the proposed bar element is a step forward in establishing a computational framework that permits large-displacement and post-buckling analyses of plane truss structures. Several truss examples are used to show the validity of the model. Therefore, the in-house nonlinear structural analysis program developed here can be used as a vital tool in the implementation of the newly proposed Performance-Based Design and Assessment Methodology.

5.2 Finite Frame Element for Large Displacement Elastic and Inelastic Analyses of Frame Structures

This work presents a simple but efficient nonlinear frame element for large displacement and large rotation analyses of elastic planar frame structures. The corotational framework is used to describe the element kinematics and kinetics at the global level while the local element response is derived based on the Euler-Bernoulli-von Karman beam theory. The Hellinger-Reissner mixed functional is used to construct the locking-free Euler-Bernoulli-von Karman frame element within the basic system. The basic element stiffness matrix and basic element force vector are obtained by linearization of the Hellinger-Reissner mixed functional using the

directional derivative operator. The standard displacement interpolation functions for a linear frame element are used in the element formulation. In accordance with theses assumed displacement interpolation functions, the force interpolation functions can be derived such that the governing differential equations are satisfied in the point-wise sense. Only linear elastic material law is of interest in this work. However, the model can naturally be extended to account for other more complex material behaviors (e.g. elastic-plastic, nonlinear elastic, etc.).

Seven benchmark structures are employed to prove the accuracy and efficiency of the proposed frame element. Examples I and II are benchmark examples of large displacement and rotation problems and consist of a single cantilever beam subjected respectively to an end force and an end moment. Correlation studies show that the proposed model is very accurate and efficient in resembling the analytical results and is not prone to the membrane-locking problem. The ability and efficiency of the proposed model to handle the snap-through instability phenomenon are shown in Example III. A pinned-fixed square diamond frame in Example IV is analyzed to demonstrate that the proposed model can handle the problem of small strains and moderately large displacements with efficiency. The ability and efficiency of the proposed model to cope with the snap-back instability phenomenon are shown in Example V. The ability of the proposed model to cope with the inelastic responses of steel and reinforced concrete frame structures is shown in Examples VI and VII, respectively.

In summary, the development of the proposed frame element is a step forward in establishing a computational framework that permits large displacement and rotation analyses of elastic plane frames. Several benchmark examples are used to show the validity and efficiency of the model. The next steps in this direction are to apply the

proposed model to assess the vulnerability of framed structures against progressive collapse scenarios induced by extreme catastrophic events (e.g. rare earthquakes, terrorist attacks, egregious construction errors, etc.).

REFERENCES

-Agardh, L. (1974). “Analytical and Numerical Analyses of Nonlinear Beam Elements with Special Consideration of Initial and Numerical Errors.” *PhD Dissertation*, Chalmers Tekniska Hogskola, Goteborg, Sweden.

-Anagnostopoulos, S. A. (1981). “Inelastic Beams for Seismic Analyses of Structures.” *Journal of the Structural Division, ASCE*, 107(7), 1297-1311.

-Argyris, J.H., Kelsey, S., and Kamel, H. (1964). ***Matrix Methods of Structural Analysis: a Precis of Recent Development***., Pergomon Press, Oxford, UK.

-Attalla, M.R., Deierlein, G.G., and McGuire, W. (1994). “Spread of plasticity: quasi plastic-hinge approach.” *Journal of Structural Engineering, ASCE*, 120, pp. 2451 2473.

-Belytschko, T., Liu, W.K., and Moran, B. (2000). “***Nonlinear Finite Elements for Continua and Structures.***” John Wiley & Sons Inc., New York, USA.

-Bathe, K.J., Ramm, E., and Wilson, E.L. (1975). “Finite Element Formulations for Large Deformation Dynamic Analysis.’, *International Journal for Numerical Methods in Engineering*, 9(2), pp. 353-386.

-Bathe, K.J. and Bolourchi, S. (1979). “Large Displacement Analysis of Three-Dimensional Beam Structures.”, *International Journal for Numerical Methods in Engineering*, 14(7), pp. 961-986.

-Bathe, K.J. (1996). ***Finite Element Procedures***. Prentice-Hall, Englewood Cliffs, New Jersey, USA.

-Batoz, J.L. and Dhatt, G. (1979). “Incremental displacement algorithm for nonlinear problems.” Int. J. Num Meth. Engng., Vol. 14, pp. 1262-1266.

-Bazan, M.L. “Response of Reinforced Concrete Elements and Structures Following Loss of Load Bearing Elements.” *Ph.D. Dissertation*, Department of Civil and Environmental Engineering, Northeastern University, Boston, USA.

-Bazant, Z.P. and Cedolin, L. (1991). Stability of Structures: Elastic, Inelastic, Fracture, and Damage Theories, Oxford University Press, New York, USA.

-Belytschko, T. and Hsieh, B.J. (1973). “Nonlinear transient finite element analysis with convected coordinates”, *International Journal for Numerical Methods in Engineering*, Vol. 7, pp. 255-271.

-Belytschko, T. and Glaum, L.W. (1979). “Applications of Higher Order Corotational Stretch Theories to Nonlinear Finite Element Analysis.”, *Computers and Structures*, 10, pp. 175-182.

-Belytschko, T., Liu, W.K., and Moran, B. (2000). ***Nonlinear Finite Elements for Continua and Structures***. John Wiley & Sons Inc., New York, USA.

-Bertero, V. V., Aktan, A. E., Charney, F. A., and Sause, R. (1984). Earthquake Simulation Tests and Associated Studies of a 1/5th-Scale Model of a 7-story R/C Frame-Wall Test Structure.” *EERC Report 84-05*, Earthquake Engineering Research Center, University of California, Berkeley.

-Berke, L. and Mallet, R.H. (1969). “Automated large deflection and stability analysis of three-dimensional structures.” In: Mar I, Liebowitz H (eds) Structures Technology for Large Radio and Radar Telescope Systems, MIT Press, Huntisville, Alabama, USA, pp. 343-381.

-Bisshop, K.E. and Drucker, D.C. (1945). “Large Deflections of Cantilever Beams.”, *Quarterly of Applied Mathematics*, 3, pp. 272-275.

-Chan, S.L. (1988). “Geometric and Material Non-Linear Analysis of Beam-Columns and Frames Using the Minimum Residual Displacement Method.”, *International Journal for Numerical Methods in Engineering*, 26(12), pp. 2657-2669.

-Chapman, S.J. (2005). MATLAB Programming for Engineers, Thomson, Australia.

-Charney, F. A. and Bertero, V. V. (1982). “An Evaluation of the Design and Analytical Seismic Response of a Seven-Story Reinforced Concrete Frame-Wall Structure.” *EERC Report 82-08*, Earthquake Engineering Research Center, University of California, Berkeley.

-Chen, W.F. and Chan, S.L. (1995). “Second-order inelastic analysis of steel frames using element with midspan and end springs.”, *Journal of Structural Engineering, ASCE*, 121, pp. 530-541.

-Ciampi, V. and Carlesimo, L. (1986). "A Nonlinear Beam Element for Seismic Analysis of Structures." *8th European Conference on Earthquake Engineering*, Lisbon, 6.3/1986, pp. 73-80.

-Cichon, C. (1984). “Large displacements in-plane analysis of elastic-plastic frames”, *Computers and Structures*, Vol. 19, No. 5-6, pp. 737-745.

-Clough, R.W., Benuska, K. L., and Wilson, E. L. (1965). “Inelastic Earthquake Response of Tall Buildings.” *Proceedings of the Third World Conference on Earthquake Engineering*, Vol. II, pp. 68-89, Wellington, New Zealand.

-Coda, H.B. and Greco, M. (2004). “A simple FEM formulation for large deflection 2D frame analysis based on position description”, *Computer Methods in Applied Mechanics and Engineering*, Vol. 193, pp. 3541-3557.

-Comite Euro-International du Beton (1996). “RC Frames under Earthquake Loading.” State of the Art Report: Task Group III/6, Thomas Telford Publishing, London, UK.

-Crespo Da Silva, M.R.M. (1988). “Nonlinear Flexural-Torsional-Extensional Dynamics of Beams.”, *International Journal of Solids and Structures*, 24(12), pp. 1225-1234.

-Crisfield, M.A. (1981). “A fast incremental/iterative solution procedure that handles snap-through.” Comput. Struct., Vol. 13, No. 1-3, pp. 55-62.

-Crisfield, M.A. (1990). “A Consistent Corotaional Formulation for Nonlinear Three Dimensional Beam Elements.”, *Computer Methods in Applied Mechanics and Engineering*, 81, 131-150.

-Crisfield, M.A. (1991). Nonlinear Finite Element Analysis of Solids and Structures: Volume I, John Wiley & Sons, New York, USA.

-de Freitas, J.A.T. and Ribeiro, A.C.B.S. (1992). “Large displacement elastoplastic analysis of space trusses.” Comput. Struct., Vol. 44, No. 5, pp. 1007-1016.

-El-Zanaty, M.H., Murray, D.W., and Bjorhovde, R. (1980). “Inelastic Behavior of Multi-Story Steel Frames.”, Structural Engineering Report No. 83, University of Alberta, Edmonton, Alberta, Canada.

-Filippou, F. C., Popov, E. P., and Bertero, V. V. (1983). “Effects of Bond Deterioration on Hysteretic Behavior of Reinforced Concrete Joints.” *EERC Report 83-19*, Earthquake Engineering Research Center, University of California, Berkeley.

-Gattass, M. and Abel, J. (1987). “Equilibrium Considerations of the Updated Lagrangian Formulation of Beam-Column with Natural Concepts.”, *International Journal for Numerical Methods in Engineering*, 24(11), pp. 2119-2141.

-Geyer, S. and Groenwold, A.A. (2003). “On reduced integration and locking of flat shell elements with drilling rotations”, *Communications in Numerical Methods in Engineering*, Vol. 19, pp. 85-97.

-Giberson, M.F. (1967). “The Response of Nonlinear Multi-Story Structures Subjected to Earthquake Excitation.” *Earthquake Engineering Research Laboratory*, California Institute of Technology, Pasadena.

-Greco, M., Gesualdo, F.A.R., Venturini, W.S., and Coda, H.B. (2006). “Nonlinear

positional formulation for space truss analysis." Finite. Elem. Anal. Des., Vol. 42, pp. 1079-1086.

-Hellesland, J. and Scordelis, A.C. (1981). "Analysis of R/C Bridge Column under Imposed Deformations." *IABSE Colloquium*, Delphi, pp. 545-559.

-Hjelmstad, K.D. and Taciroglu, E. (2003). "Mixed variational methods for finite element analysis of geometrically non-linear, inelastic Bernoulli-Euler beams", *Communications in Numerical Methods in Engineering*, Vol. 19, pp. 809-832.

-Holzapfel, G.A. (2000). Nonlinear Solid Mechanics: A Continuum Approach for Engineering, John Wiley & Sons, West Sussex, England

- Hughes, T.J.R. and Pister, K.S. (1978). "Consistent linearization in mechanics of solids and structures", *Computers and Structures*, Vol. 8, pp. 391-397.

-Hughes, T.J.R. (1987), ***The Finite Element Method: Linear Static and Dynamic Finite Element Analysis***. Prentice-Hall, Englewood Cliffs, New Jersey, USA.

-ICC (2012). International Building Code, International Code Council, Country Club Hills, Illinois, USA.

-Iura, M. and Atluri, S.N. (1988). "Dynamic Analysis of Finitely Stretched and Rotated Three-Dimensional Space Curved Beams.", *Computers and Structures*, 29(5), pp. 875-889.

-Iura, M. (1994). "Effects of coordinate system on the accuracy of corotational formulation for Bernoulli-Euler's beam", *International Journal of Solids and Structures*, Vol. 31, No. 20, pp. 2793-2806.

-Jiang, J. and Olson, M.D. (1994). "Large elastic-plastic deformations of slender beams: corotational theory vs. von Karman theory", *Computational Mechanics*, Vol. 15, pp. 117-128.

-Jenkins, J.A., Seitz, T.B. and Przemieniecki, J.S. (1966). "Large deflections of diamond-shaped frames", *International Journal of Solids and Structures*, Vol. 2, pp. 591-603.

-Kent, D. C. and Park, R. (1971). "Flexural Members with Confined Concrete." *Journal of the Structural Division, ASCE*, 97 (7), pp. 1964-1990.

-Ketter, R.L., Kaminsky, E.L., and Beedle, L.S. (1995). "Plastic deformation of wide-flange beam columns.", *Transactions ASCE*, 120, pp. 1028-1069.

-King, W.S., While, D.W., and Chen, W.F. (1992). "Second-order inelastic analysis methods for steel-frame design." *Journal of Structural Engineering, ASCE*, 118,

pp. 408-428.

-Kondoh, K. and Atluri, S.N. (1985). “Influence of the local buckling on global instability: simplified, large deformation, post-buckling analysis of plane trusses.” Comput. Struct., Vol. 21, No. 4, pp. 613-627.

-Krenk, S., Vissing-Jorgensen, C., and Thesbjerg, L. (1999). “Efficient Collapse Analysis of Frames.”, *Computers and Structures*, 72, pp. 481-496.

-Lai, S. S., Will, G. T., and Otani, S. (1984). “Model for Inelastic Biaxial Bending of Concrete Members.” *Journal of Structural Engineering, ASCE,* 110(11), pp. 2563 2584.

-Lee, S., Manuel, F.S., and Rossow, E.C. (1968). “Large Deflections and Stability of Elastic Frames.”, *Journal of Engineering Mechanics Division, ASCE,* 2, pp. 521-547.

-Lee, K. (1997). “Analysis of large displacements and large rotations of three-dimensional beams by using small strains and unit vectors”, *Communications in Numerical Methods in Engineering*, Vol. 13, pp. 987-997.

-Lee, C.-L. and Filippou, F.C. (2009). “Frame Elements with Mixed Formulation for Singular Section Response.”, *International Journal for Numerical Methods in Engineering*, 78(11), pp. 1320-1344.

-Limkatanyu, S. (2002). “Reinforced Concrete Models with Bond-Interfaces for the Nonlinear Static and Dynamic Analysis of Reinforced Concrete Frame Structure.” *Ph.D. Dissertation*, Department of Civil, Environmental, and Architectural Engineering, University of Colorado, Boulder, USA.

-Limkatanyu, S. and Spacone, E. (2002). “Reinforced Concrete Frame Element with Bond Interfaces. Part I: Displacement-Based, Force-Based, and Mixed Formulations.” *Journal of Structural Engineering*, ASCE; V.128, No.3: 346-355.

-Limkatanyu, S. and Spacone, E. (2006). Frame Element with Lateral Deformable Supports: Formulation and Numerical Validation. *Computers and Structures*, 84(13-14), pp. 942-954.

-Mahin, S. A. and Bertero, V. V. (1975). “An Evaluation of Some Methods for Predicting Seismic Behavior of Reinforced Concrete Buildings.” *EERC Report 75/05*, Earthquake Engineering Research Center, University of California, Berkeley.

-Mallet, R.H. and Schmit, L.A. (1967). “Nonlinear structural analysis by energy search.” J. Struct. Div., ASCE., Vol. 93, No. 6, pp. 221-234.

-Malvern, L.E. (1969). ***Introduction to the Mechanics of a Continuous Medium***. Prentice-Hall, Englewood Cliffs, New Jersey, USA.

-Mattiasson, K. (1981). “Numerical Results from Large Deflection Beam and Frame Problems Analyzed by Means of Elliptic Integrals.”, *International Journal for Numerical Methods in Engineering*, 17, pp. 145-153.

-Milner, H.R. (1981). “Accurate finite element analysis of large displacements in skeletal frames”, *Computers and Structures*, Vol. 14, No. 3-4, pp. 205-210.

-Menegotto, M., and Pinto, P. E. (1973). “Method of Analysis for Cyclically Loaded Reinforced Concrete Plane Frames Including Changes in Geometry and Inelastic Behavior of Elements under Combined Normal Force and Bending.” *IABSE Symposium on Resistance and Ultimate Deformability of Structures Acted on by Well-Defined Repeated Loads*, Final Report, Lisbon.

-Nanakorn, P. and Vu, L.N. (2006). “A 2D Field-Consistent Beam Element for Large Displacement Analysis Using the Total Lagrangian Formulation.”, *Finite Elements in Analysis and Design*, 42, pp. 1240-1247.

-Oran, C. (1973). “Tangent Stiffness in Plane Frames.”, *Journal of Structural Division, ASCE*, 99(6), pp. 973-985.

-Pacoste, C. and Eriksson, A. (1997). “Beam Elements in Instability Problems.”, *Computer Methods in Applied Mechanics and Engineering*, 14, 163-197.

-Pai, P.F., Anderson, T.J., and Wheater, E.A. (2000). “Large-deformation tests and total- Lagrangian finite-element analyses of flexible beams, *International Journal of Solids and Structures*, Vol. 37, pp. 2951-2980.

-Papadrakakis, M. (1983). “Inelastic post-buckling analysis of trusses.” J. Struct. Div., ASCE., Vol. 109, No. 9, pp. 2129-2147.

-Perego, U.A. (2000). “A variationally consistent generalized variable formulation for enhanced strain finite elements”, *Communications in Numerical Methods in Engineering*, Vol. 16, pp. 151-163.

-Pignataro, M., Rizzi, N. and Luongo, A. (1991). *Stability, Bifurcation, and Post-Critical Behavior of Elastic Structures*, Elsevier.

-Powell, G.H. (1968). “Theory of Nonlinear Elastic Structures”, *Journal of Structural Division, ASCE*, 95(12), pp. 2687-2701.

-Prager, W. and Hodge, P. (1951). “***Theory of Perfectly Plastic Solids***.” John Wiley and Sons, New York.

-Rankin, C.C. and Brogan, F.A. (1984). “An Element-Independent Corotaional Procedure for the Treatment of Large Rotations”, *Collapse Analysis of Structures, ASME*, New York, USA.

-Reddy, J.N. (2002). *Energy Principles and Variational Methods in Applied Mechanics*, John Wiley & Sons.

-Reddy, J.N. (2005). ***An Introduction to the Finite Element Method***. 3rd Edition, McGraw-Hill Inc., New York, USA.

-Reddy, J.N. (2008). *An Introduction to Continuum Mechanics*, Cambridge University Press.

-Reissner, E. (1972). “On One-Dimensional Finite-Strain Beam Theory: the Plane Problem.”, Journal of Applied Mathematics and Physics, 23, pp. 795-804.

-Riks, E. (1972). “The application of Newton’s method to the problem of elastic stability.” J. Appl. Mech., Vol. 39, pp. 1060-1066.

-Rohde, F.V. (1953). “Large Deflections of a Cantilever Beam wit Uniformly Distributed Load.”, *Quarterly of Applied Mathematics*, 11, pp. 337-338.

-Rubiano-Benavides, N.R. (1998). "Predictions in the Inelastic Seismic Response of Concrete Structures Including Shear Deformations and Anchorage Slip." *Ph.D. dissertation*, Dept. of Civil Engineering, University of Texas, Austin.

-Rungamornrat, J. and Tangnovarad, P. (2011). “Analysis of linearly elastic inextensible frames undergoing large displacement and rotation”, *Mathematical Problems in Engineering*, Vol. 2011(592958), pp. 1-37.

-Saje, M. and Srpčič, S. (1985). “Large deformations of in-plane beam”, *International Journal of Solids and Structures*, Vol. 21, pp. 1181-1195.

-Saje, M. (1990). “A Variational Principle for Finite Planar Deformation of Straught Slender Elastic Beams.”, *International Journal of Solids and Structures*, 24(12), pp. 887-900.

-Schmidt, L.C., Morgan, P.R., and Clarkson, J.A. (1976). “Space trusses with brittle type strut buckling.” J. Struct. Div., ASCE., Vol. 102, No. 7, pp. 1479-1492.

-Scott, B.D., Park, R., and Priestley, M.J.N. (1982). “Stress-Strain Behavior of Concrete Confined by Overlapping Hoops at Low and High Strain Rates.” *ACI Journal*, 79(1), pp. 13-27.

-Scott, M.H. and Filippou, F.C. (2007). “Response Gradients for Nonlinear Beam-Column Elements under Large Displacements.”, *Journal of Structural Engineering*, ASCE; V.133, No.2: 155-165.

-Shugyo, M. (2003). “Elastoplastic Large Deflection Analysis of Three-Dimensional Steel Frames.”, *Journal of Structural Engineering*, ASCE; V.129, No.9: 1259-1267.

-Simo, J.C., Armero, F. and Taylor, R.L. (1993). “Improved versions of assumed enhanced strain tri-linear elements for 3D finite deformation problems”, *Computer Methods in Applied Mechanics and Engineering*, Vol. 110, pp. 359-386.

-Spacone, E. (1994). "Flexibility-Based Finite Element Models for the Nonlinear Static and Dynamic Analysis of Concrete Frame Structures." *Ph.D. dissertation*, Department of Civil and Environmental Engineering, University of California, Berkeley.

-Spacone, E., Filippou, F.C., and Taucer, F.F. (1996). “Fiber Beam-Column Model for Nonlinear Analysis of R/C Frames. Part I: Formulation.” *Earthquake Engineering and Structural Dynamics*, 25(7), pp. 711-725.

-Spacone, E., Ciampi. V. and Filippou, F.C. (1996). “Mixed formulation of nonlinear beam finite element”, *Computers and Structures*, Vol. 58, pp. 71-83.

-Urthaler, Y. and Reddy, J.N. (2005). “A corotational finite element formulation for the analysis of planar beams”, *Communications in Numerical Methods in Engineering*, Vol. 21, pp. 553-570.

-Taylor, R.L. (2000). *FEAP: A Finite Element Analysis Program, User Manual: Version 7.3*. Department of Civil and Environmental Engineering, University of California, Berkeley.

-Taylor, R.L., Filippou, F.C., Saritas, A., and Auricchio, F. (2003). "A Mixed Finite Element Method for Beam and Frame Problems", *Computational Mechanics*, Vol. 31, No. 1-2, pp. 192-203.

-Thompson, J.M.T. and Hunt, G.W. (1973). A General Theory of Elastic Stability, Clowes and Sons Ltd, UK.

-Tonti, E. (1977). “The reason for analogies between physical theories.” Appl. Math. Model., Vol. 1, pp. 37-50.

-Torkamani, M.A.M. and Shieh, J.H. (2011). “Higher-order stiffness matrices in nonlinear finite element analysis of plane truss structures.” Eng. Struct., Vol. 33, No. 12, pp. 3516-3526.

-Vu, L.N. (2006). “A 2D Field-Consistent Beam Element for Large Displacement Analysis Using the Total Lagrangian Formulation.”, Master Thesis:CE-MS-2005-02, Sirindhorn International Institute of Technology, Thammasat University, Thailand.

-Washizu, K. (1982). Variational Method in Elasticity and Plasticity, 3rd edn, Pergamon Press, New York, USA.

-Waszczyszyn, Z. and Janus-Michalska, M. (1998). “Numerical approach to the exact finite element analysis of in-plane finite displacements of framed structures”, *Computers and Structures*, Vol. 69, pp. 525-535.

-Wen, R.K. and Rahimzadeh, J. (1983). “Nonlinear elastic frame analysis by finite element”, *ASCE Journal Structural Division*, Vol. 109, No. 8, pp. 1952-1971.

-White, D.W. (1985). “Material and Geometric Nonlinear Analysis of Local Planar Behavior in Steel Frames Using Interactive Computer Graphics.”, Master Thesis, Cornell University, Ithaca, USA.

-William, F.W. (1964). “An Approach to Nonlinear Behavior of the Members of a Rigid Joined Place Framework with Finite Deflections.”, *Quarterly of Applied Mathematics*, 17, pp. 451-469.

-Wolf, J.P. (1971). “Post buckling strength of large space truss.” J. Struct. Div., ASCE., Vol. 99, No.7, pp. 1708-1712.

-Yang, Y.B. and McGuire, W. (1986). “Stiffness Matrix for Geometric Nonlinear Analysis.”, *Journal of Structural Engineering*, ASCE; V.112, No.4: 853-877.

-Yang, Y.B. and Chiou, H.T. (1987). “Rigid body motion test for nonlinear analysis with beam elements”, *ASCE Journal of Engineering Mechanics*, Vol. 113, pp. 1404-1419.

-Yang, Y.B. and Shieh, M.S. (1990). “Solution method for nonlinear problems with multiple critical points.” AIAA. J., Vol. 28, pp. 2110-2116.

-Yang, Y.B. and Leu, L.J. (1991). “Force Recovery Procedures in Nonlinear Analysis.”, *Computers and Structures*, 41(6), pp. 1255-1261.

-Yang, Y.B. and Kuo, S.R. (1994). Theory and Analysis of Nonlinear Framed Structures, Prentice-Hall, Singapore.

-Yassin, Mohd H.M. (1994). "Nonlinear Analysis of Prestressed Concrete Structures under Monotonic and Cyclic Loads." *Ph.D. dissertation*, Dept. of Civil and Environmental Engineering, University of California, Berkeley.

-Yi, W.J., He, Q.F., Xiao, Y., and Kunnath, S.K. (2008). “Experimental Study on Progressive Collapse-Resistant Behavior of Reinforced Concrete Frame Structures.”, *ACI Structural Journal*, 105(4), pp. 433-439.

-Zienkiewicz, O.C., Valliapan, S., and King, I.P. (1969). “Elasto-plastic solutions of engineering problems: initial stress finite element approach.” Int. J. Num. Meth. Engng., Vol. 1, pp. 75-100.

OUTPUTS

International Journal:

Limkatanyu, S., Prachasaree, W., Kaewkulchai, G., and Spacone, E. (2014) "Unification of Mixed Euler-Bernoulli-von Karman Planar Frame Model and Corotational Approach." *Mechanics Based Design of Structures and Machines: An International Journal*, 42(4), pp. 419-441.
(ISI Impact Factor (2013/2014) = 0.69)

Limkatanyu, S., Prachasaree, W., Kaewkulchai, G., and Kwon, M. (2013) "Total Lagrangian Formulation of 2D Bar Element Using Vectorial Kinematical Description", *KSCE Journal of Civil Engineering*, 17(6), pp. 1348-1358.
(ISI Impact Factor (2013/2014) = 0.511)